# Dual-Readout Calorimetry

Sehwook Lee (Kyungpook National Univ.)
CALOR 2024, Tsukuba, Japan
May 22, 2024

# Dual-Readout Calorimetry since 1997

- 1986-1992: the secret of compensation was unraveled
- 1997: Dual-Readout Calorimeter was proposed in CALOR 1997, Tucson, USA
- 1997-2009: DREAM (Dual-REAout Method) Collaboration
  - Proved the Dual-Readout principle with the proto-type DREAM module (Cu-fibers)
- 2010-2018: RD52 Collaboration
  - Improvement of the performance of the dual-readout calorimeter (Cu-fiber, Pb-fiber)
- 2019-present: Studying for future collider experiments

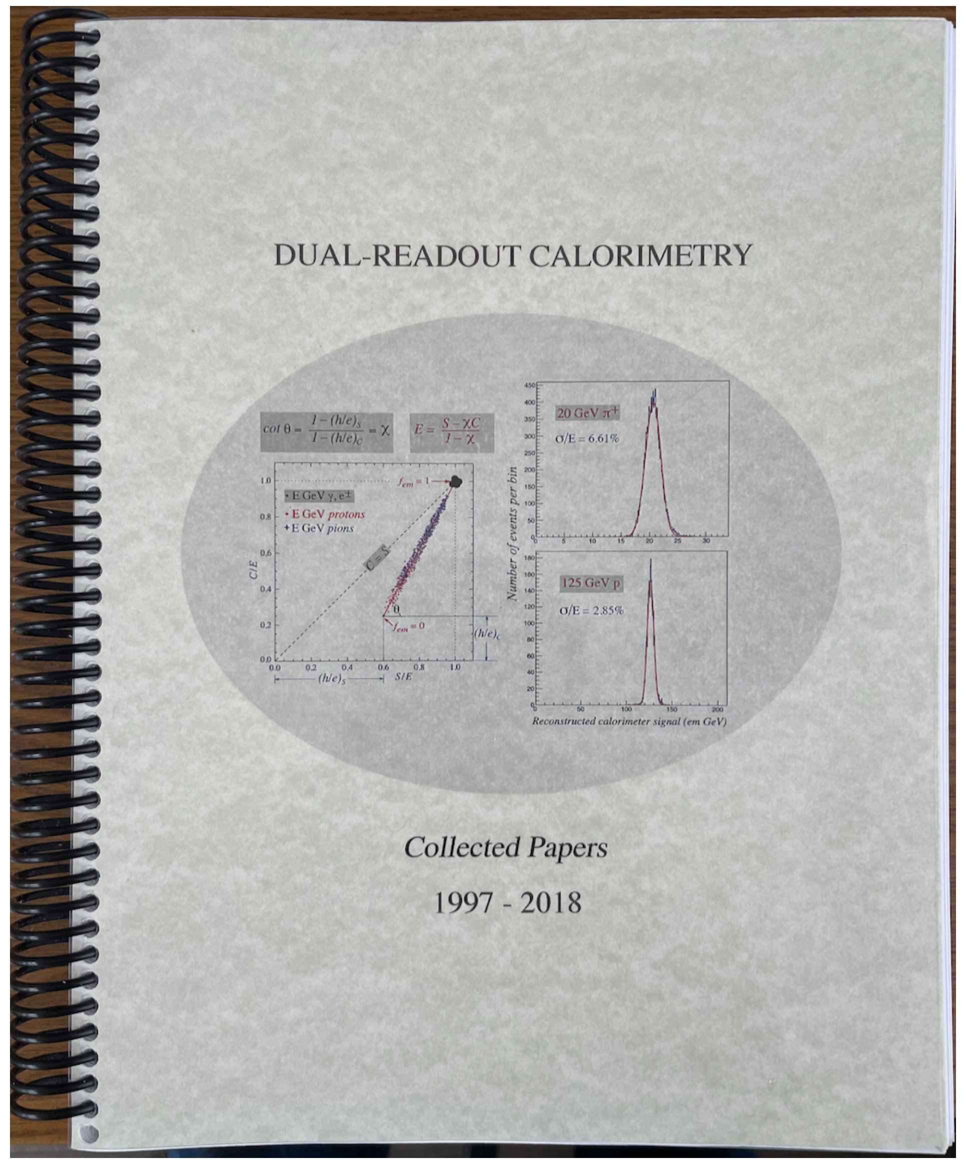


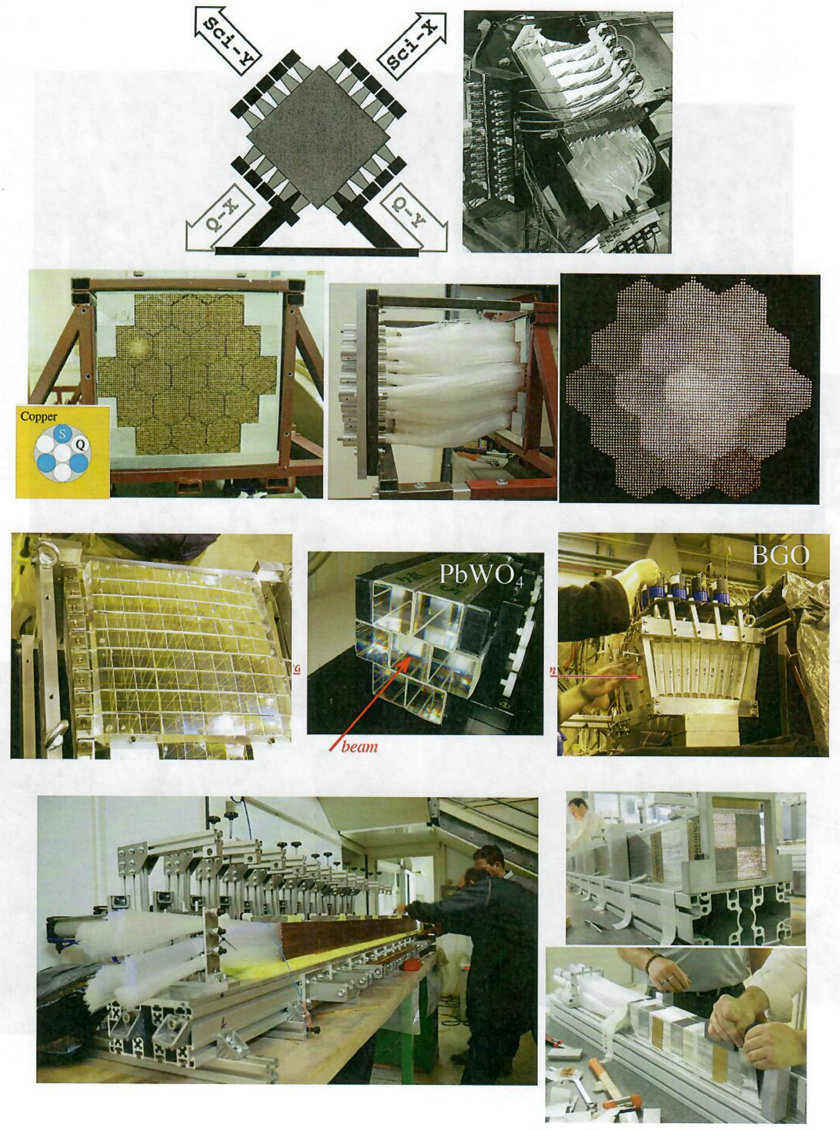


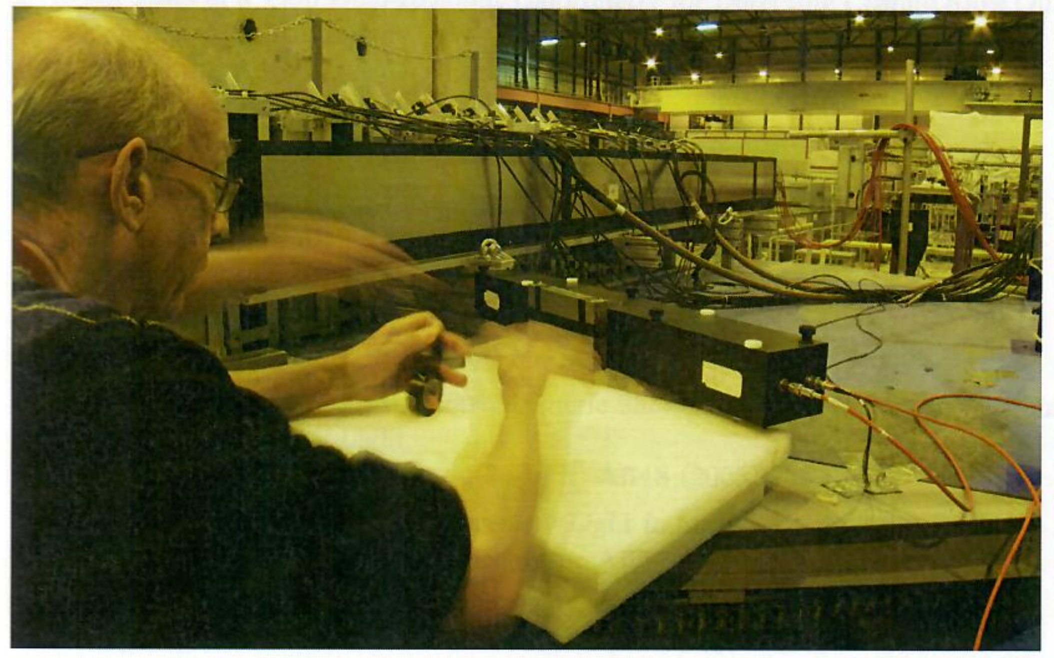

*In memory of our wonderful friend and colleague*

*GUIDO CIAPETTI*

# RD52 Collaboration (2010-2018)


[35] S. Lee, M. Livan, R. Wigmans, Dual-Readout Calorimetry, Rev. Mod. Phys. 90 (2018) 025002.

[34] Sehwook Lee, John Hauptman, Richard Wigmans, Where the energy goes?, 2018 Physics World Focus on Instruments and Vacuum, August 2018

[33] M. Antonello, et al, Tests of a dual-readout fiber calorimeter with SiPM light sensors, Nucl. Instr. and Meth. in Phys. Res. A 899 (2018) 52.

[32] S. Lee, M. Livan, R. Wigmans, On the limits of the hadronic energy resolution of calorimeters, Nucl. Instr. and Meth. in Phys. Res. A 882 (2018) 148.

[31] S. Lee, et al., Hadron detection with a dual-readout fiber calorimeter, Nucl. Instr. and Meth. in Phys. Res. A 866 (2017) 76.

[30] R. Wigmans, New results from the RD52 project, Nucl. Instr. and Meth. in Phys. Res. A 824 (2016) 721.

[29] A. Cardini, et al., The small-angle performance of a dual-readout fiber calorimeter, Nucl. Instr. and Meth. in Phys. Res. A 808 (2016) 41.

[28] N. Akchurin, et al., Lessons from Monte Carlo simulations of the performance of a dual-readout fiber calorimeter, Nucl. Instr. and Meth. in Phys. Res. A 762 (2014) 100.

[27] N. Akchurin, et al., Particle identification in the longitudinally unsegmented RD52 calorimeter, Nucl. Instr. and Meth. in Phys. Res. A 735 (2014) 120.

[26] N. Akchurin, et al., The electromagnetic performance of the RD52 fiber calorimeter, Nucl. Instr. and Meth. in Phys. Res. A 735 (2014) 130.

[25] N. Akchurin, et al., Detection of electron showers in Dual-Readout crystal calorimeters, Nucl. Instr. and Meth. in Phys. Res. A 686 (2012) 125.

[24] N. Akchurin, et al., A comparison of BGO and BSO crystals used in the dual-readout mode, Nucl. Instr. and Meth. A 640 (2011) 91.

[23] N. Akchurin, et al., Polarization as a tool for dual-readout calorimetry, Nucl. Instr. and Meth. A 638 (2011) 47.

[22] Gabriella Gaudio, New result from the DREAM project, Nucl. Instr. and Meth. A 628 (2011) 339.

[21] N. Akchurin, et al., Optimization of crystals for applications in dual-readout calorimetry, Nucl. Instr. and Meth. A 621 (2010) 212.

[20] R. Wigmans, The DREAM project - Towards the ultimate in calorimetry, Nucl, Instr. and Meth. A 617 (2010) 129.


# DREAM (Dual-REAdout Method) Collaboration (1997-2009)

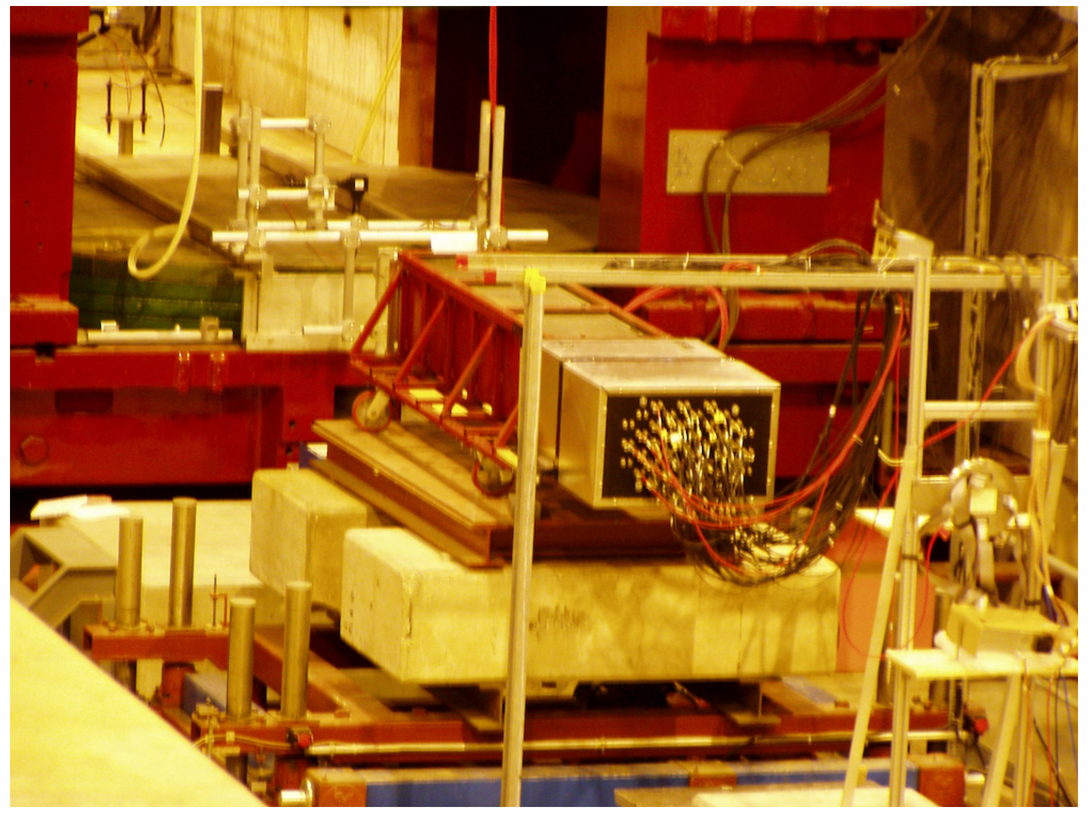


[19] N. Akchurin, et al., Dual-readout calorimetry with a full-size BGO electromagnetic section, Nucl. Instr. and Meth. A 610 (2009) 488.

[18] N. Akchurin, et al., New crystals for dual-readout calorimetry, Nucl. Instr. and Meth. A 604 (2009) 512.

[17] N. Akchurin, et al., Dual-Readout Calorimetry with Crystal Calorimeters, Nucl. Instr. and Meth. A 598 (2009) 710.

[16] N. Akchurin, et al., Neutron Signals for Dual-Readout Calorimetry, Nucl. Instr. and Meth. A 598 (2009) 422.

[15] M. Nikl et al., Luminescence and scintillation characteristics of heavily Pr^{3+}-doped PbWO4 single crystals, Journal of Applied Physics 104, (2008) 093514.

[14] N. Akchurin, et al., Separation of crystal signals into scintillation and Cherenkov components, Nucl. Instr. and Meth. A 595 (2008) 359.

[13] N. Akchurin, et al., Effects of the temperature dependence of the signals from lead tungstate crystals, Nucl. Instr. and Meth. A 593 (2008) 530.

[12] N. Akchurin, et al., Comparison of High-Energy Hadronic Shower Profiles Measured with Scintillation and Cerenkov Light, Nucl. Instr. and Meth. A 584 (2008) 304.

[11] N. Akchurin, et al., Dual-Readout Calorimetry with Lead Tungstate Crystals, Nucl. Instr. and Meth. A 584 (2008) 273.

[10] N. Akchurin, et al., Contributions of Cherenkov light to the signals from lead tungstate crystals, Nucl. Instr. and Meth. A 582 (2007) 474.

[9] N. Akchurin, et al., Measurement of the Contribution of Neutrons to Hadron Calorimeter Signals, Nucl. Instr. and Meth. A 581 (2007) 643.

[8] R. Wigmans, The DREAM project-Results and plans, Nucl. Instr. and Meth. A 572 (2007) 215.

[7] N. Akchurin, et al., Separation of Scintillation and Cerenkov Light in an Optical Calorimeter, Nucl. Instr. and Meth. A 550 (2005) 185.

[6] N. Akchurin, et al., Comparison of High-Energy Electromagnetic Shower Profiles Measured with Scintillation and Cerenkov Light, Nucl. Instr. and Meth. A 548 (2005) 336.

[5] N. Akchurin, et al., Hadron and jet detection with a dual-readout calorimeter, Nucl. Instr. and Meth. A 537 (2005) 537.

[4] N. Akchurin, et al., Electron detection with a dual-readout calorimeter, Nucl. Instr. and Meth. A 536 (2005) 29.

[3] N. Akchurin, et al., Muon detection with a dual-readout calorimeter, Nucl. Instr. and Meth. A 533 (2005) 305.

[2] Richard Wigmans, Status and perspectives of detectors for experiments in HEP and related fields, Nucl. Instr. and Meth. A 518 (2004) 9.

[1] Vladimir Nagaslaev, Alan Sill, Richard Wigmans, Beam tests of a thin dual-readout calorimeter for detecting cosmic rays outside the Earth's atmosphere, Nucl. Instr. and Meth. A 462 (2001) 411


# Proposal (1997)


[0] Richard Wigmans (Texas Tech. University, USA), Quartz Fibers and the Prospects for Hadron Calorimetry at the 1% Resolution Level, CALOR 1997 Tucson, USA

# Dual-Readout Principle

## Improvement of Hadron Calorimeter Performance

- The performance of hadronic calorimeters is worse than that of electromagnetic calorimeters.
- Non-Gaussian fluctuations of EM component and nuclear binding energy loss are responsible for the poor hadronic performance.
- Hadron showers
  - EM component ($\pi^0$)
  - Non-EM component (mainly soft protons)
- EM component is relativistic and can generate Cerenkov light, while charged shower particles produce dE/dx signals
- **Dual-Readout Principle**: measure $f_{em}$ event-by-event by comparing Cerenkov and dE/dx signals

# CALOR 1997, Tucson, USA

## 1997

- Quartz Fibers and the Prospects for Hadron Calorimetry at the 1% Resolution Level
- Richard Wigmans proposed a fiber calorimeter consisting of scintillating and quartz fibers
  - Scintillating fibers: the visible energy
  - Quartz fibers: the em energy

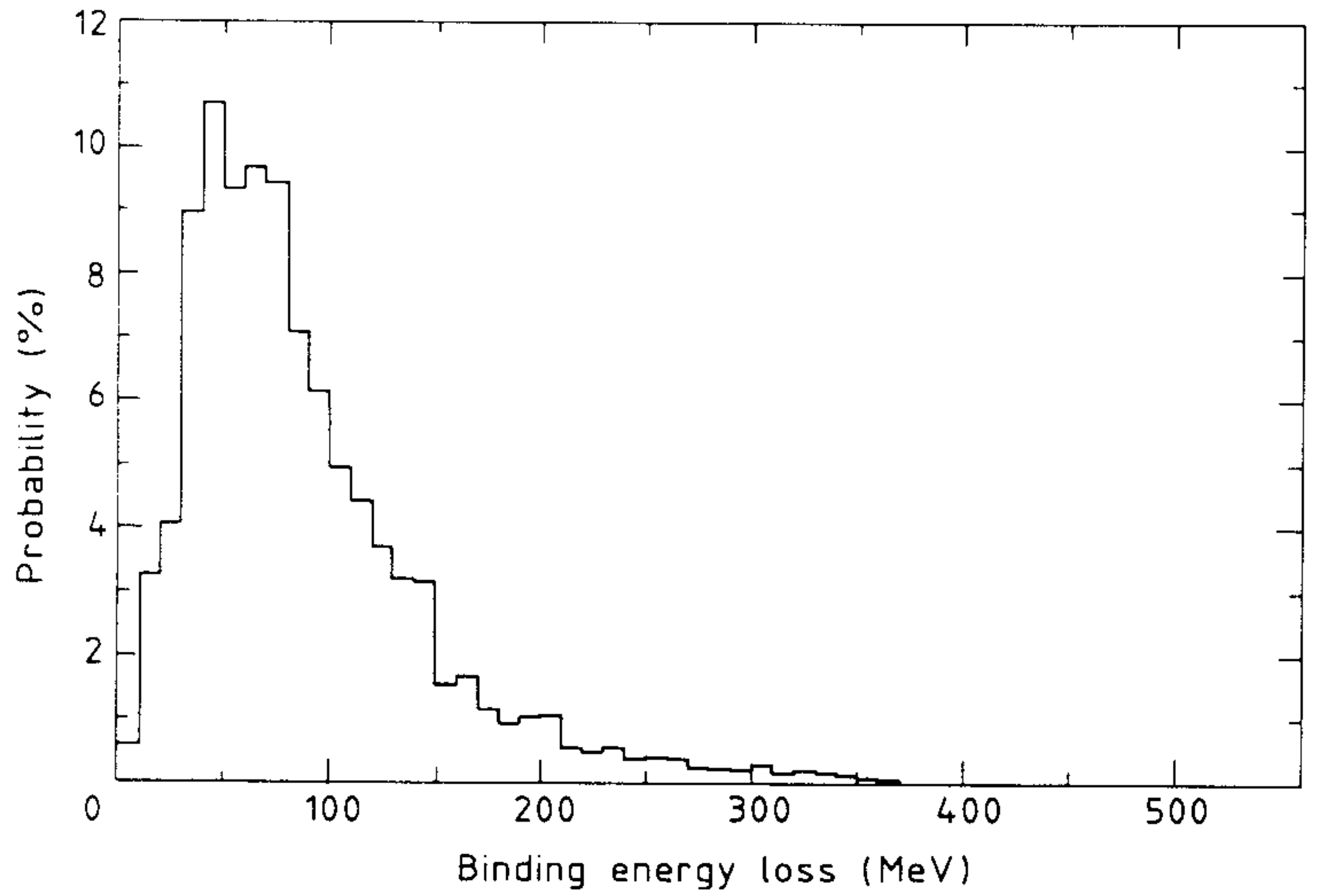


Figure 4: The nuclear binding energy lost in spallation reactions induced by 1 GeV pions on $^{63}$Cu nuclei.

# ACCESS

## 2001

- This calorimeter was designed to detect high-energy cosmic rays at International Space Station
- Total depth: 1.4 $\lambda_{int}$
  - Absorber: 39 Pb plates, 6.4 mm thick each
  - Active medium: ribbons of plastic scintillator and quartz
  - Tested with high-energy pions (up to 375 GeV) at CERN

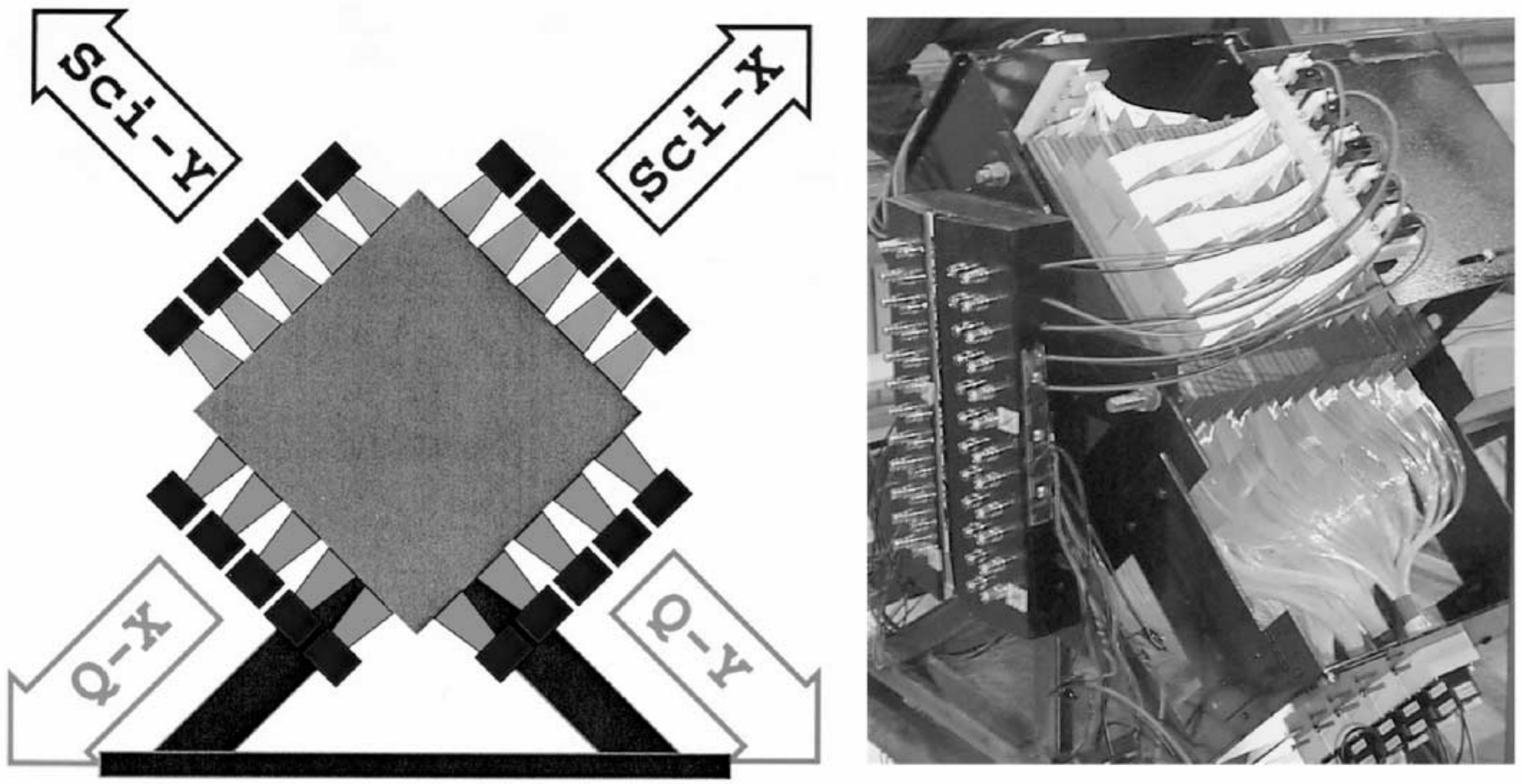


Fig. 1. Schematic layout and a photograph of the dual-readout calorimeter. Thin lead plates are interleaved with 4 cm wide ribbo scintillating and quartz fibers, which both provide readout in two coordinates.

# ACCESS

## NIM A 462 (2001) 411-425

- The calorimeter response to high-energy hadrons is determined by leakage fluctuation
- In the first nuclear reaction, some fraction of the initial pion energy is converted into neutral pion
- If that fraction is large (Q/S is large), the leakage is relatively small, and the signal is relatively large
- If that fraction is small (Q/S is small), the leakage is relatively large, and the signal is relatively small
- The C/S ratio provides information on the energy containment

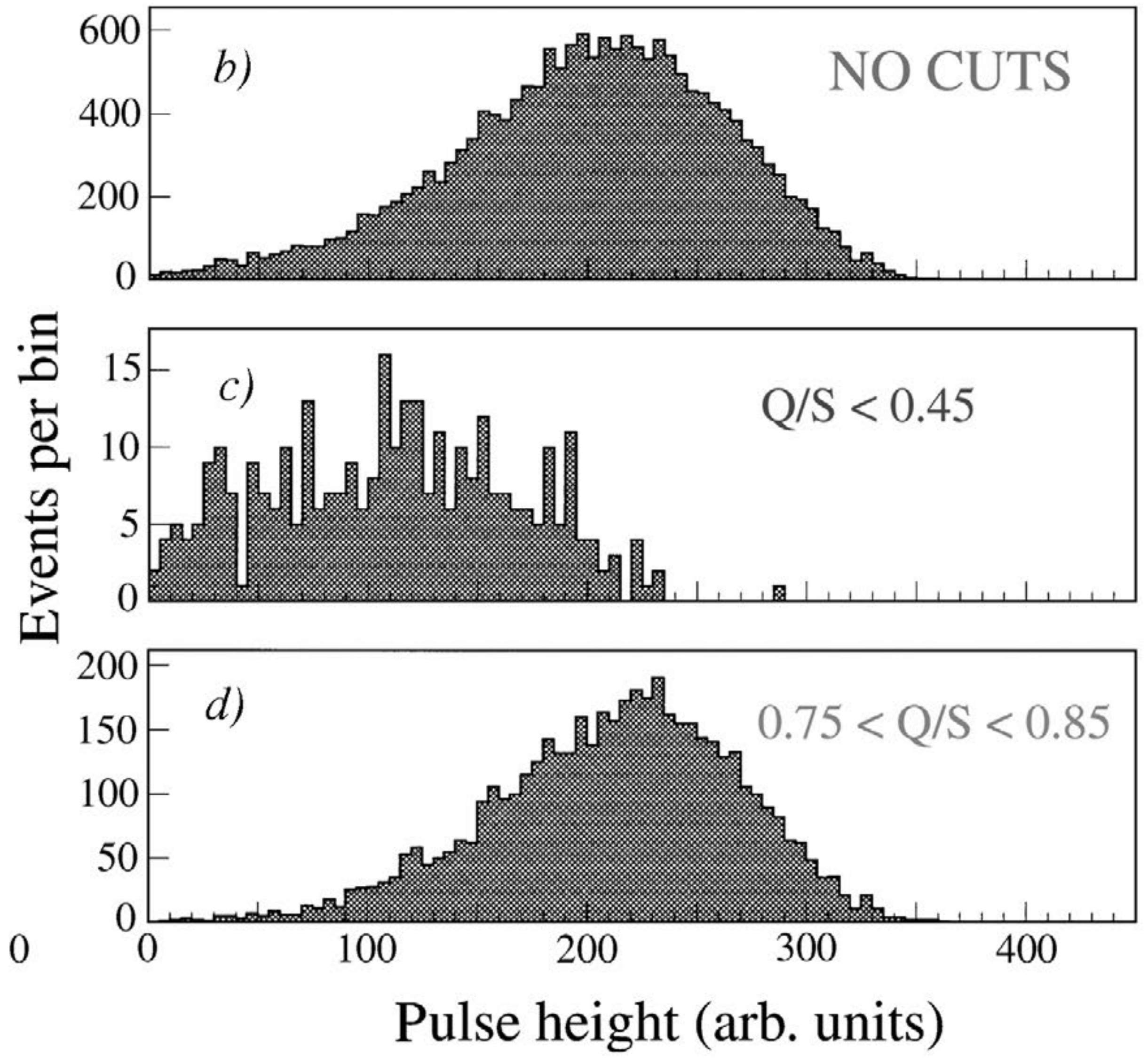


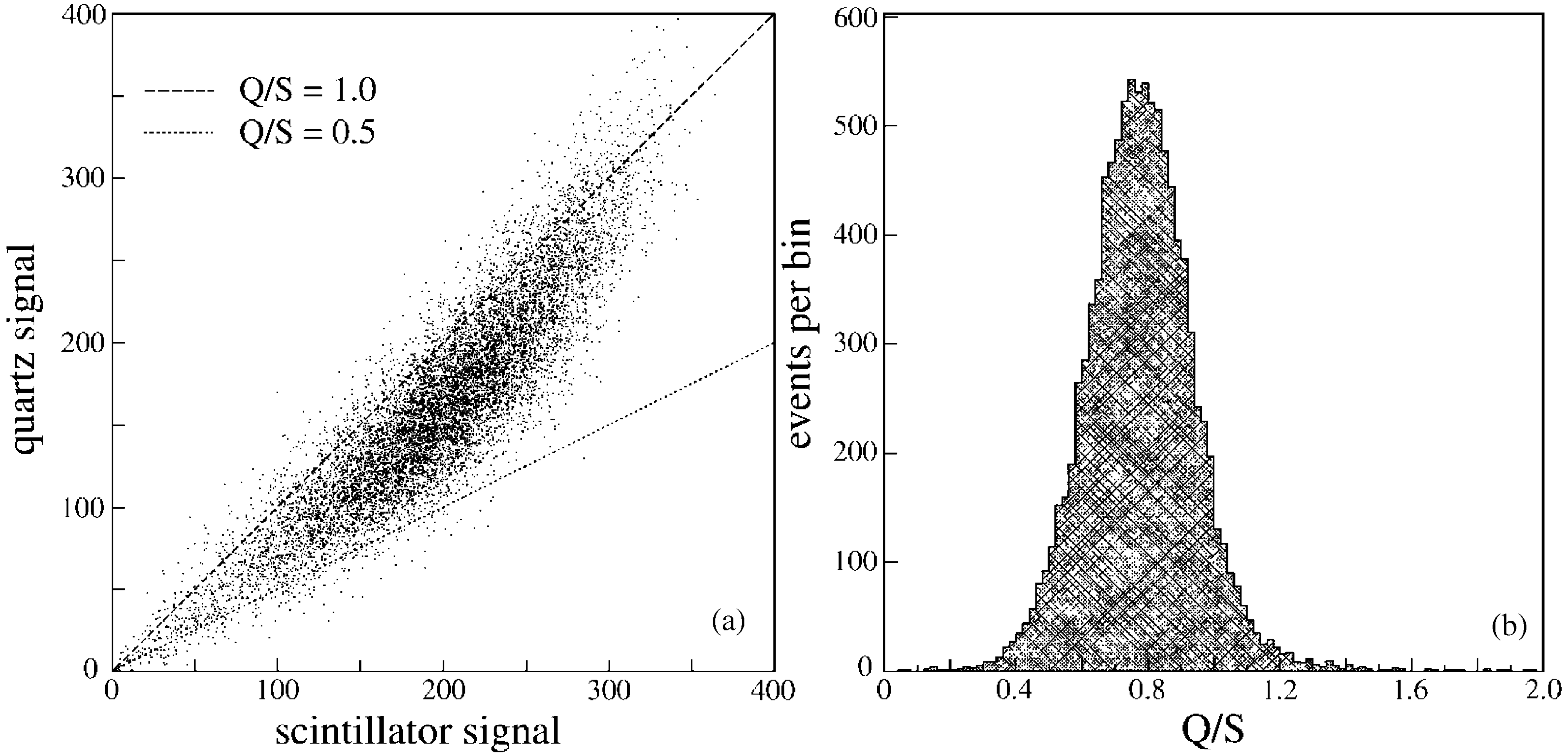


Fig. 8. Results of tests of the dual-readout calorimeter with 375 GeV pions. Scatter plot of the signals recorded in the quartz fibers vs. those in the scintillating fibers (a). Distribution of the ratio of the signals observed in the quartz fibers and the scintillating fibers (b).

# Prototype DREAM Module

- Depth: 200 cm (10 $\lambda_{int}$)
- Effective radius: 16.2 cm (0.81 $\lambda_{int}$, 8 $\rho_M$)
- Mass: 1030 kg
- Number of fibers: 35910, diameter 0.8 mm, total length≈90 km
- Hexagonal towers: 19, each read out by 2 PMTs

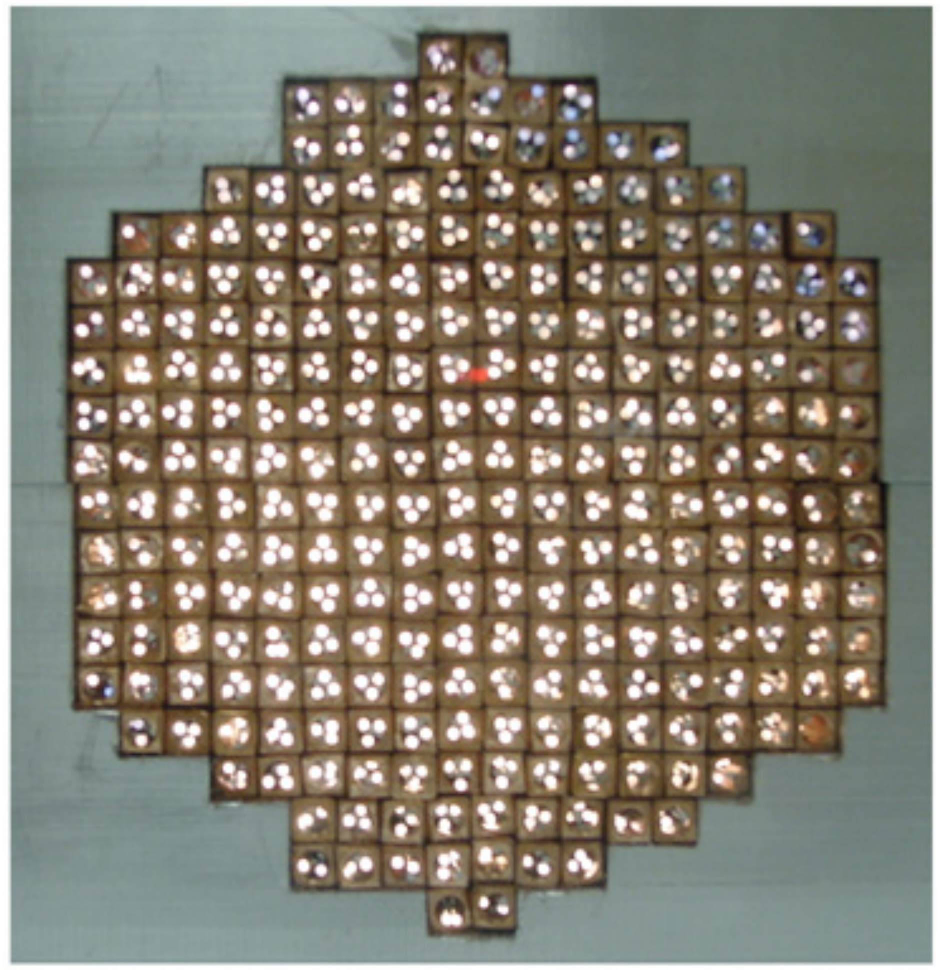

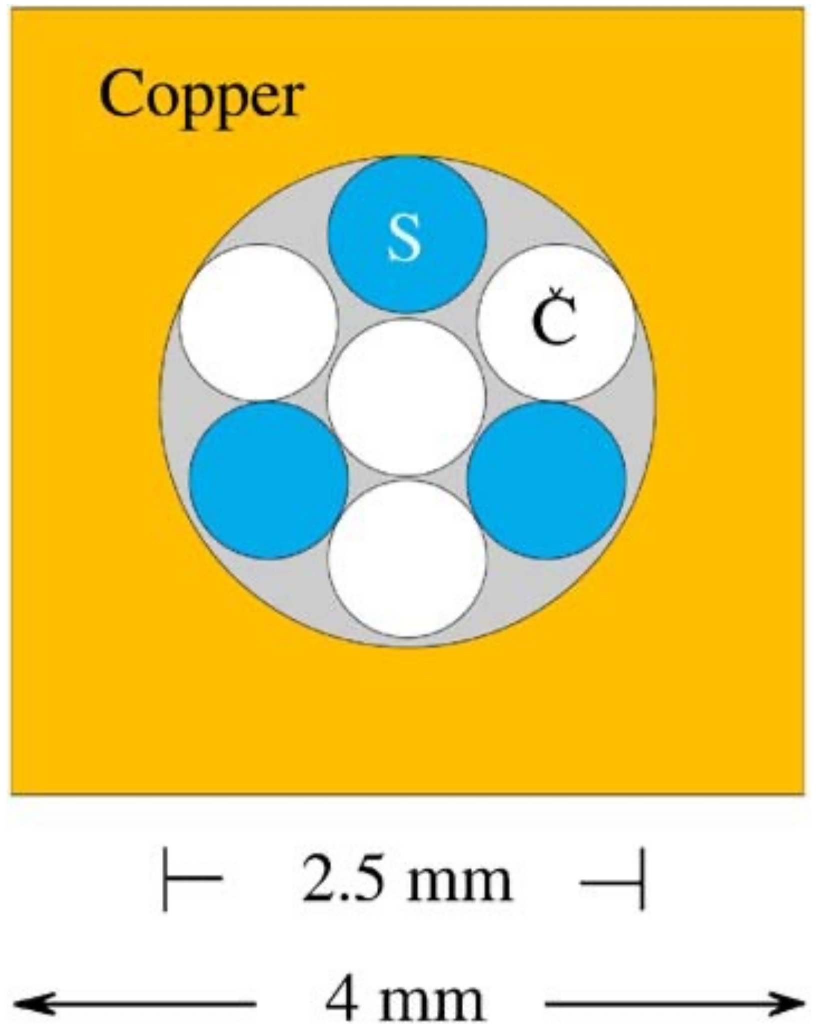


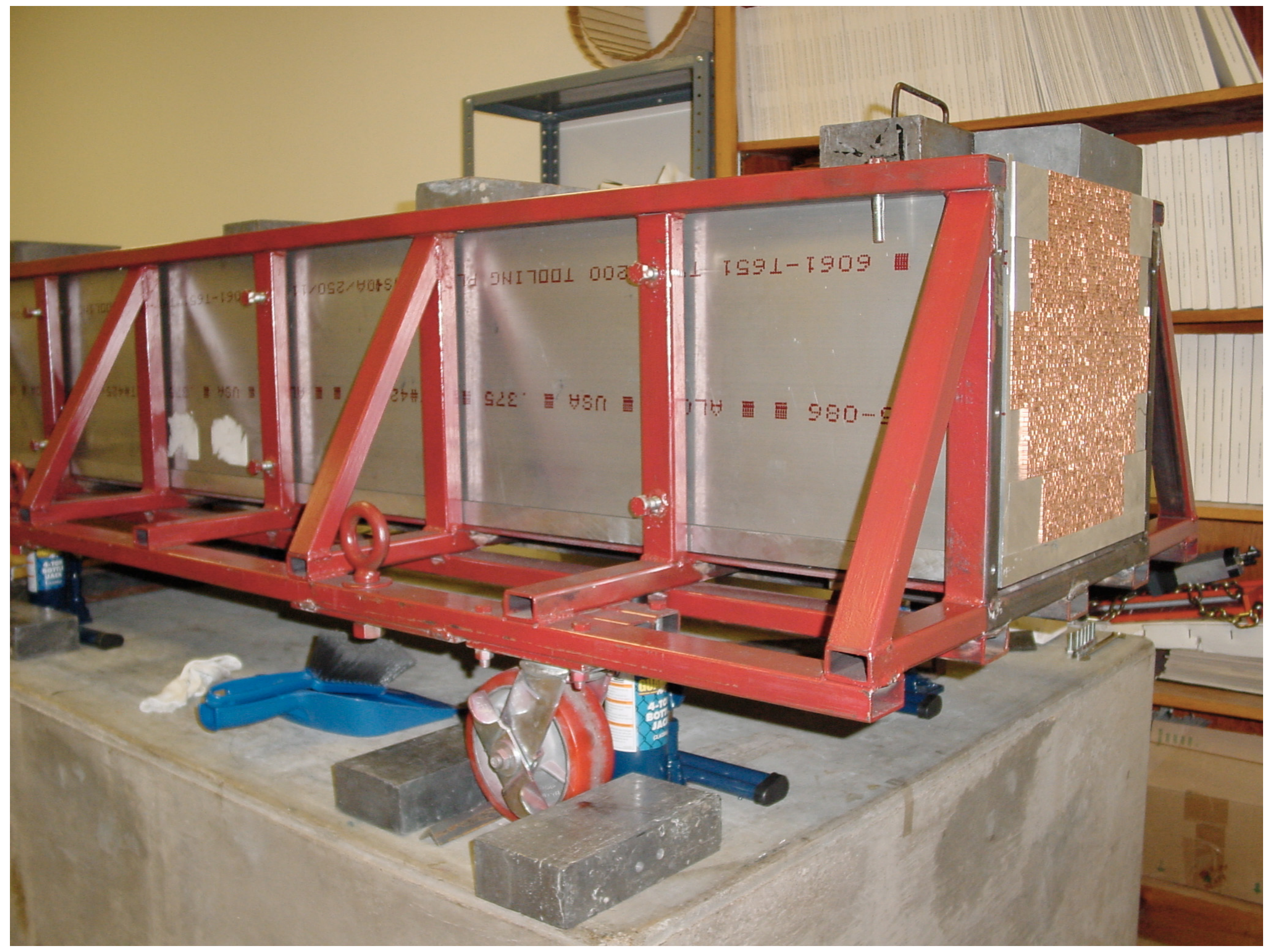

# Muon detection with a dual-readout calorimeter

## NIM A 533 (2005) 305

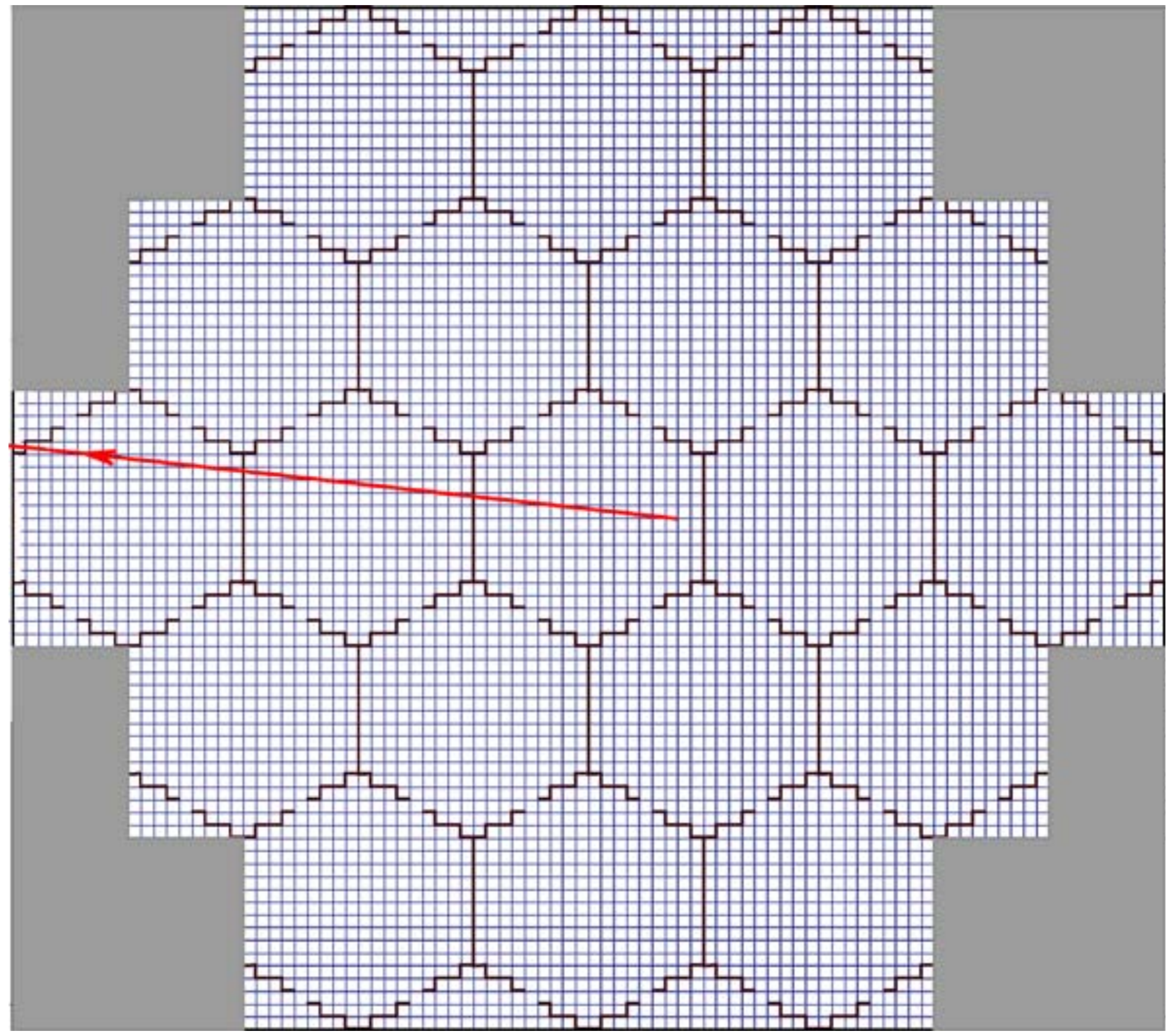

Fig. 2. Layout of the DREAM calorimeter. The detector consists of 19 hexagonal towers. A central tower is surrounded by two hexagonal rings, the Inner Ring (6 towers) and the Outer Ring (12 towers). The towers are not longitudinally segmented. The arrow indicates the (projection of the) trajectory of a muon traversing the calorimeter oriented in position D(6°, 0.7°).

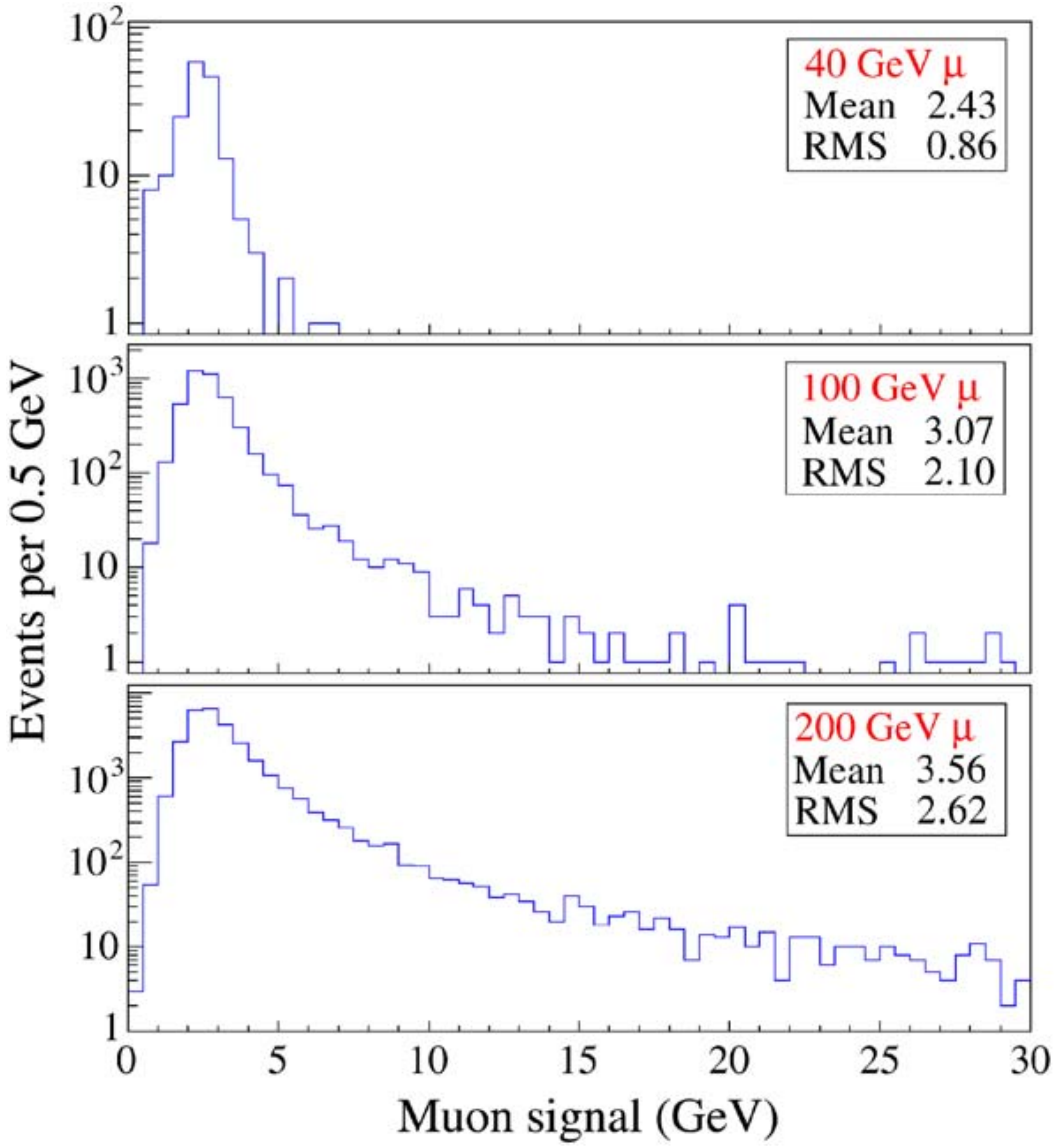


Fig. 14. Signal distributions for 40, 100 and 200 GeV muons, measured with the scintillating fibers in the DREAM calorimeter.

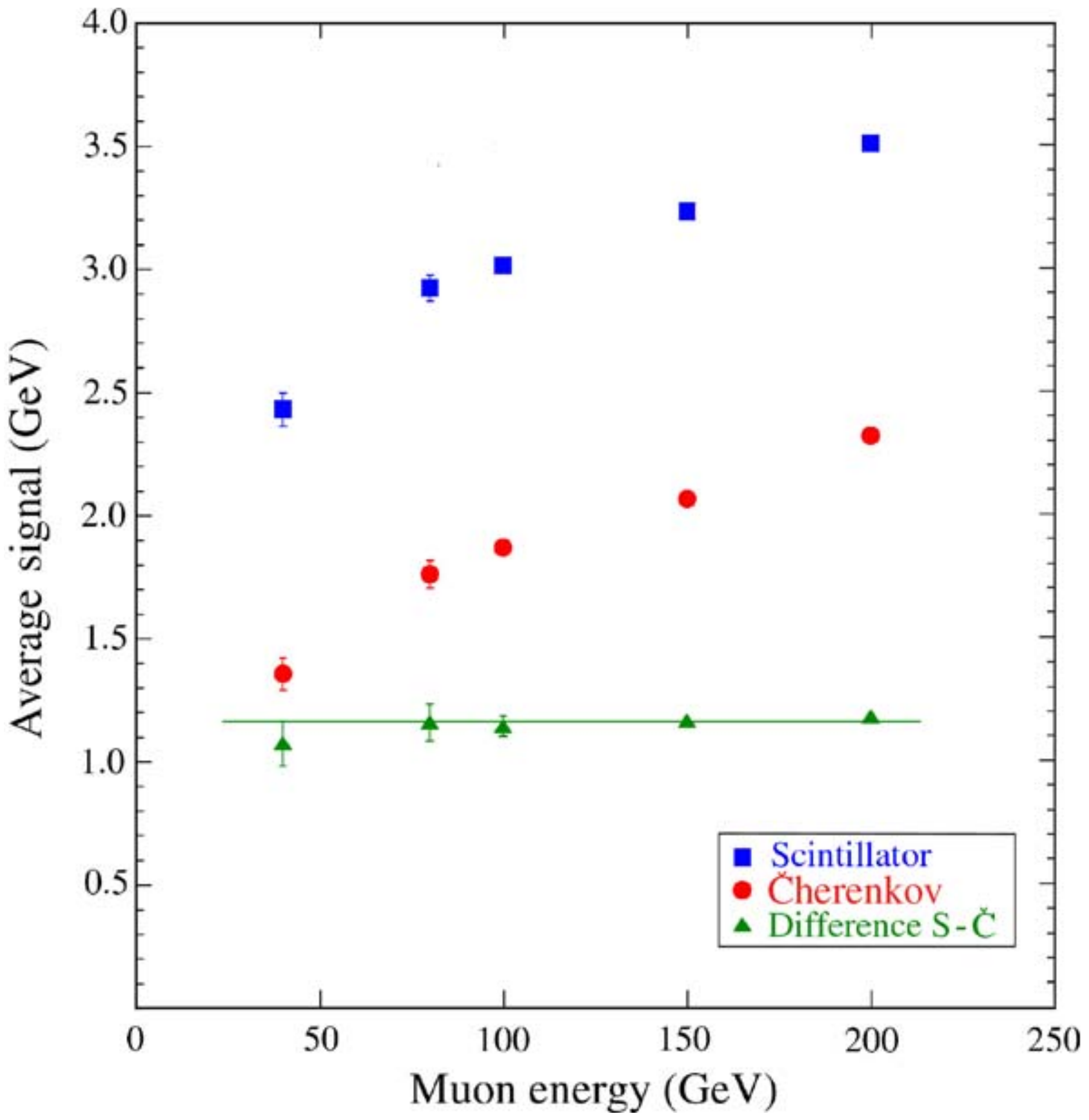


Fig. 18. Average signal from muons traversing the DREAM calorimeter, as a function of the muon energy. The detector was oriented in position D(6°, 0.7°). Results are given separately for the scintillating and the Cherenkov fibers. Also shown is the *difference* between the average signal values from both media.

# Electron detection with a dual-readout calorimeter

## NIM A 536 (2005) 29

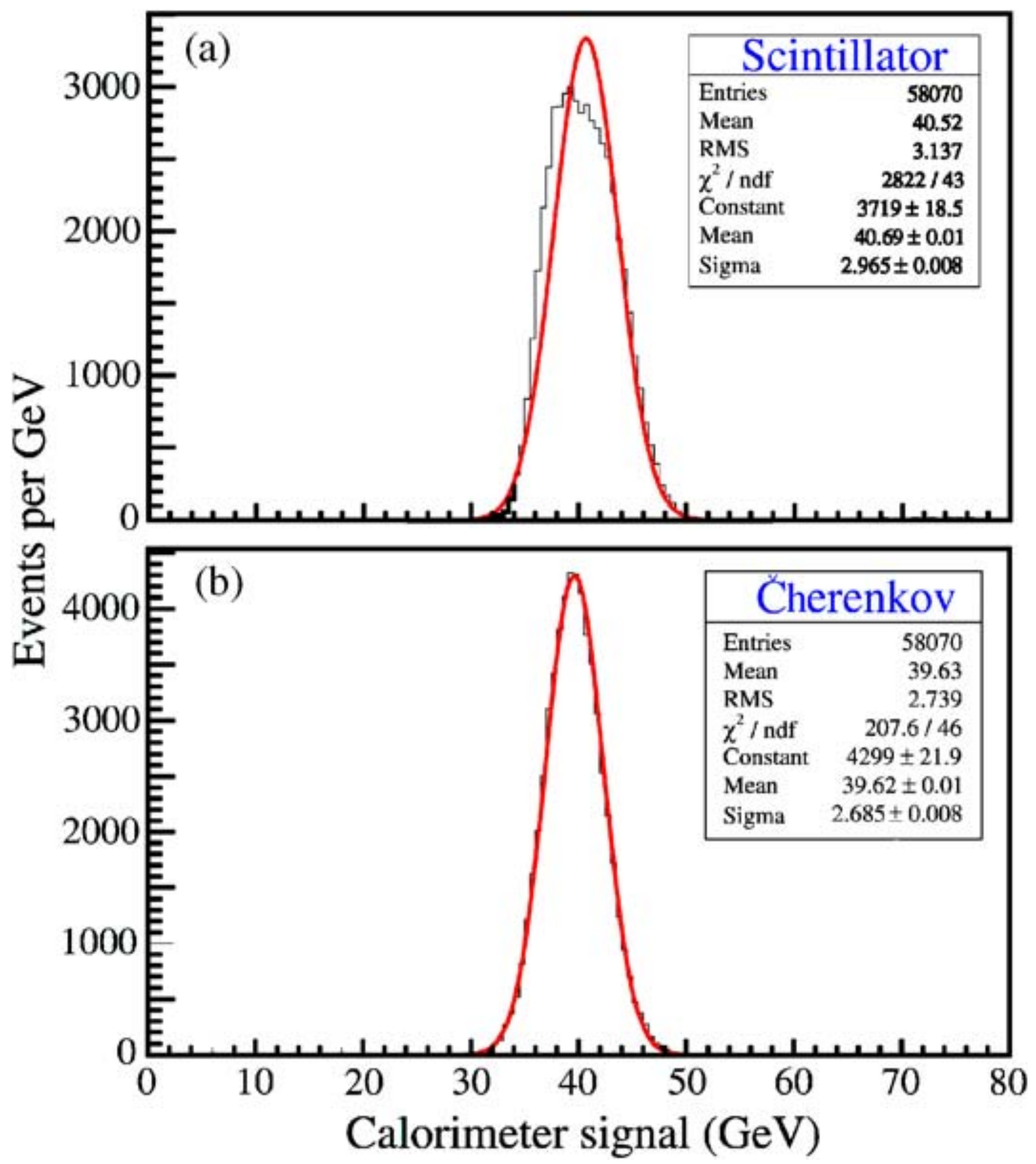


Fig. 7. Signal distributions for 40 GeV electrons, recorded from the scintillating (a) and the Cherenkov (b) fibers, with the DREAM calorimeter in the untilted position, A(2°, 0.7°).

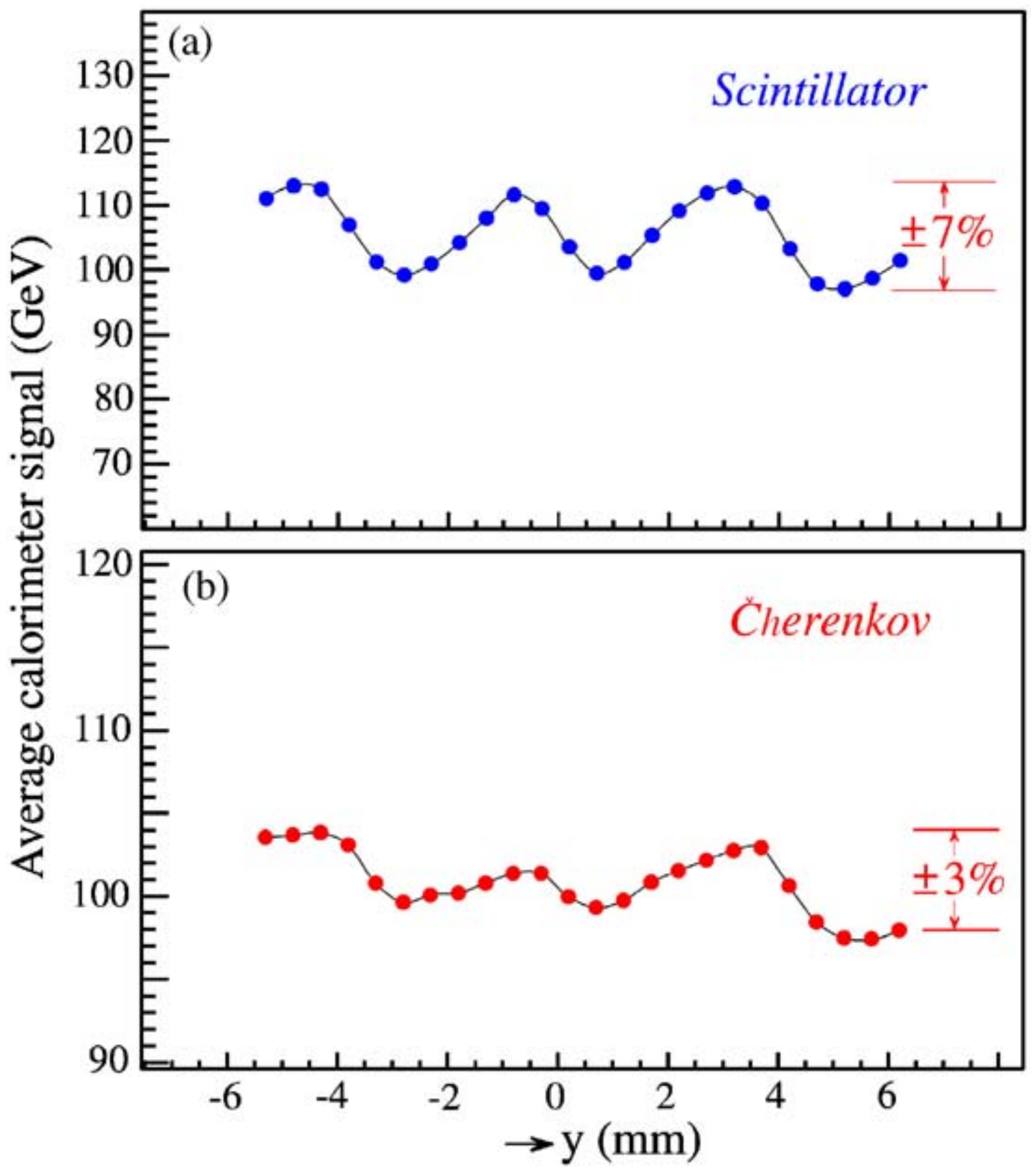


Fig. 11. Average calorimeter signal as a function of the *y*-coordinate of the impact point, for the scintillator (a) and Cherenkov (b) signals from 100 GeV electrons entering the DREAM calorimeter oriented in the untilted position, A(2°, 0.7°). Note the different vertical scales.

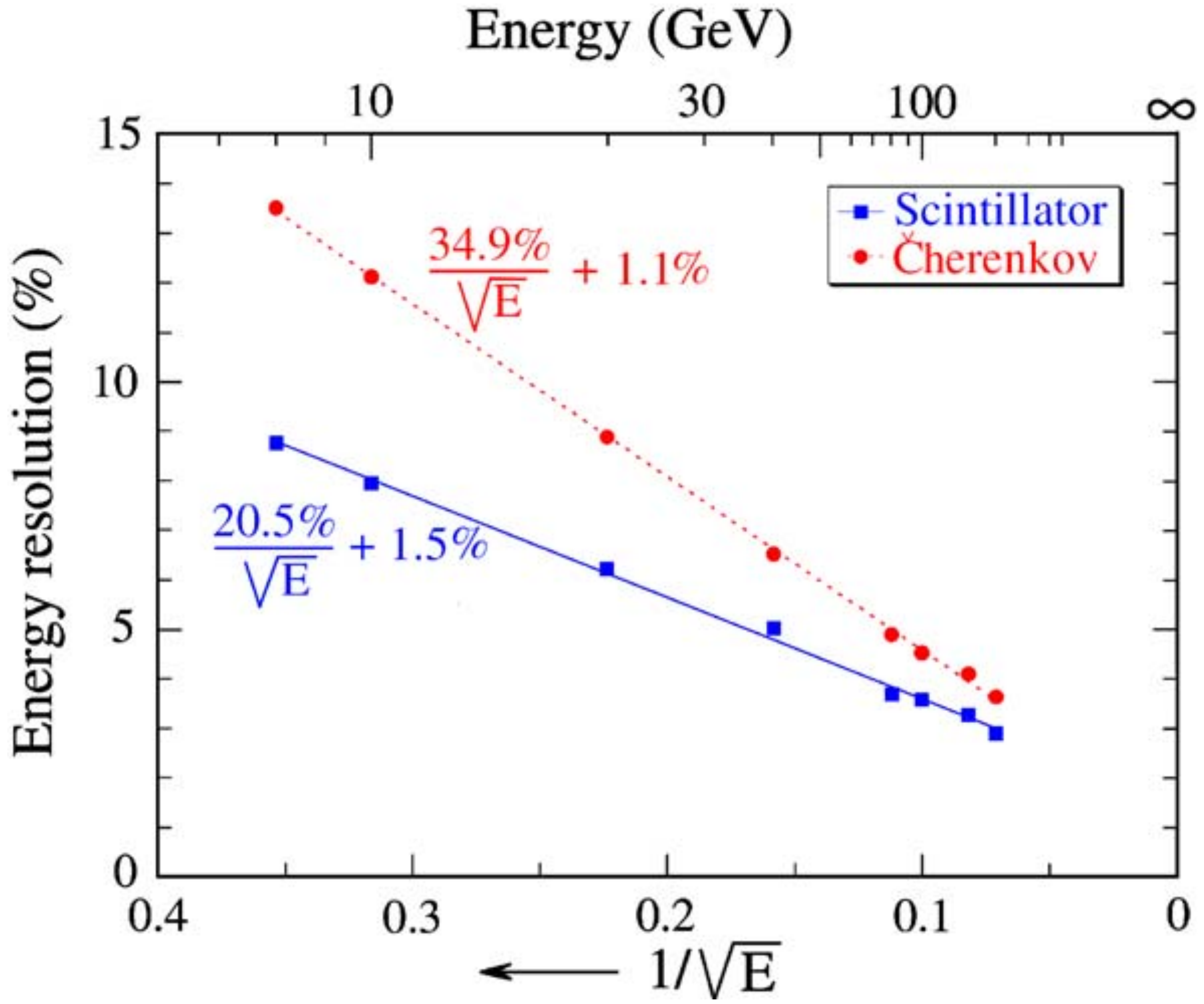


Fig. 20. The energy resolution as a function of energy, measured with the scintillating (squares) and Cherenkov fibers (circles), for electrons entering the calorimeter in the tilted position, B(3°, 2°).

# Hadron and jet detection with a dual-readout calorimeter

## NIM A 537 (2005) 537

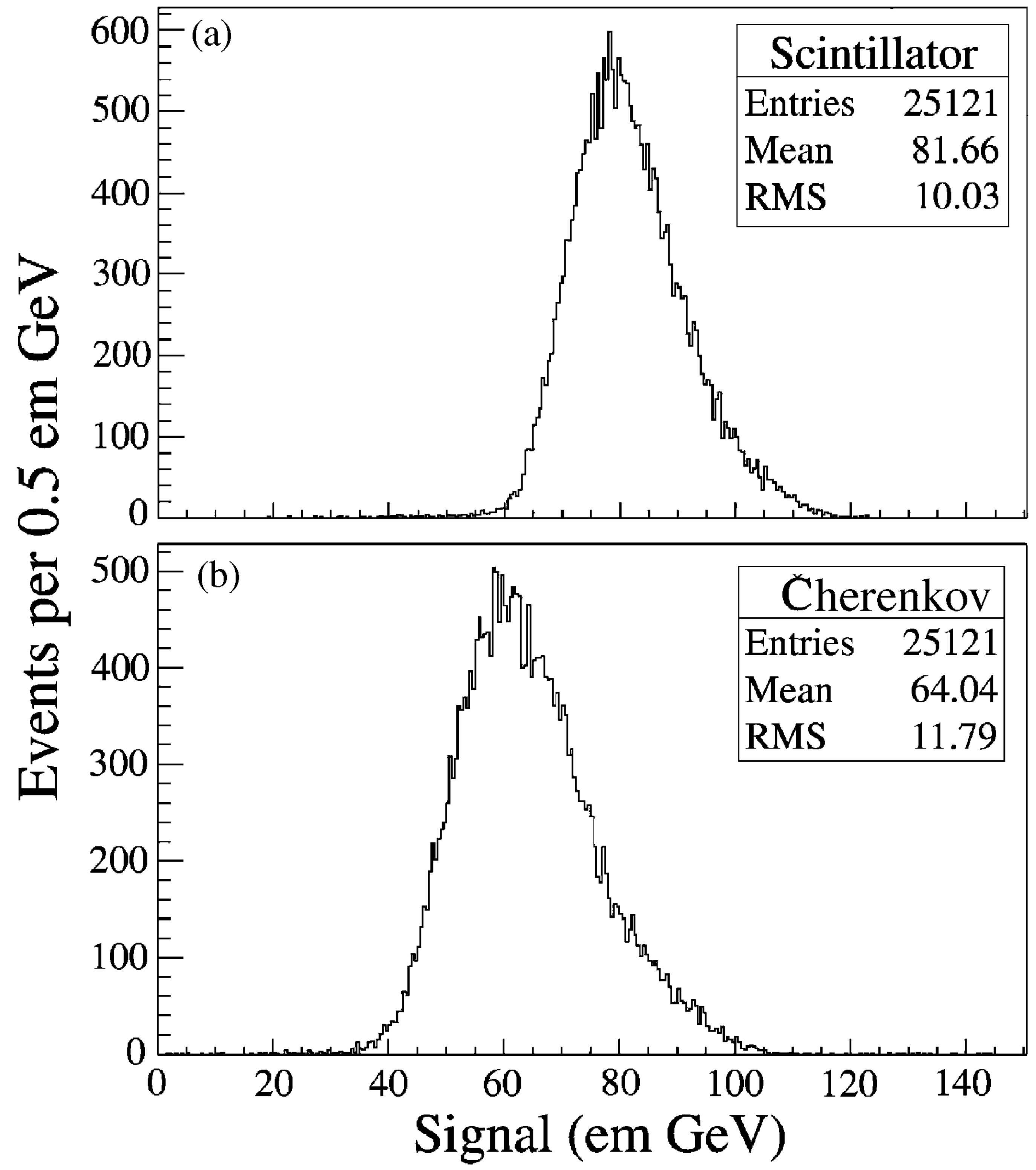


Fig. 9. Signal distributions for 100 GeV $\pi^-$ recorded by the scintillating (a) and Cherenkov (b) fibers of the DREAM calorimeter, oriented in the untilted position, $A(2°, 0.7°)$. The signals are expressed in the same units as those for em showers, which were used to calibrate the detector (em GeV).

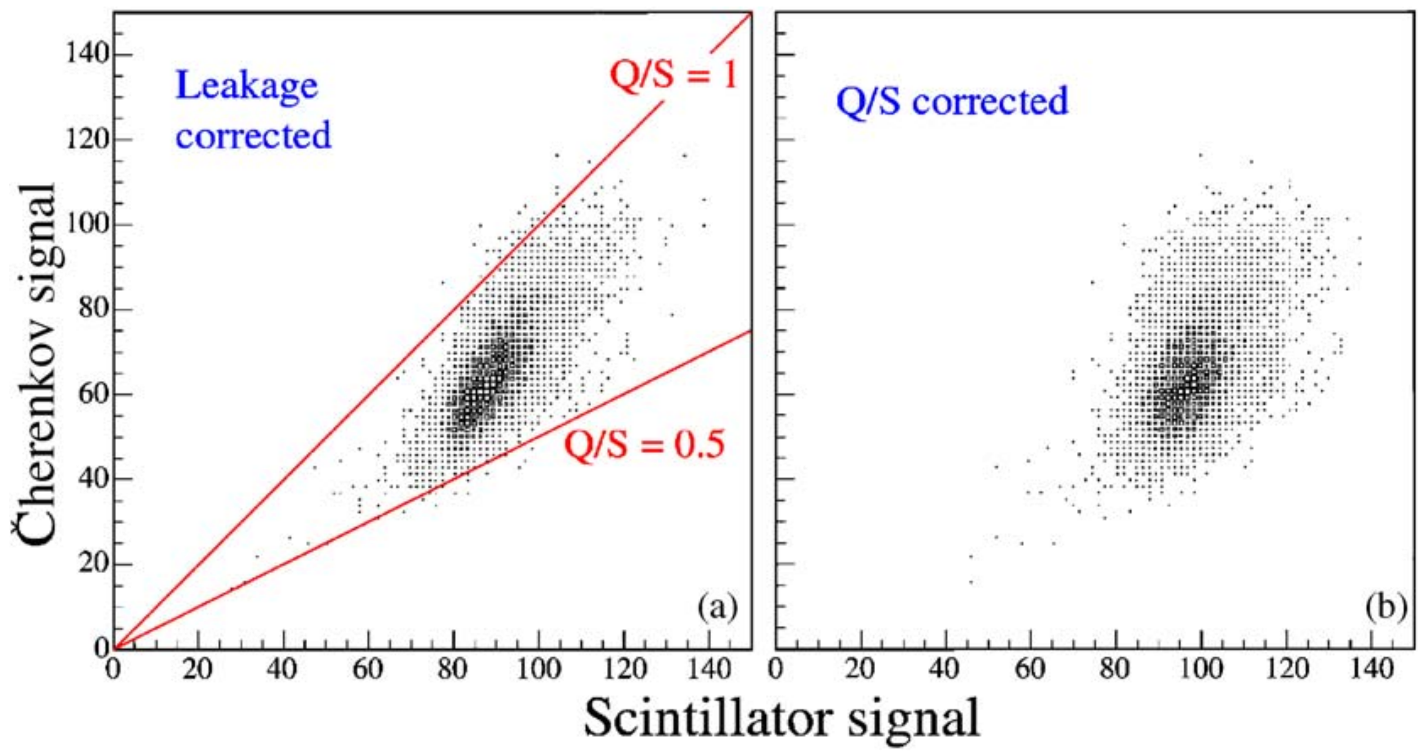


Fig. 24. Cherenkov signals versus scintillator signals for 100 GeV $\pi^-$ in the DREAM calorimeter. These plots were derived from the raw data (Fig. 12) after applying corrections for shower leakage, using Eq. (6) (a) and, in addition, for the effects of non-compensation, using Eq. (7) (b).

$$S = E\left[f_{em} + \frac{1}{(e/h)_S}(1 - f_{em})\right]$$

$$Q = E\left[f_{em} + \frac{1}{(e/h)_Q}(1 - f_{em})\right]$$

$e.g.$ If $e/h = 1.3$ (S), 4.7 (Q)

$$\frac{Q}{S} = \frac{f_{em} + 0.21\,(1 - f_{em})}{f_{em} + 0.77\,(1 - f_{em})}$$

$$E = \frac{S - \chi Q}{1 - \chi}$$

with $\chi = \dfrac{1 - (h/e)_S}{1 - (h/e)_Q}$

# Hadron and jet detection with a dual-readout calorimeter

## NIM A 537 (2005) 537

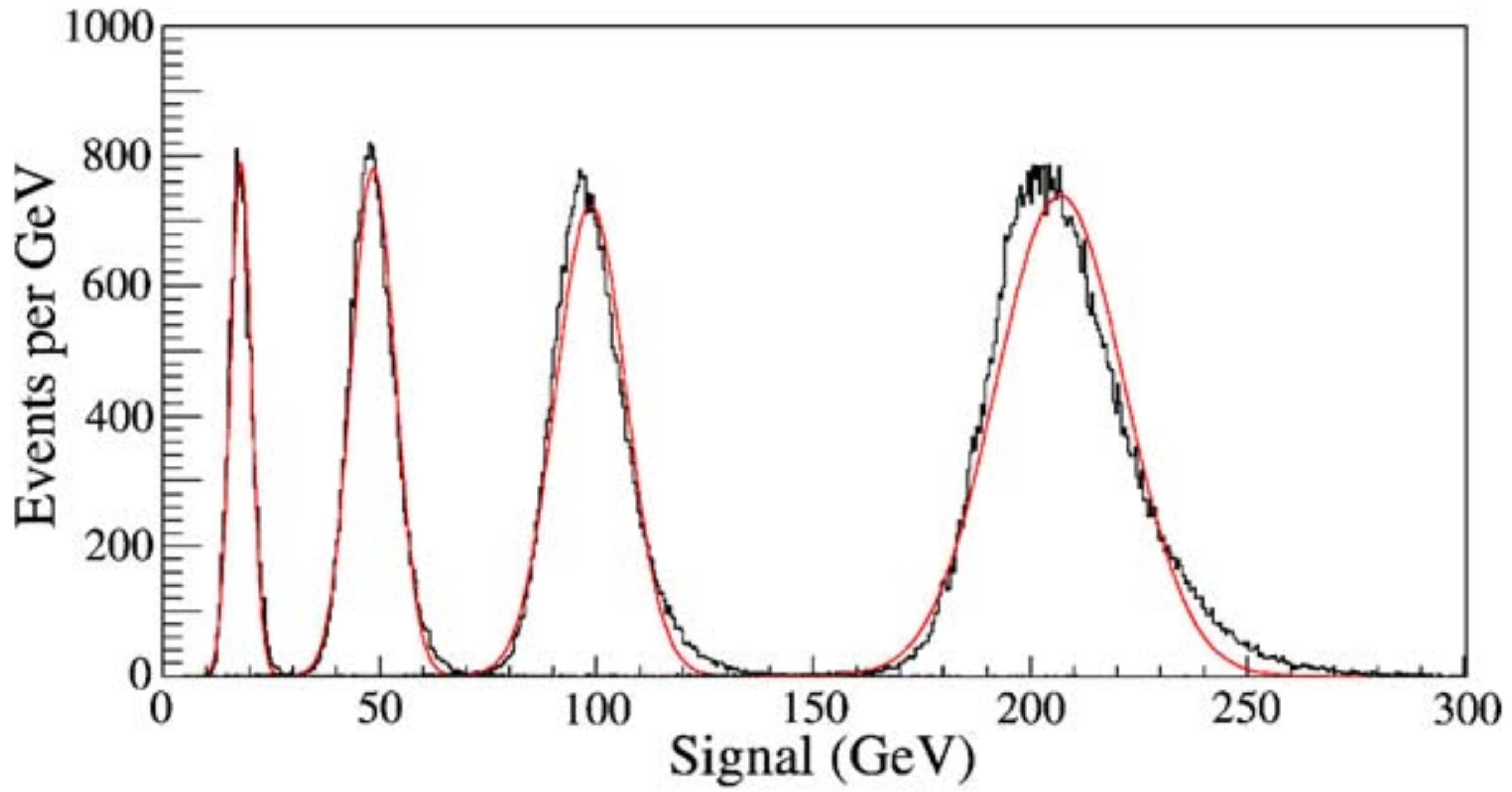


Fig. 33. $Q/S$-corrected scintillator signal distributions for single pions at 20, 50, 100 and 200 GeV. The curves represent Gaussian fits.

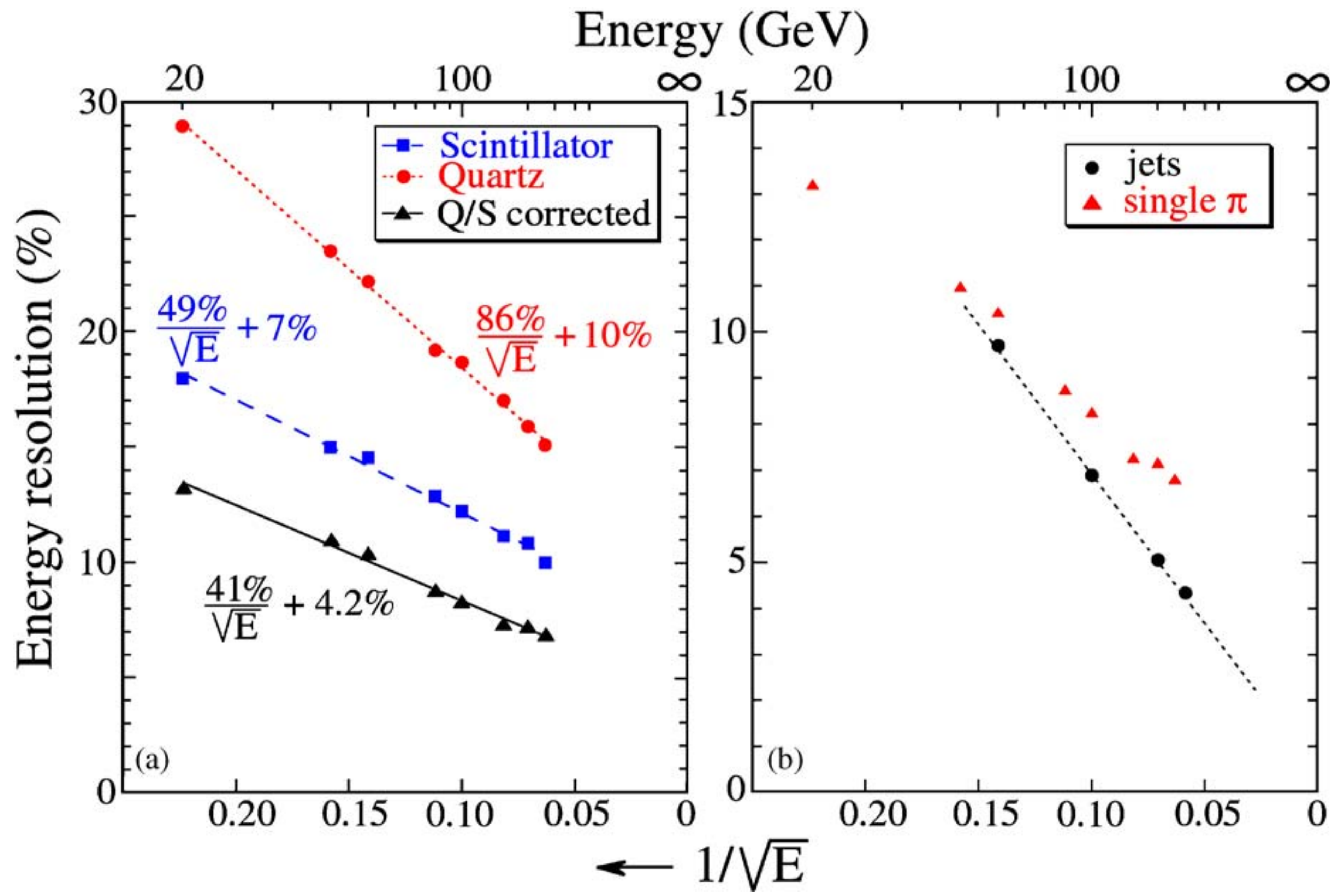


Fig. 32. The energy resolution for single pions as a function of energy, measured with the scintillation fibers and the Cherenkov fibers, and after corrections made on the basis of the measured $Q/S$ signal ratio (a). Comparison of the corrected resolutions for jets and single pions (b).

# What we learned with the prototype DREAM calorimeter

- Reduction of shower leakage (leakage fluctuations) → Build a larger detector
- Increase Cerenkov light yield
  - Prototype DREAM: 8 p.e./GeV → light yield fluctuations contribute by 35%/√E
- Reduction of sampling fluctuations
  - contribute ~40%/√E to hadronic resolution

# RD52 Cu- and Pb-fiber Calorimeters

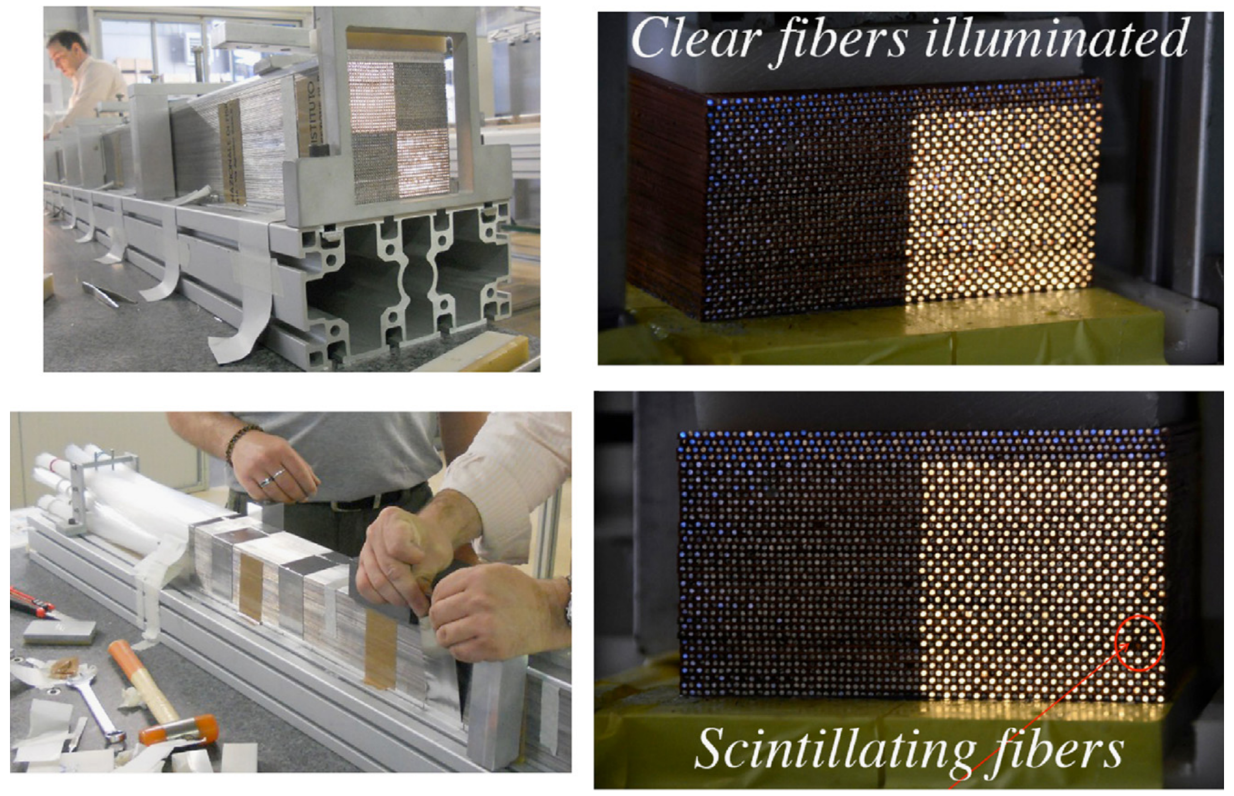


**Fig. 2.** Pictures of the first SuperDREAM modules built with lead (*left*) or copper (*right*) as absorber material. The alternating arrangement of clear and scintillating fibers in each row of the copper modules is illustrated by illuminating the fiber bunches from the rear end.

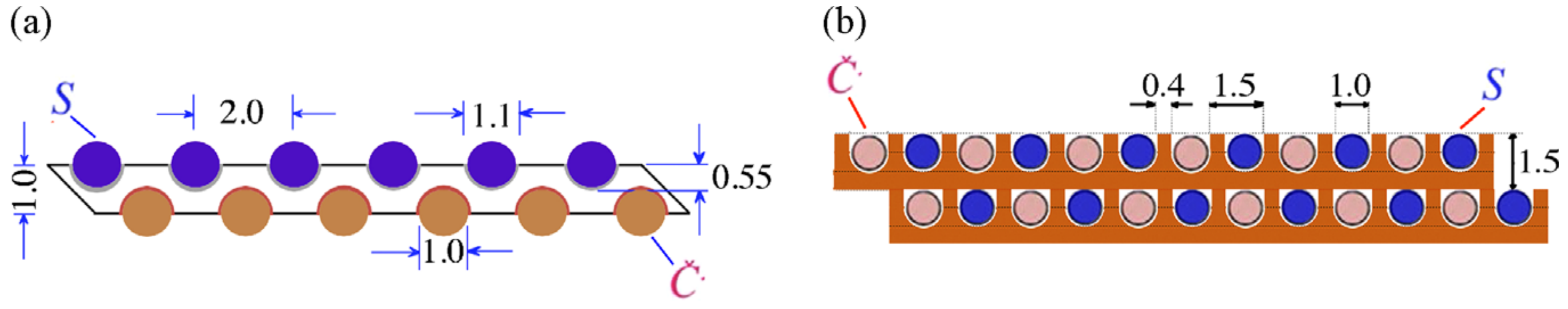


**Fig. 3.** Basic structure of the new lead (a) and copper (b) based RD52 fiber calorimeters.

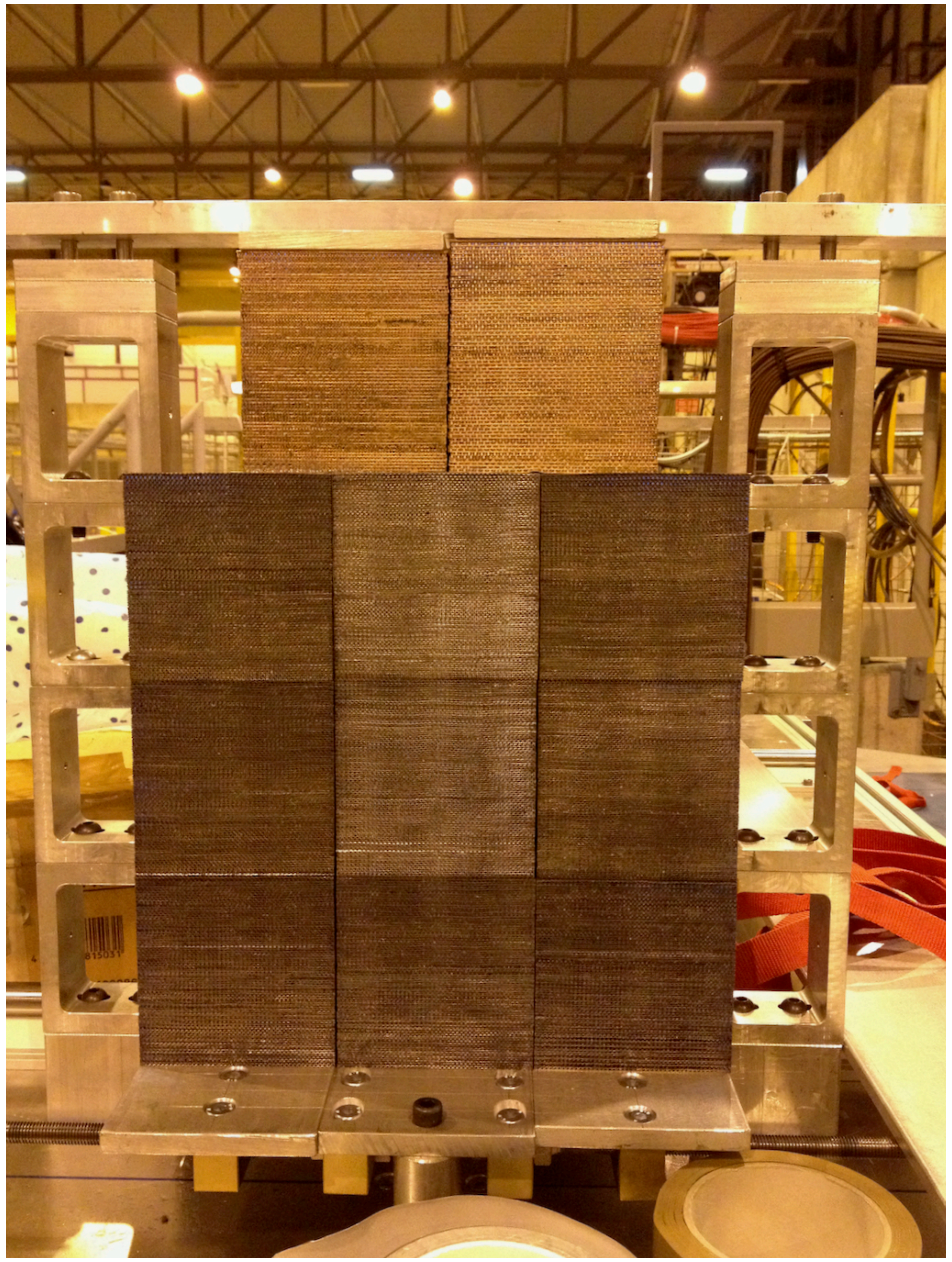

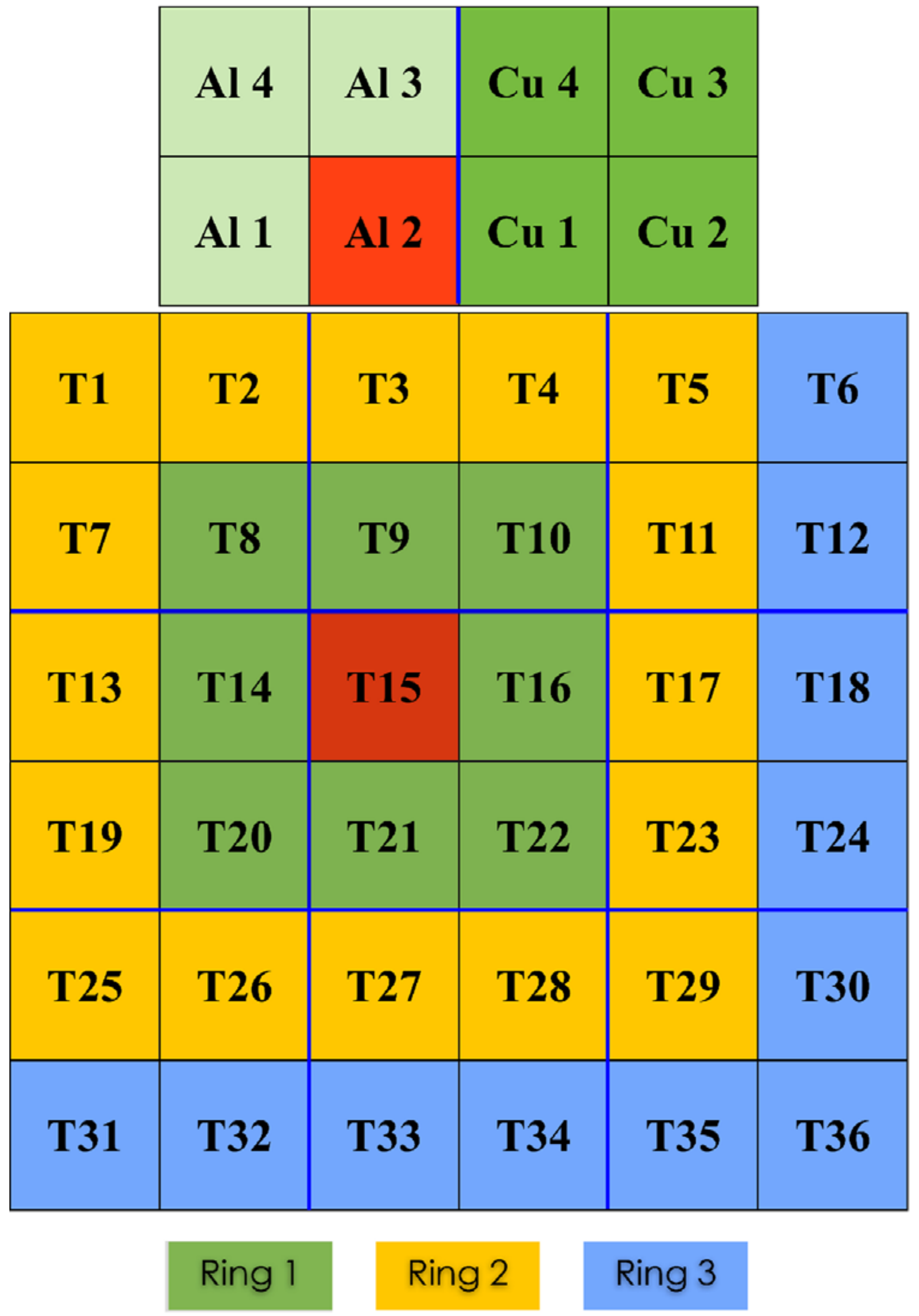


**Fig. 4.** The RD52 SuperDREAM calorimeter as tested at the end of 2012. It consisted of 9 lead-based modules, each consisting of 4 towers (towers 1–36), and two copper-based modules, placed on top of the lead array. The left copper module (of which the towers are marked as "Al") is equipped with Cherenkov fibers with an aluminized upstream end face. For readout purposes, the lead calorimeter consists of a central tower (T15), surrounded by 3 square rings of towers.

# The electromagnetic performance of the RD52 fiber calorimeter

# NIM A 735 (2014) 130

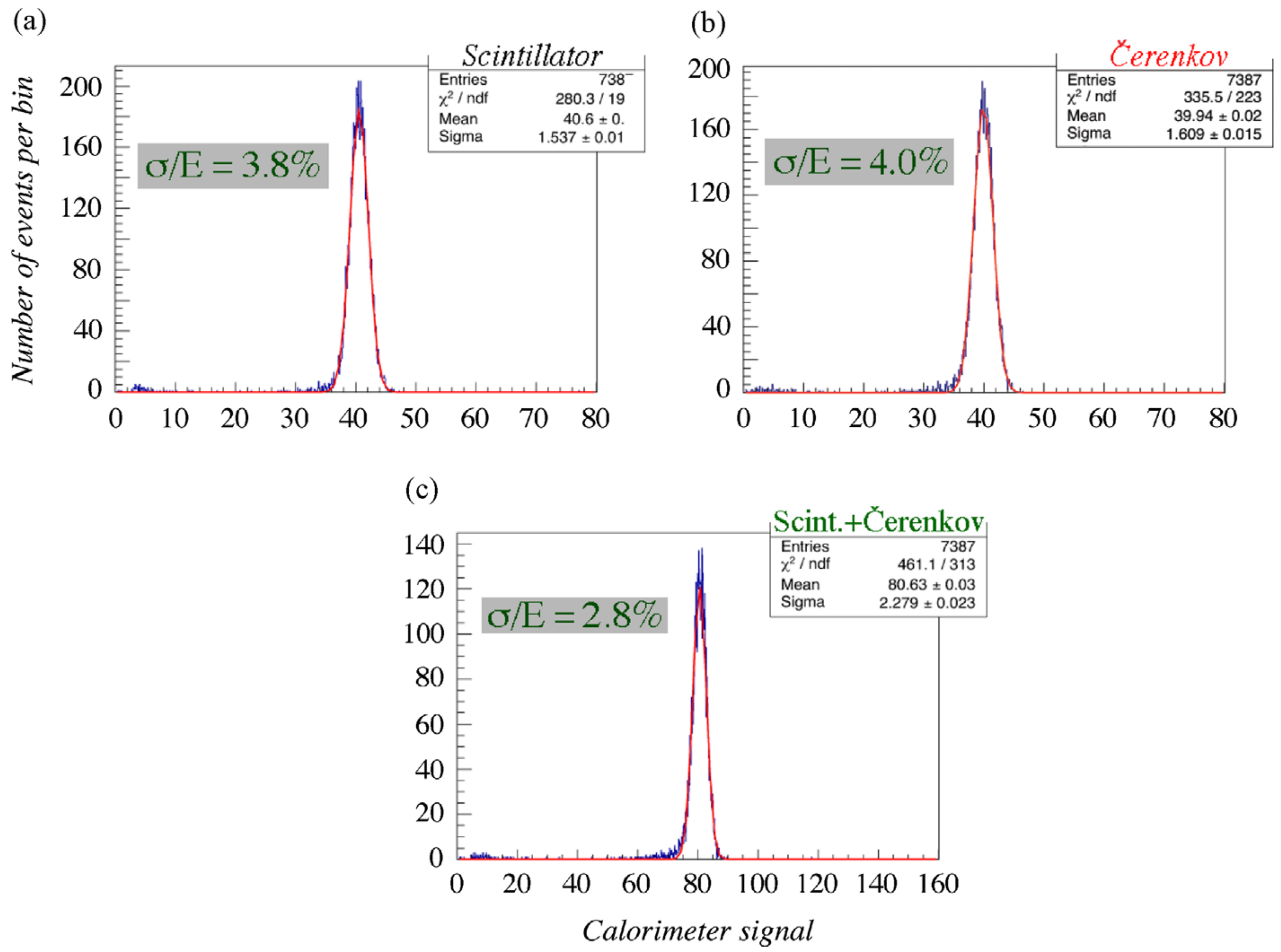


**Fig. 8.** Signal distributions for 40 GeV electrons in the copper-fiber calorimeter. Shown are the distributions measured with the scintillating fibers (a), the Cherenkov fibres (b) and the sum of all fibers (c). The angle of incidence of the beam particles ($\theta$, $\phi$) was (1.5°, 1.0°). The size of the beam spot was 10 × 10 $mm^2$.

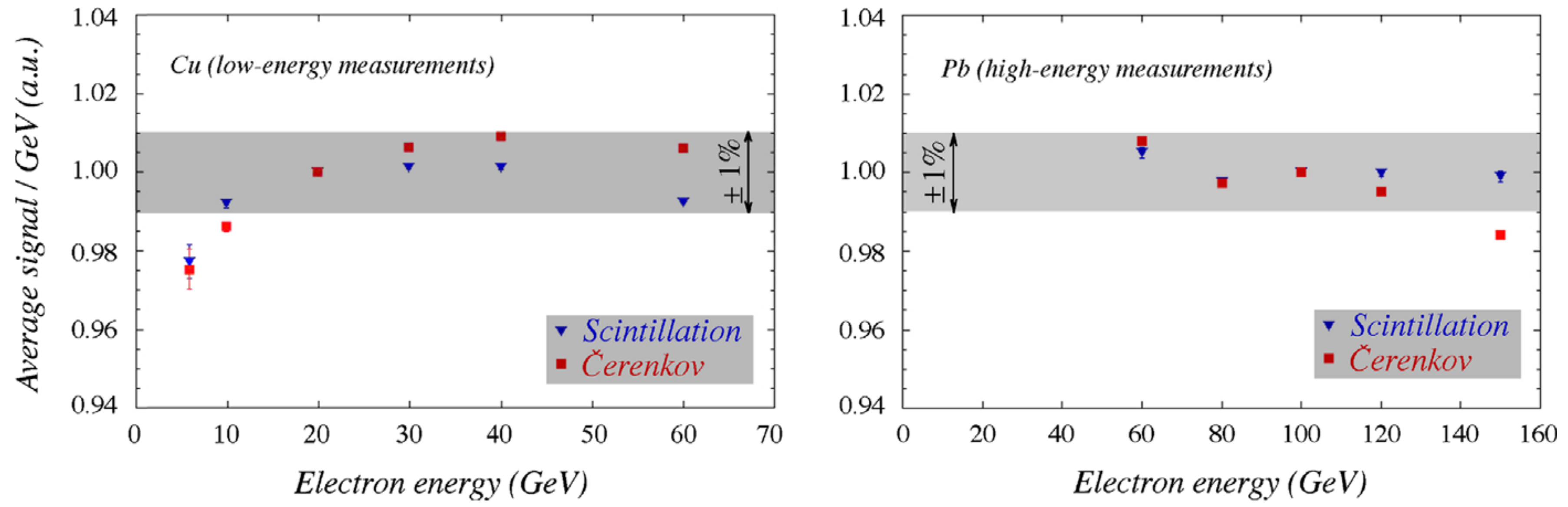


**Fig. 9.** The linearity of the copper (a) and lead (b) based fiber calorimeters for em shower detection in the scintillation and Cherenkov channels. See text for details.

# The electromagnetic performance of the RD52 fiber calorimeter

## NIM A 735 (2014) 130

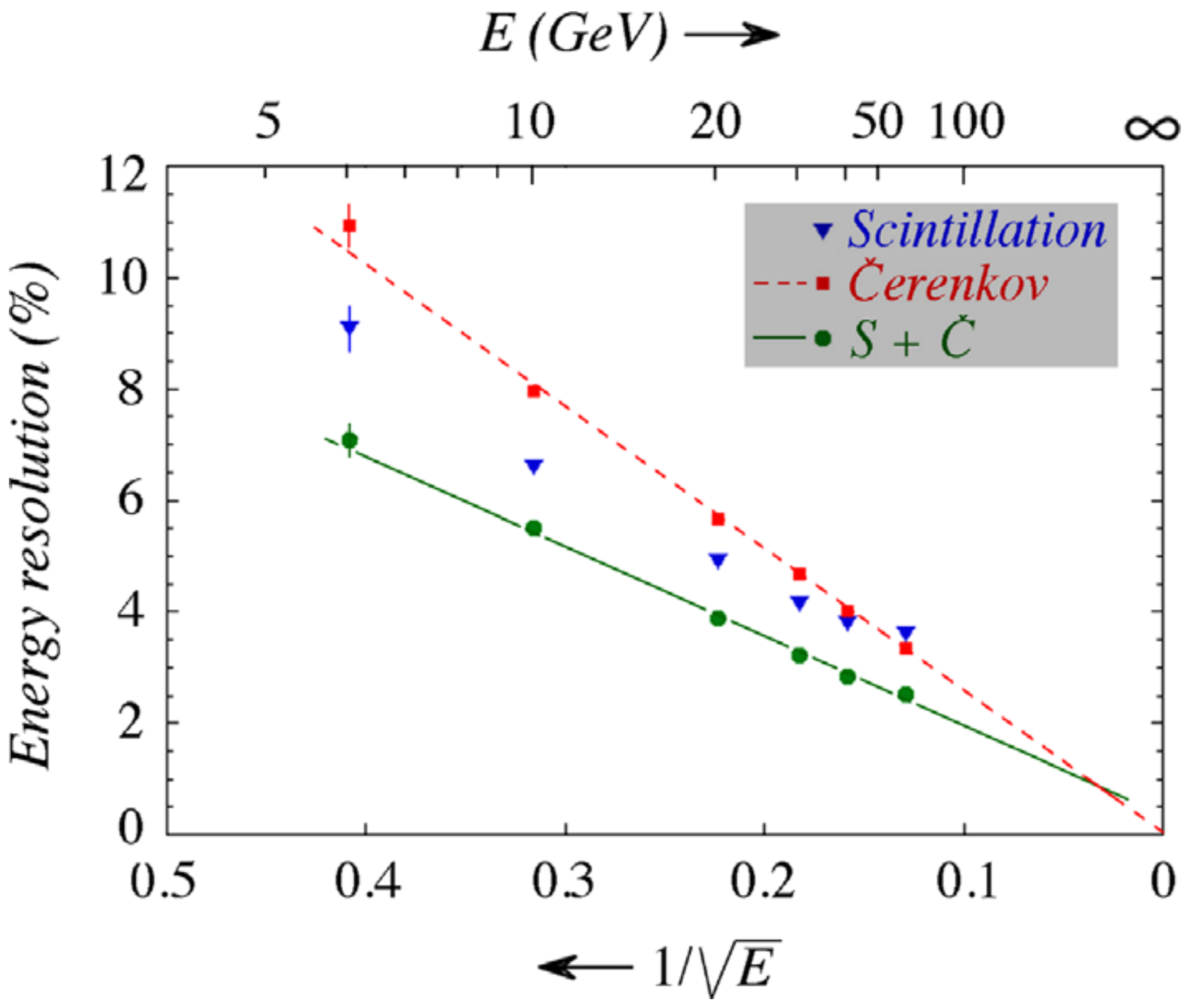


**Fig. 13.** The energy resolution for electrons in the copper-fiber module, as a function of the beam energy. Shown are the results for the two types of fibers, and for the combined signals. The angle of incidence of the beam particles ($\theta$, $\phi$) was (1.5°, 1.0°). The size of the beam spot was $10 \times 10$ mm$^2$.

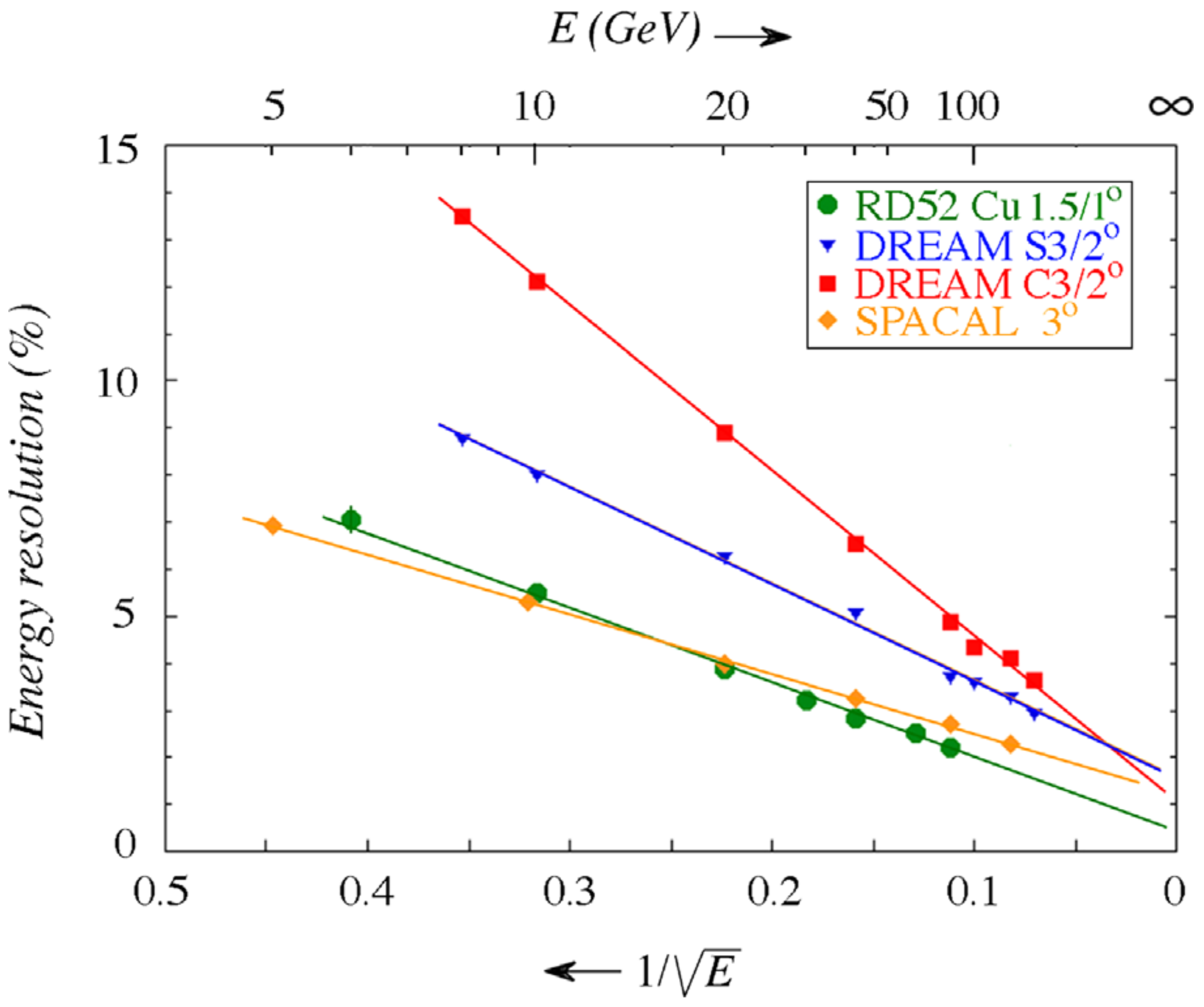


**Fig. 22.** Comparison of the em energy resolution measured with the RD52 copper-fiber calorimeter, the original DREAM copper-fiber calorimeter [3], and the SPACAL lead-fiber calorimeter [4].

# Lessons from Monte Carlo simulations of the performance of a dual-readout fiber calorimeter

## NIM A 762 (2014) 100

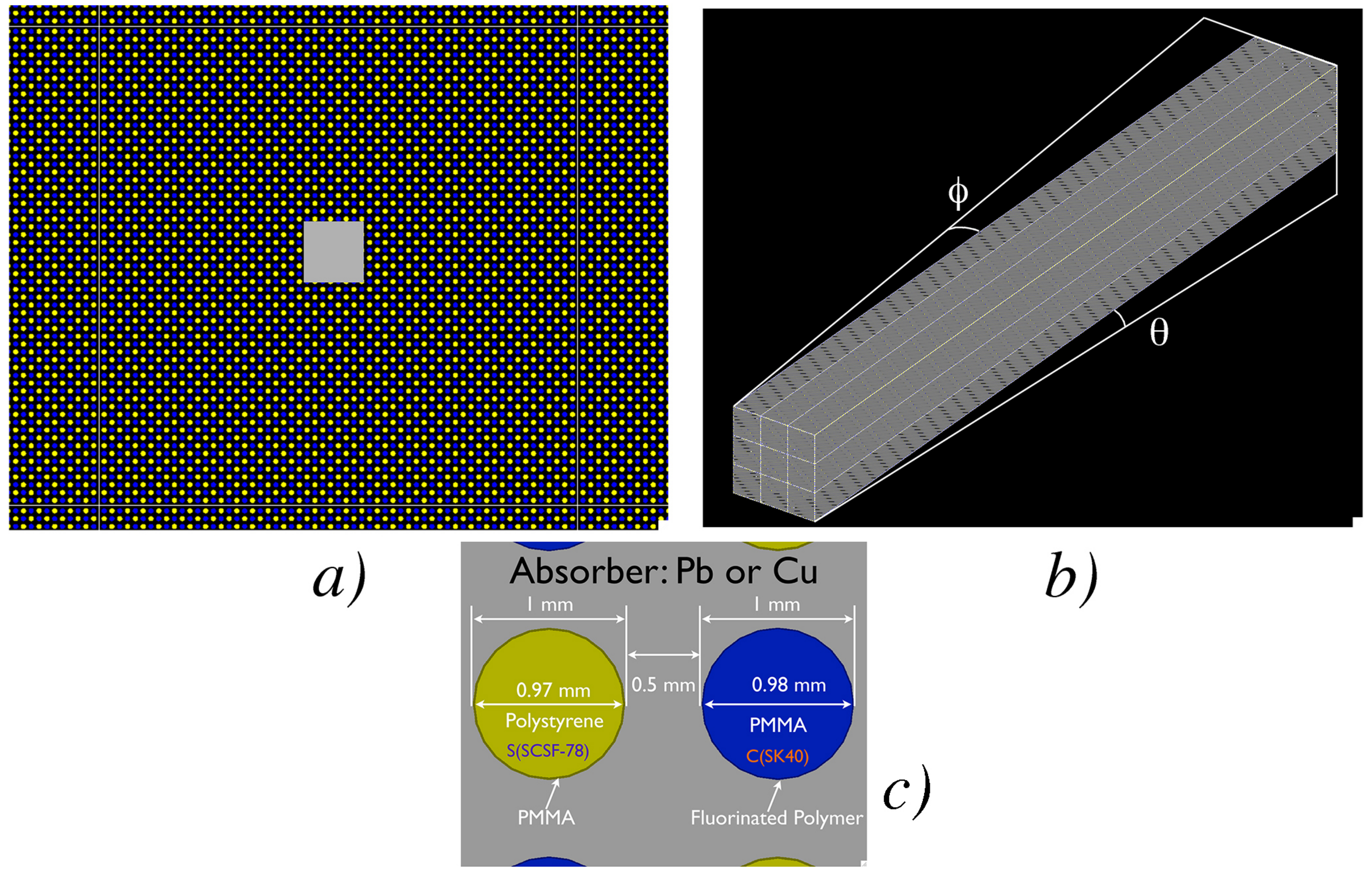


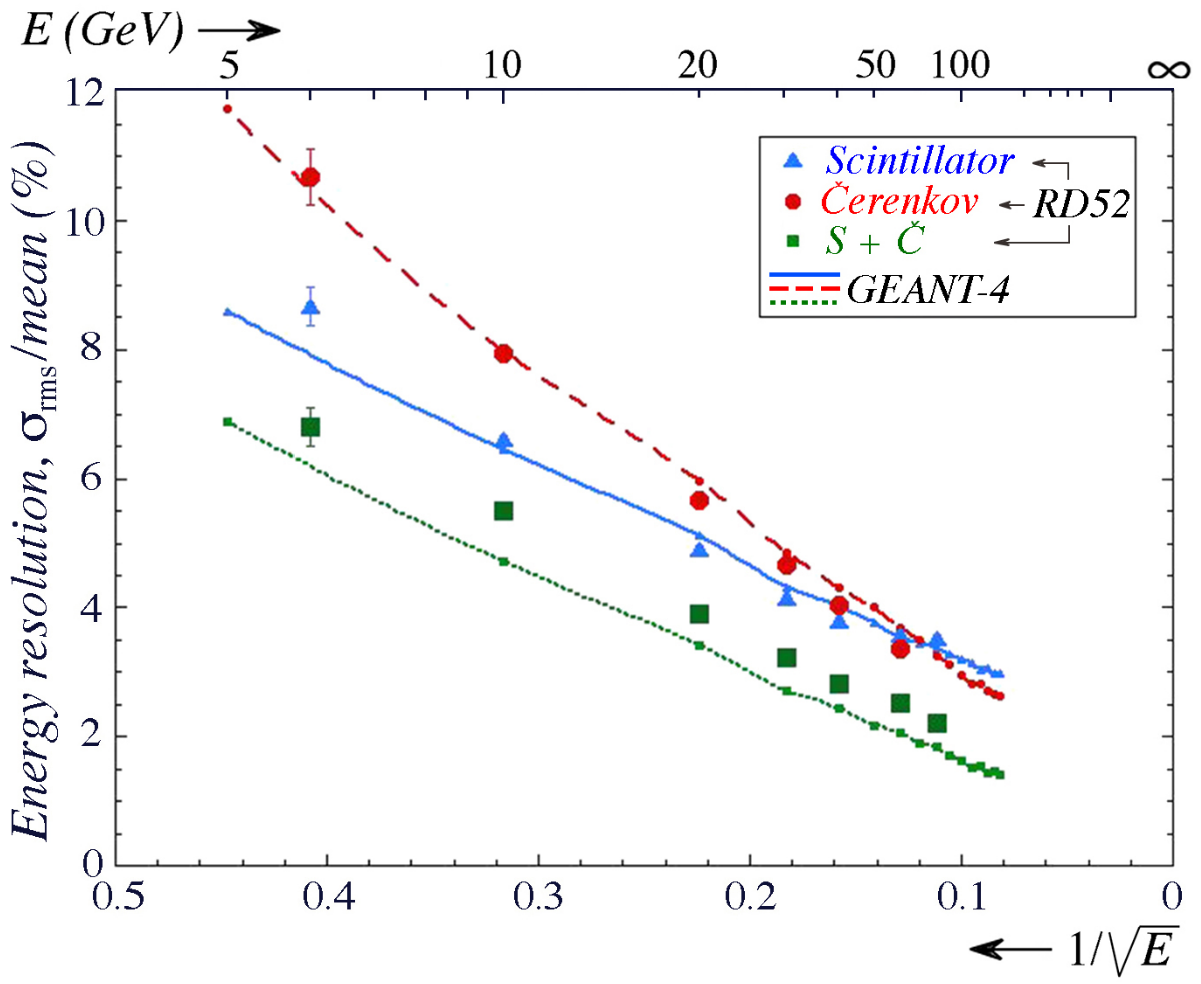


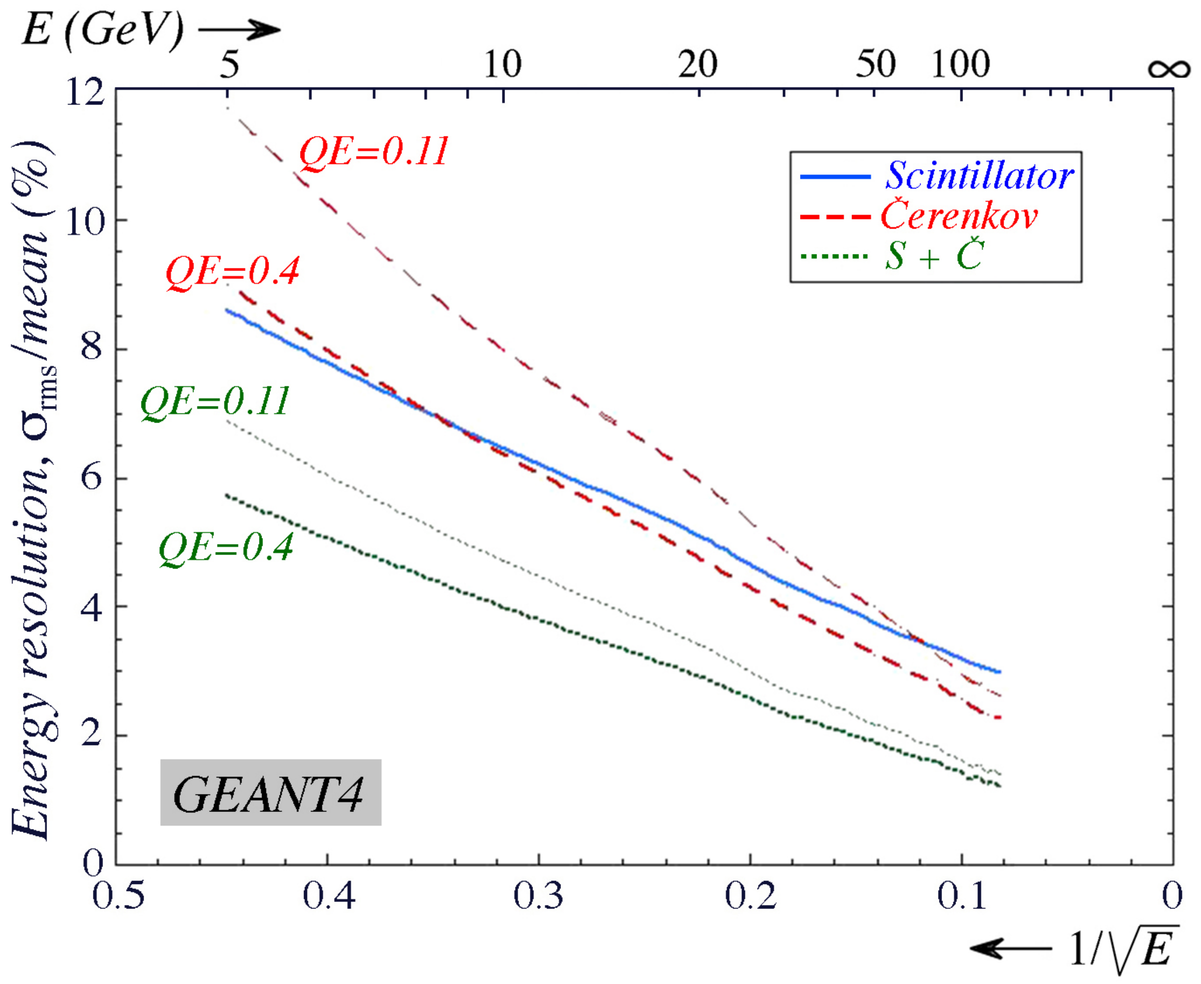


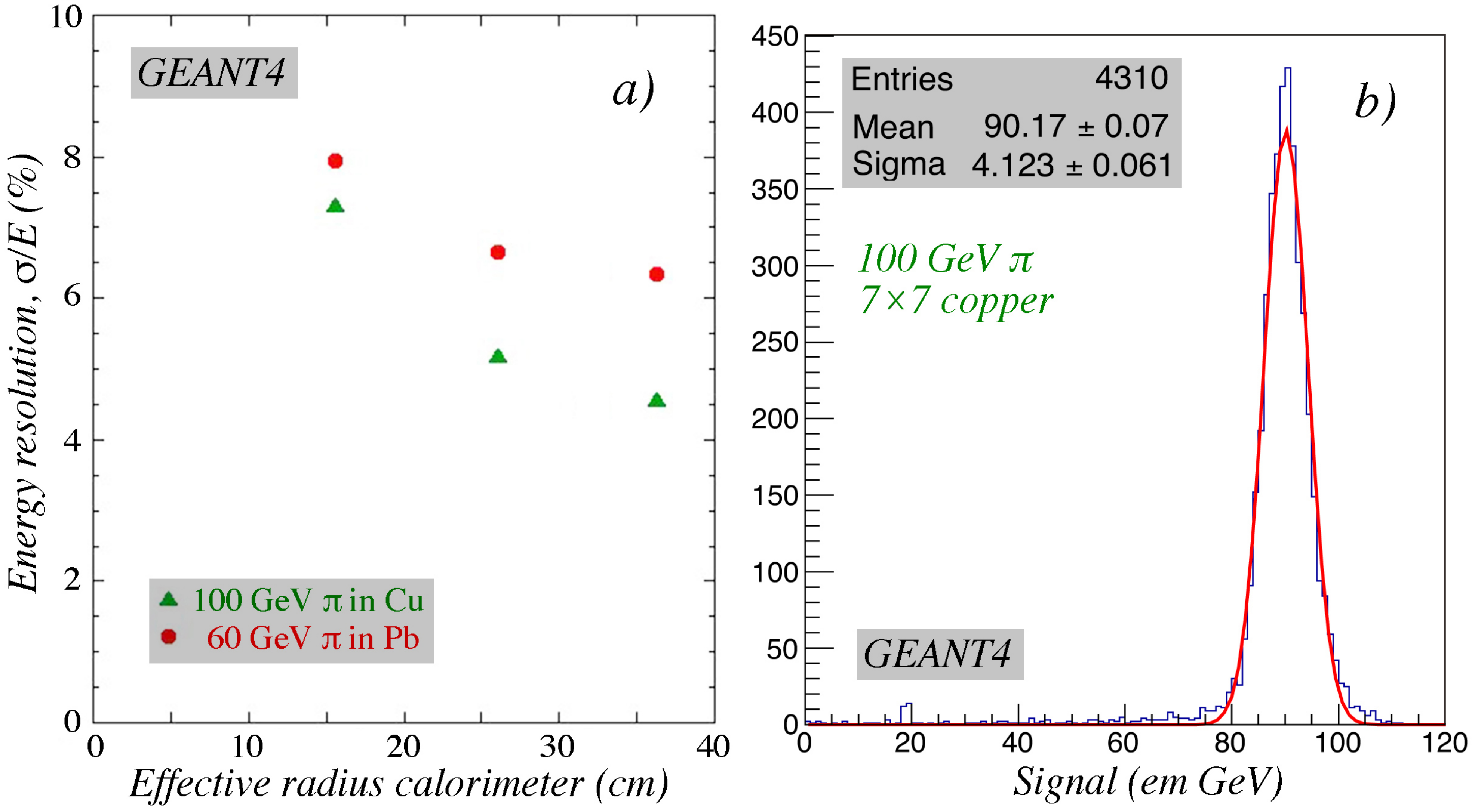

# Hadron detection with a dual-readout fiber calorimeter

## NIM A 866 (2017) 76

$$E = \frac{S - \chi C}{1 - \chi}, \quad \text{with} \quad \chi = \frac{\left[1 - (h/e)_S\right]}{\left[1 - (h/e)_C\right]} \approx 0.3.$$

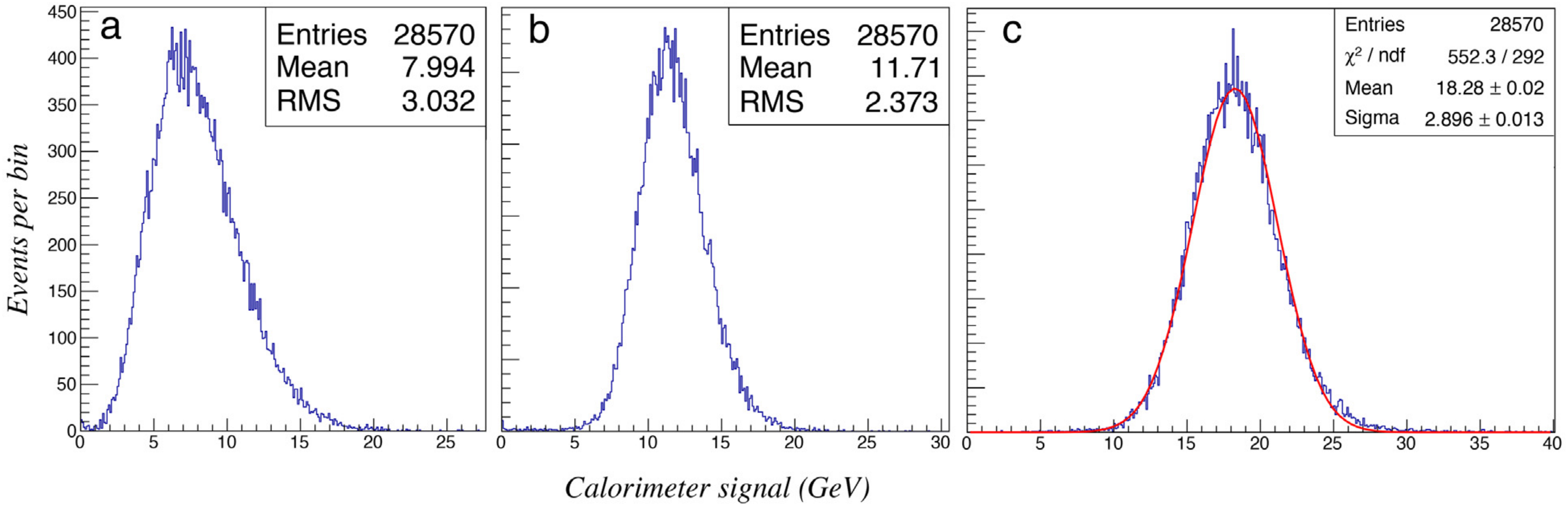


**Fig. 11.** Signal distributions for 20 GeV $\pi^-$ particles. Shown are the measured Čerenkov (a) and scintillation (b) signal distributions as well as the signal distribution obtained by combining the two signals according to Eq. (2), using $\chi = 0.45$ (c).

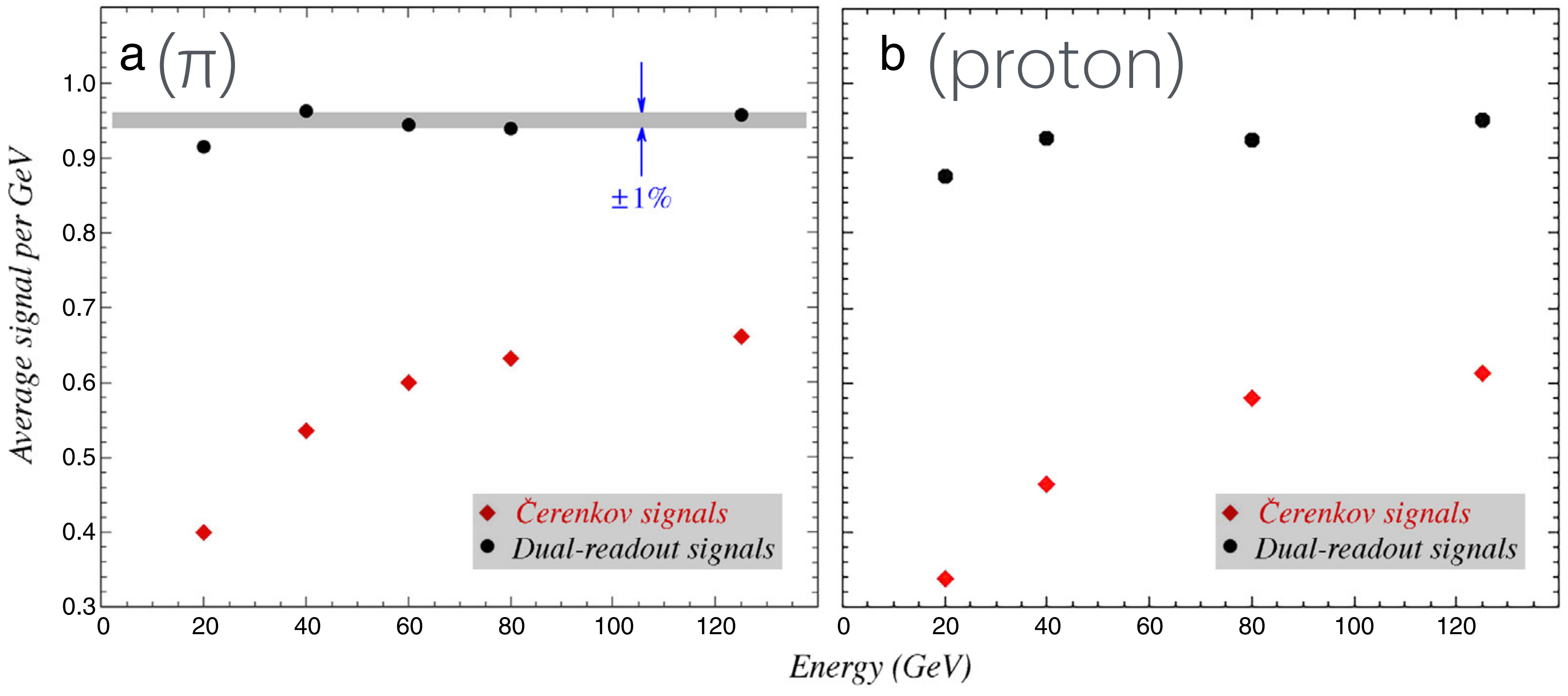


**Fig. 12.** The hadronic response of the RD52 lead–fiber dual-readout calorimeter, for single pions (a) and protons (b). Shown are the average Čerenkov signal and the dual-readout signal (Eq. (2)) per unit deposited energy, as a function of the energy.

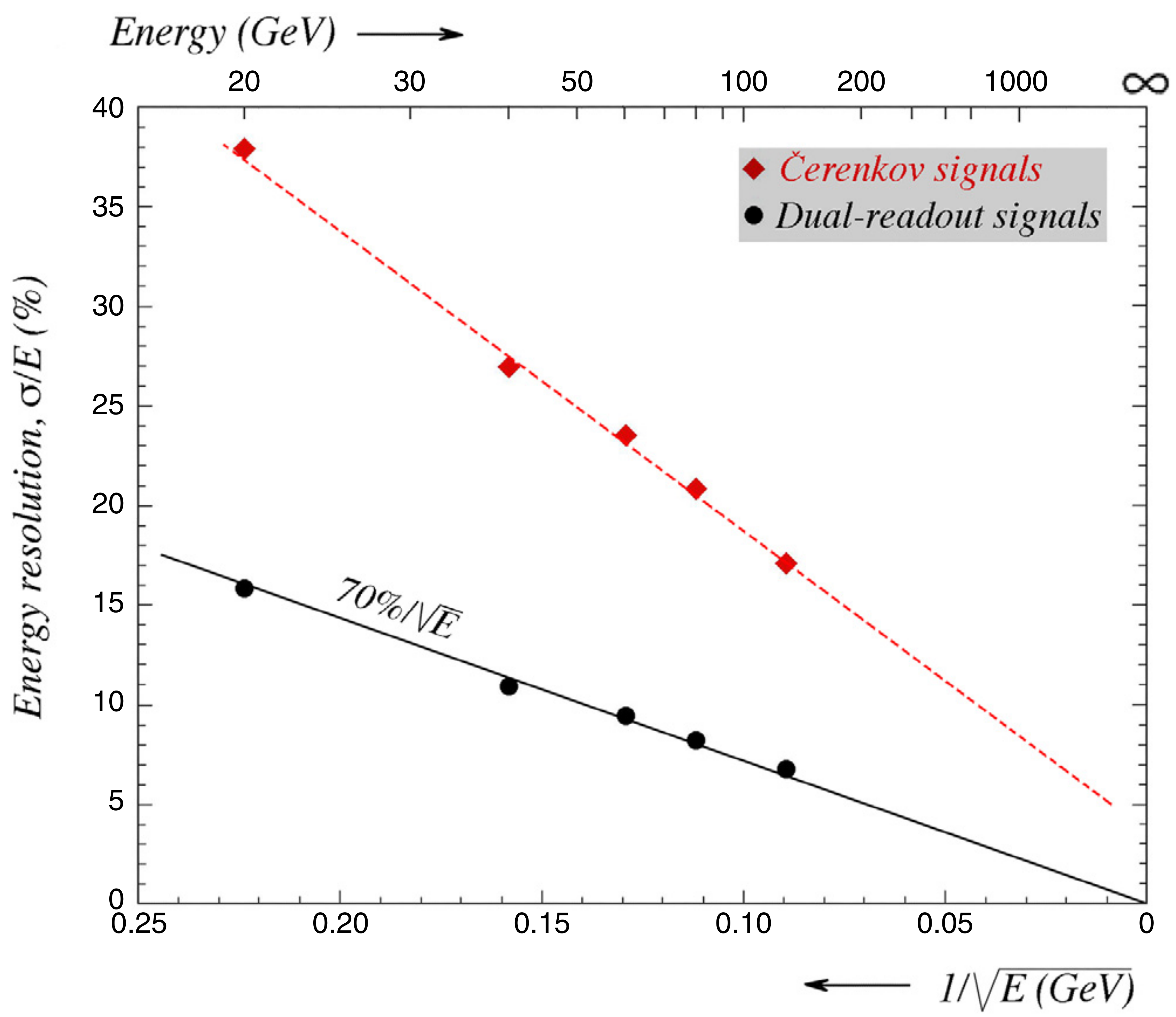


**Fig. 13.** The hadronic energy resolution of the RD52 lead–fiber dual-readout calorimeter, for single pions. Shown are the results for the Čerenkov signals alone, and for the dual-readout signals, obtained with Eq. (2).

# Hadron detection with a dual-readout fiber calorimeter

## NIM A 866 (2017) 76

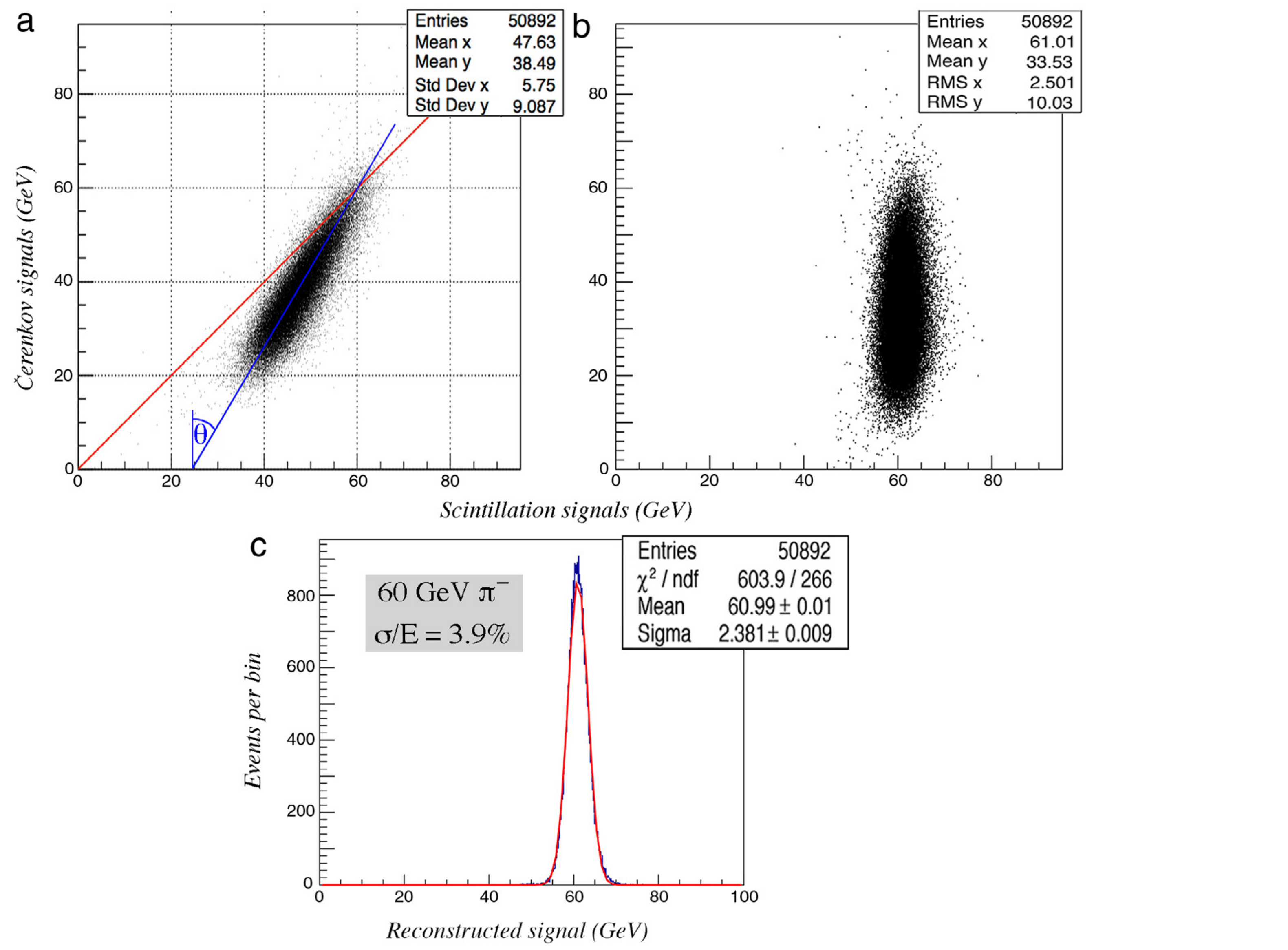


**Fig. 14.** Signal distributions of the RD52 Dual-Readout lead/fiber calorimeter for 60 GeV pions. Scatter plot of the two types of signals as recorded for these particles (a) and rotated over an angle $\theta = 30°$ around the point where the two lines from diagram a intersect (b). Projection of the latter scatter plot on the $x$-axis (c).

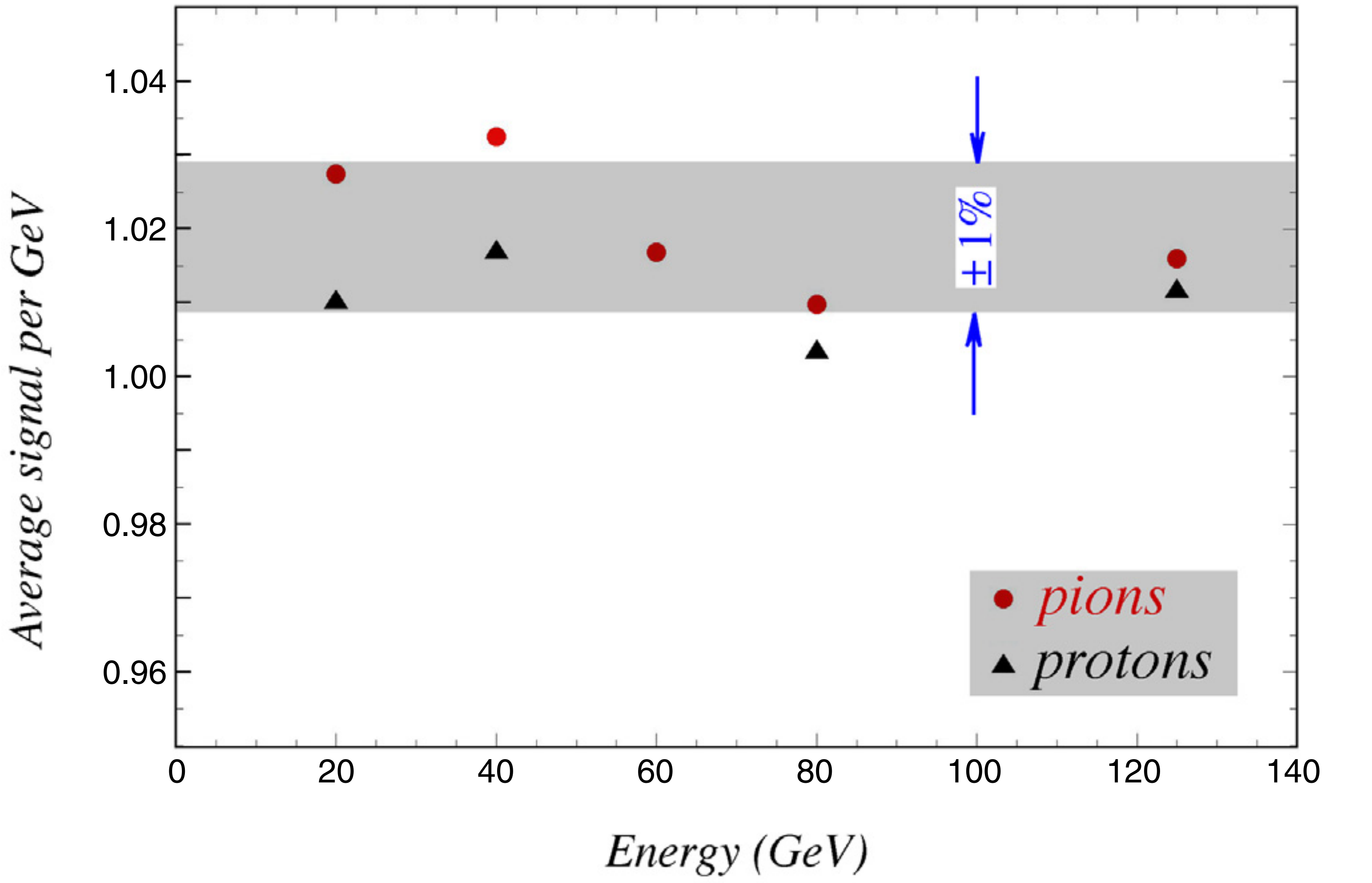


**Fig. 16.** The calorimeter response, *i.e.,* the average signal for protons and pions per GeV, as a function of energy. The vertical scale is normalized to the electron response.

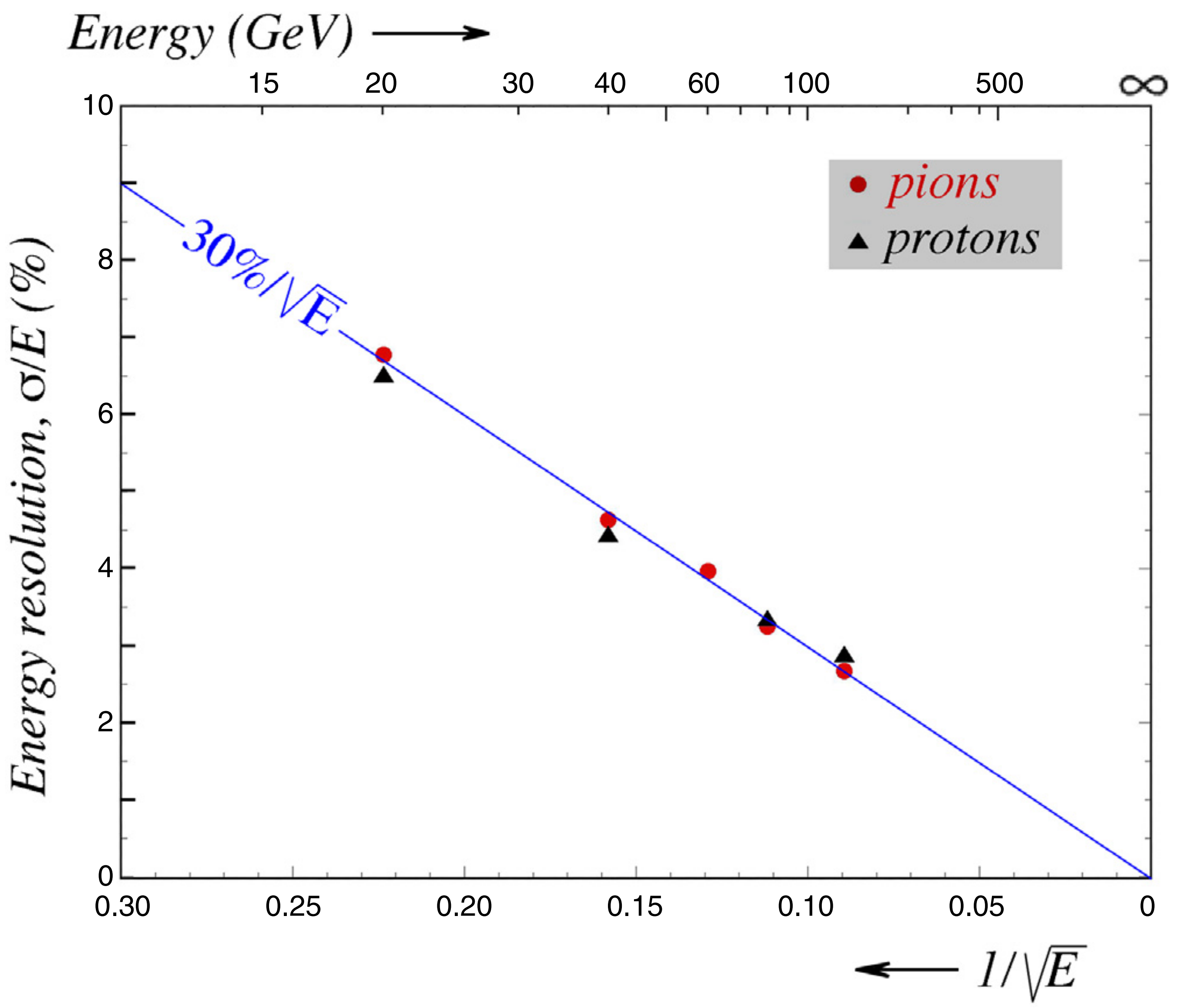


**Fig. 18.** The fractional width of the signal distribution, $\sigma/E$, as a function of energy, for pions and protons in the 20–125 GeV energy range. The line represents $\sigma/E = 30\%/\sqrt{E}$.

# On the limits of the hadronic energy resolution of calorimeters

## NIM A 882 (2018) 148

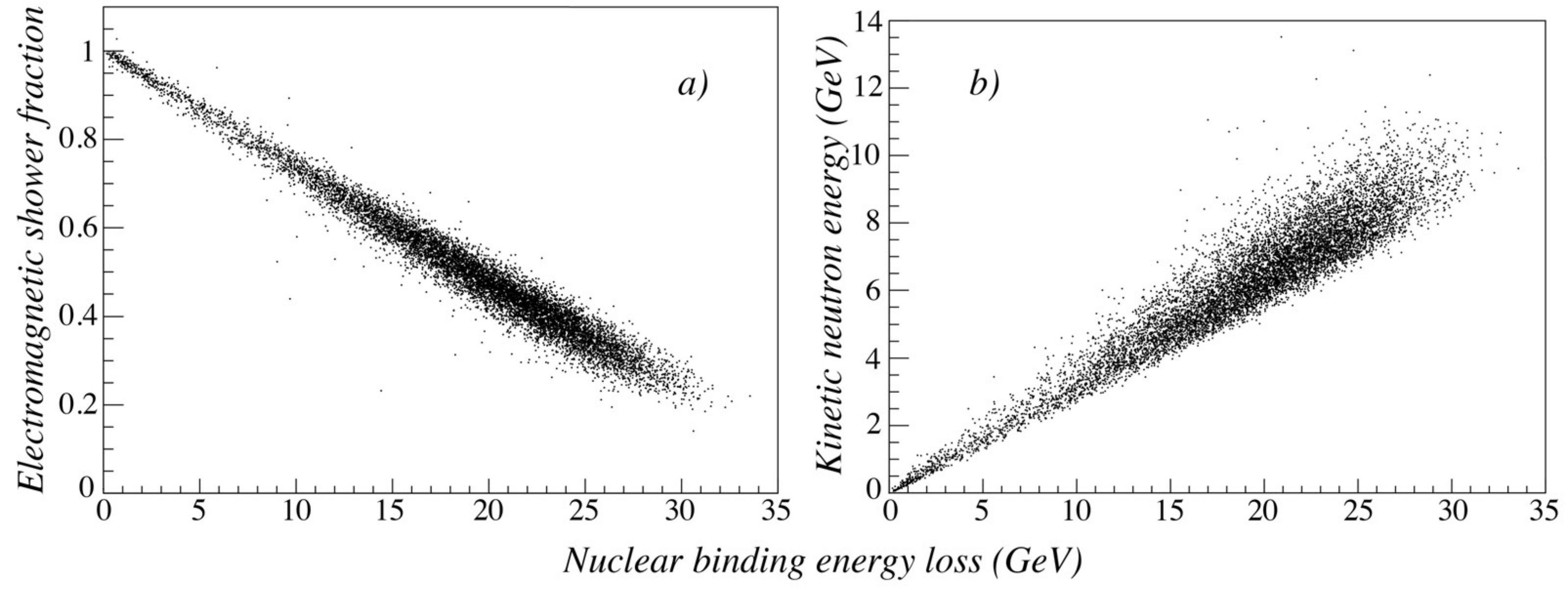


**Figure 6.** The correlations between the binding energy loss and the em shower fraction (a), and the neutron kinetic energy (b) obtained from GEANT 4 simulation in the case that 100 GeV pions produce hadron showers in the lead absorber.

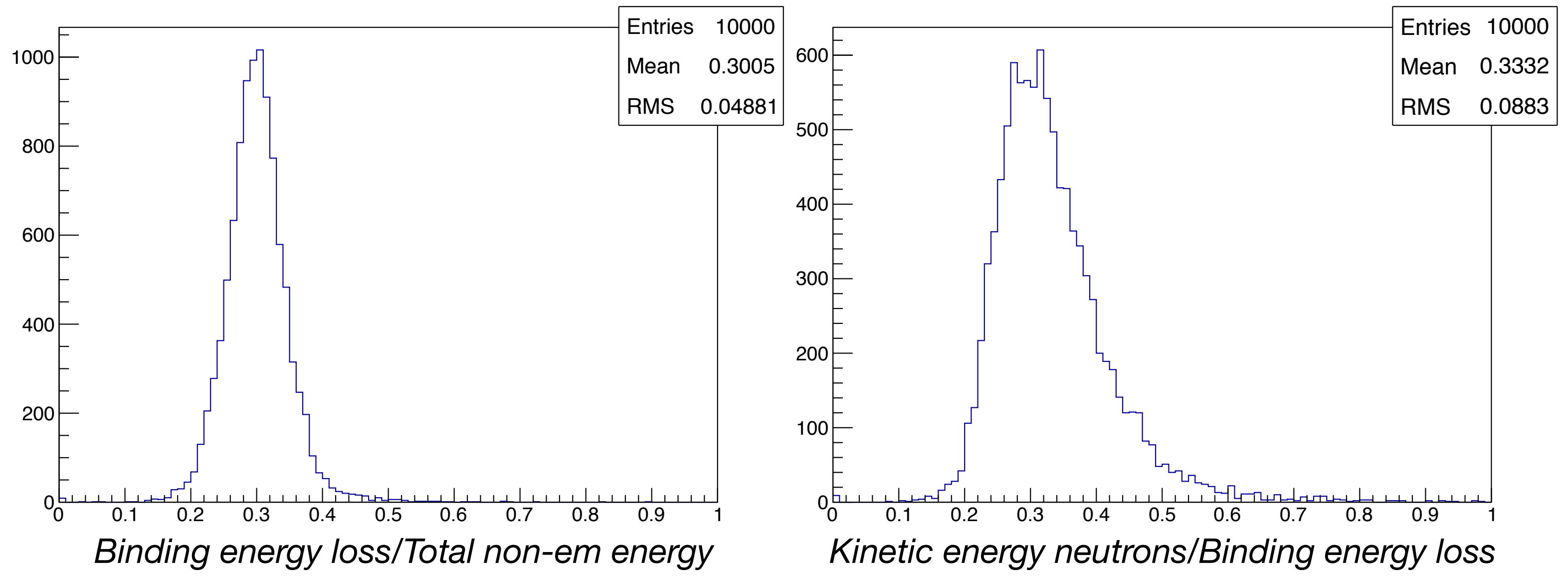


**Figure 7.** Correlations between the binding energy loss and the total non-em energy (left), and the neutron kinetic energy (right) for hadron showers produced with 20 GeV pions.

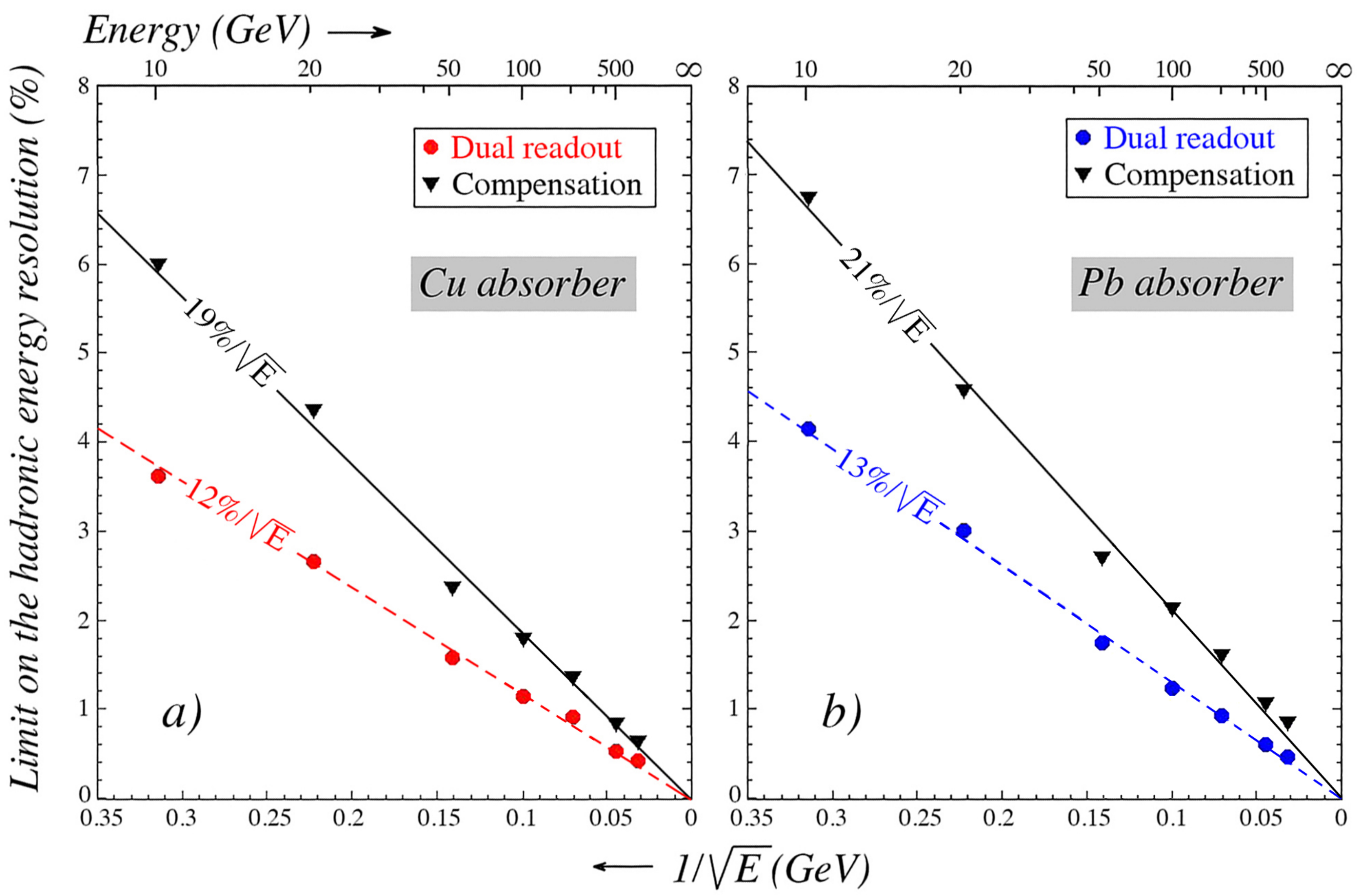


**Figure 9.** The limits of the hadronic energy resolutions for dual-readout and compensation obtained by the simulations with pion showers developing in Cu (a) and Pb (b) absorbers.

# Study for Future Lepton Collider Experiments

# Simulation study for Dual-Readout Calorimeter

- **Jet energy resolution and energy separation between bosons**
  - **Jet energy resolution** estimated by GEANT4
    - With **DR correction**, stochastic term is **~34.6%**
    - **For 100 GeV jet, resolution is ~3.7%, satisfying the requirement**
  - **Detector response with energy that corresponds to bosons energy**
    - shows **great energy separation**
    - **which is the most important part for Higgs factory experiment**

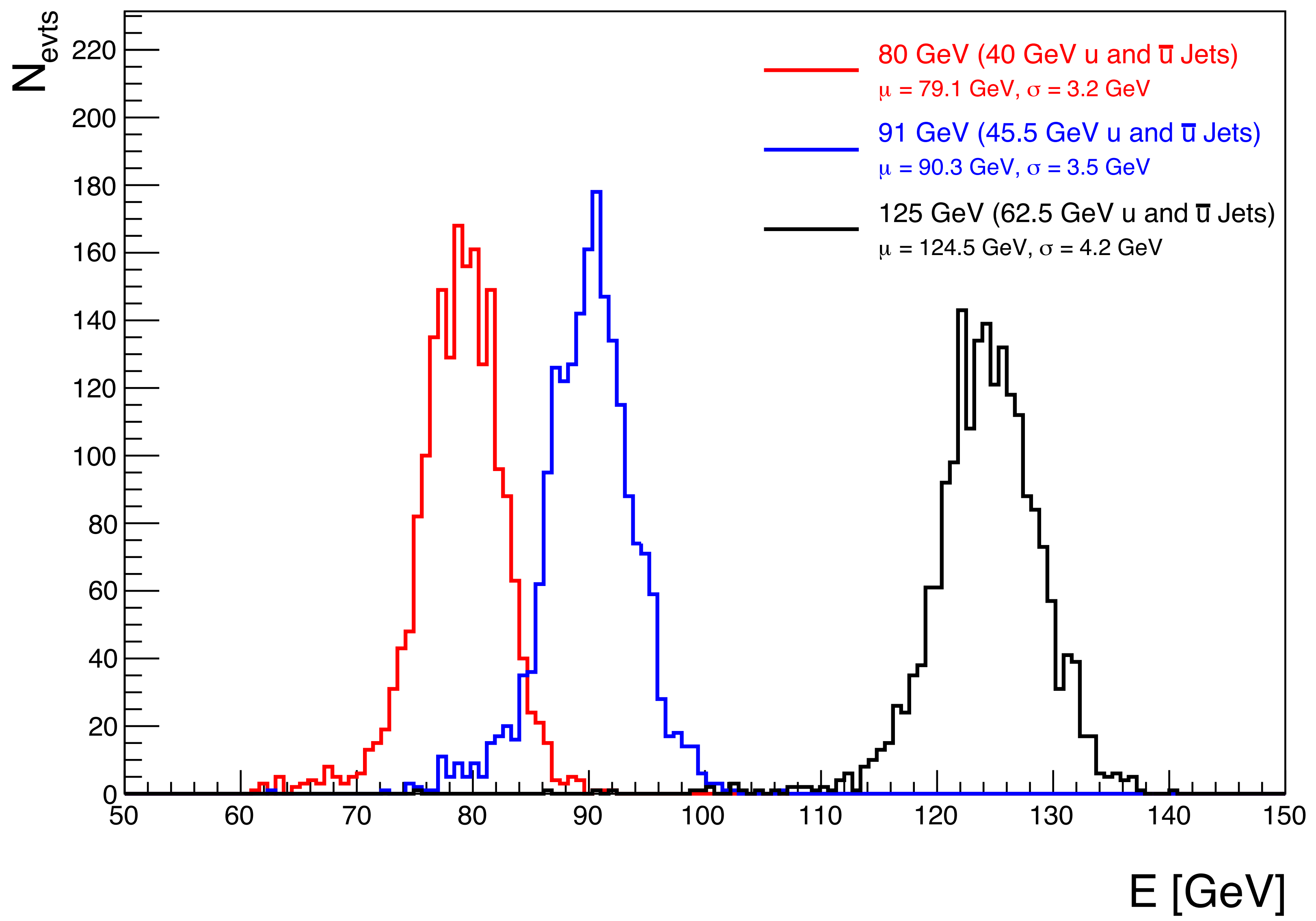


Kyuyeong Hwang, May 23

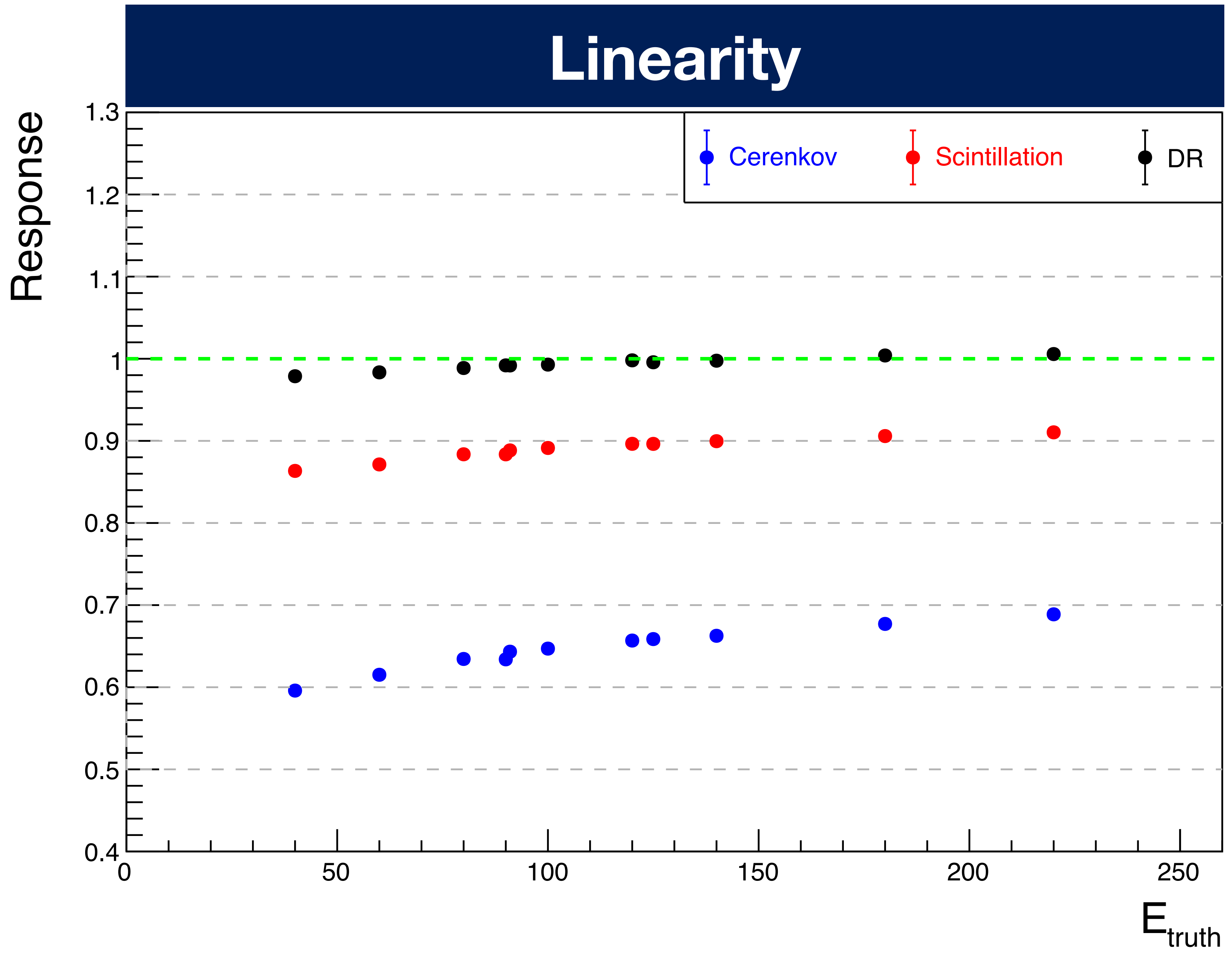


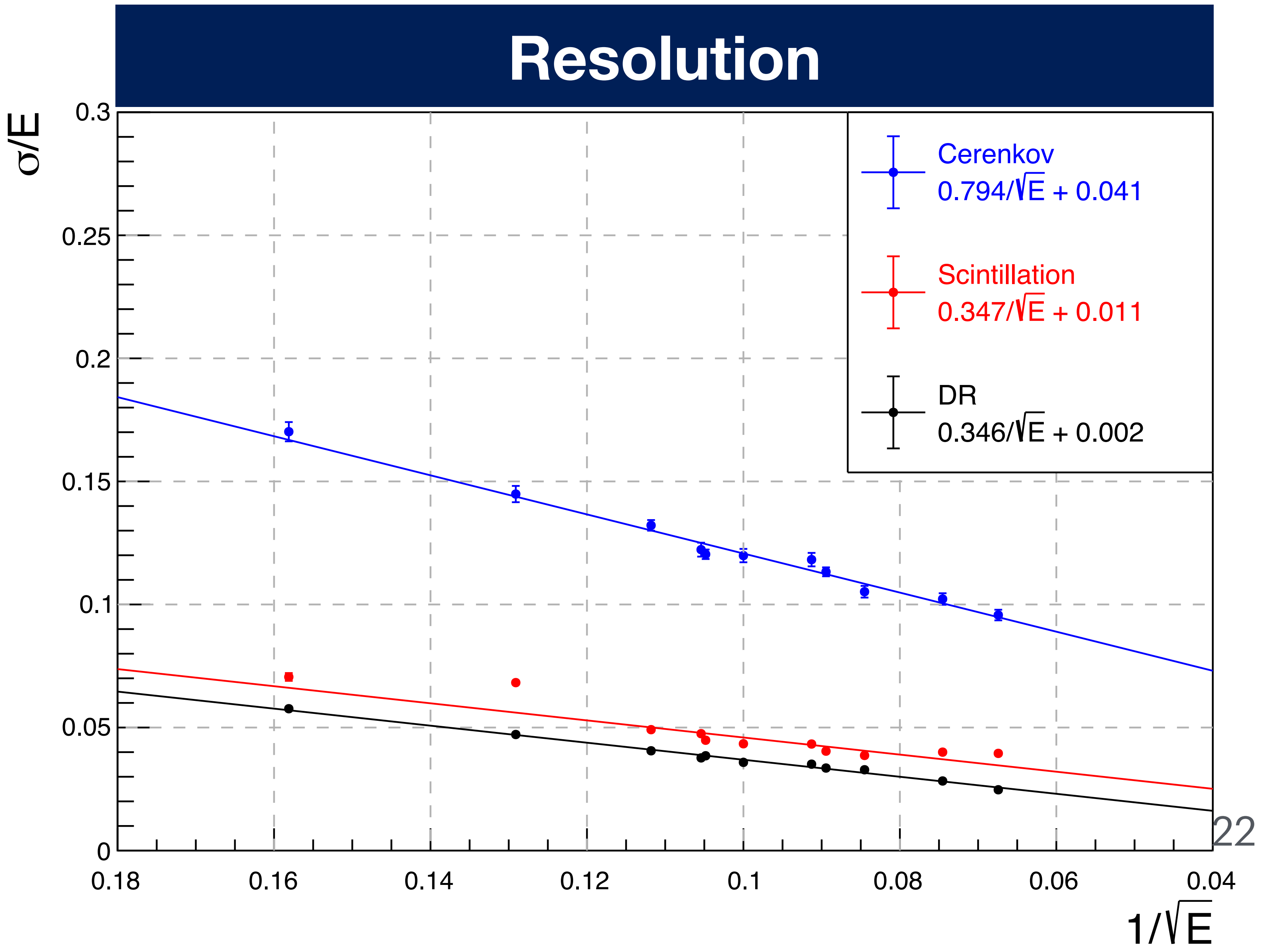

# Particle reconstruction for dual-readout calorimeter using deep learning

Shower data(position, timing, energy) as Point cloud format trained for classification and reconstruction of variables using deep learning model.

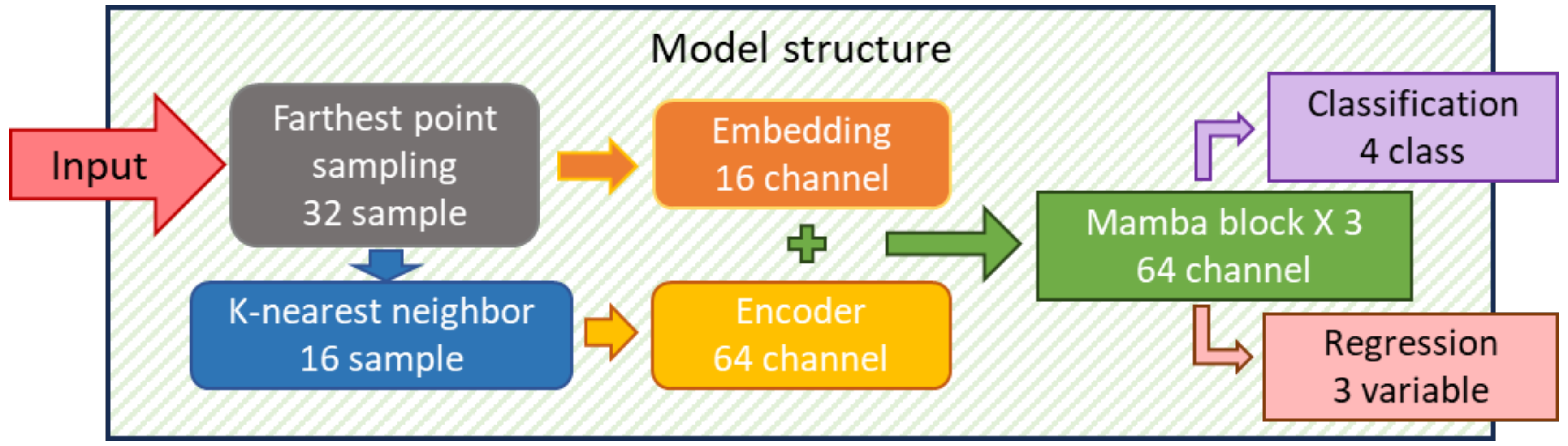


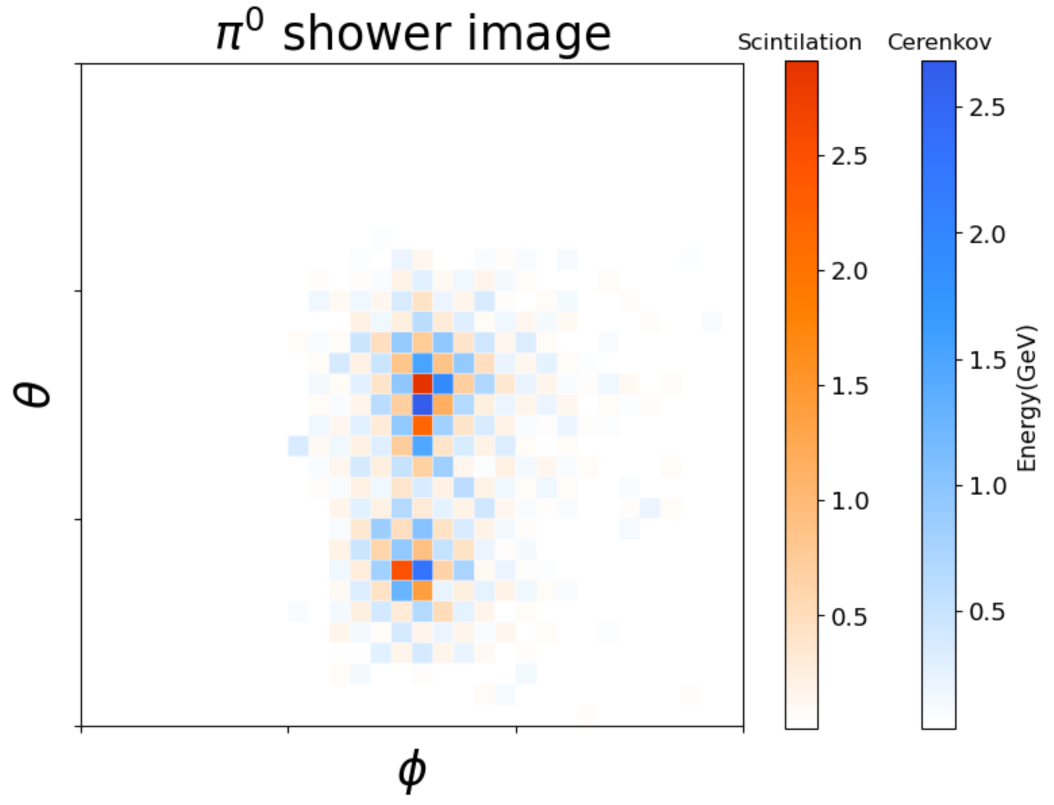


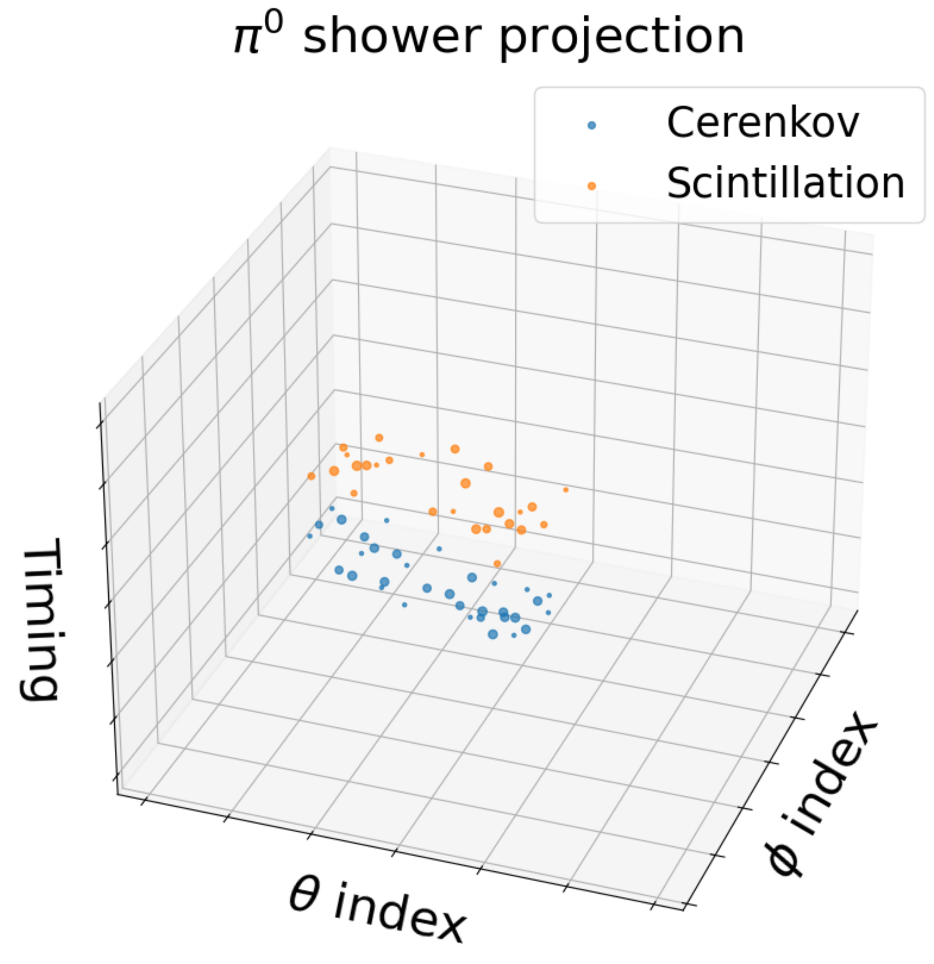


ROC curves of

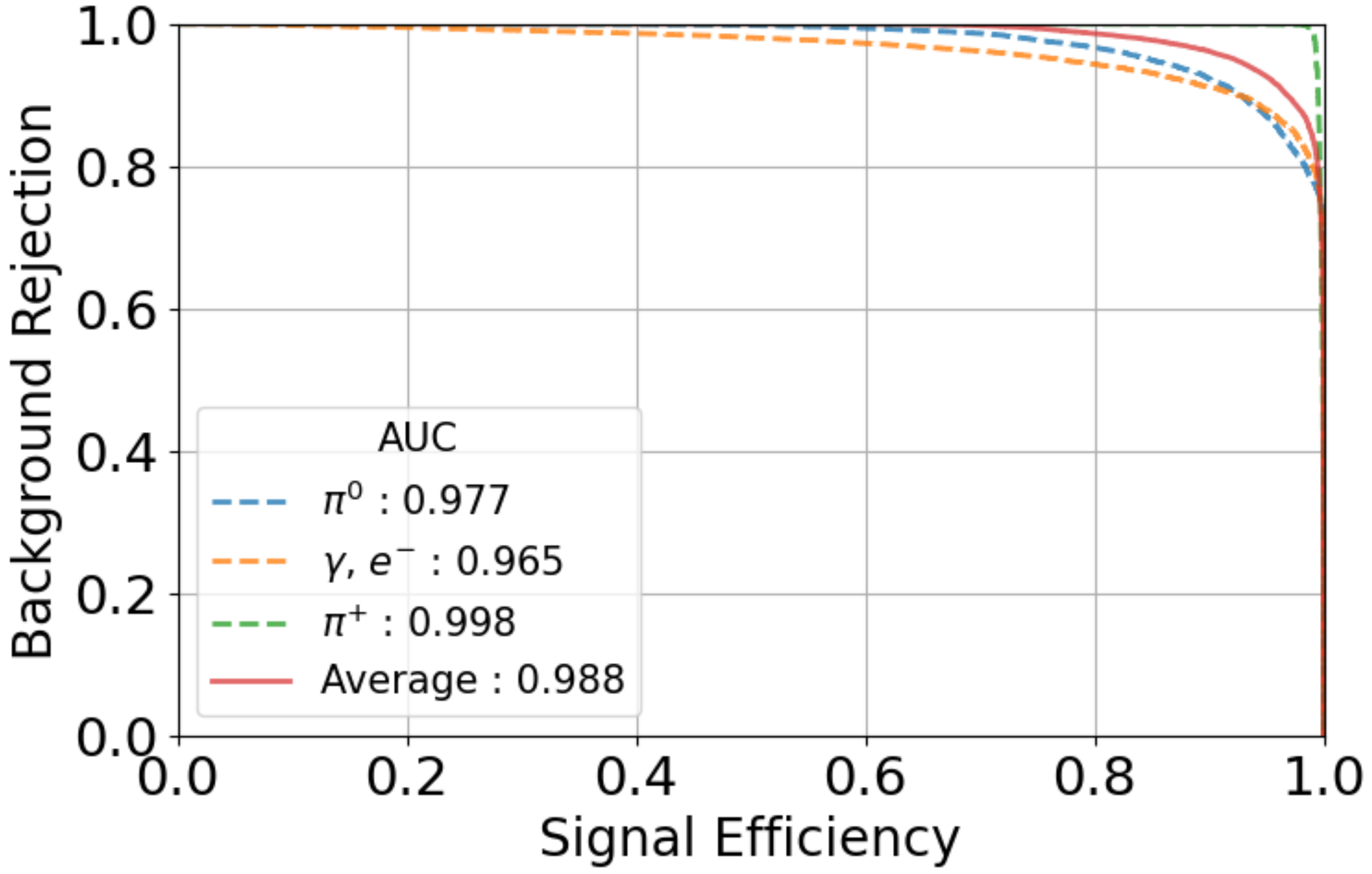


## Direction reconstruction

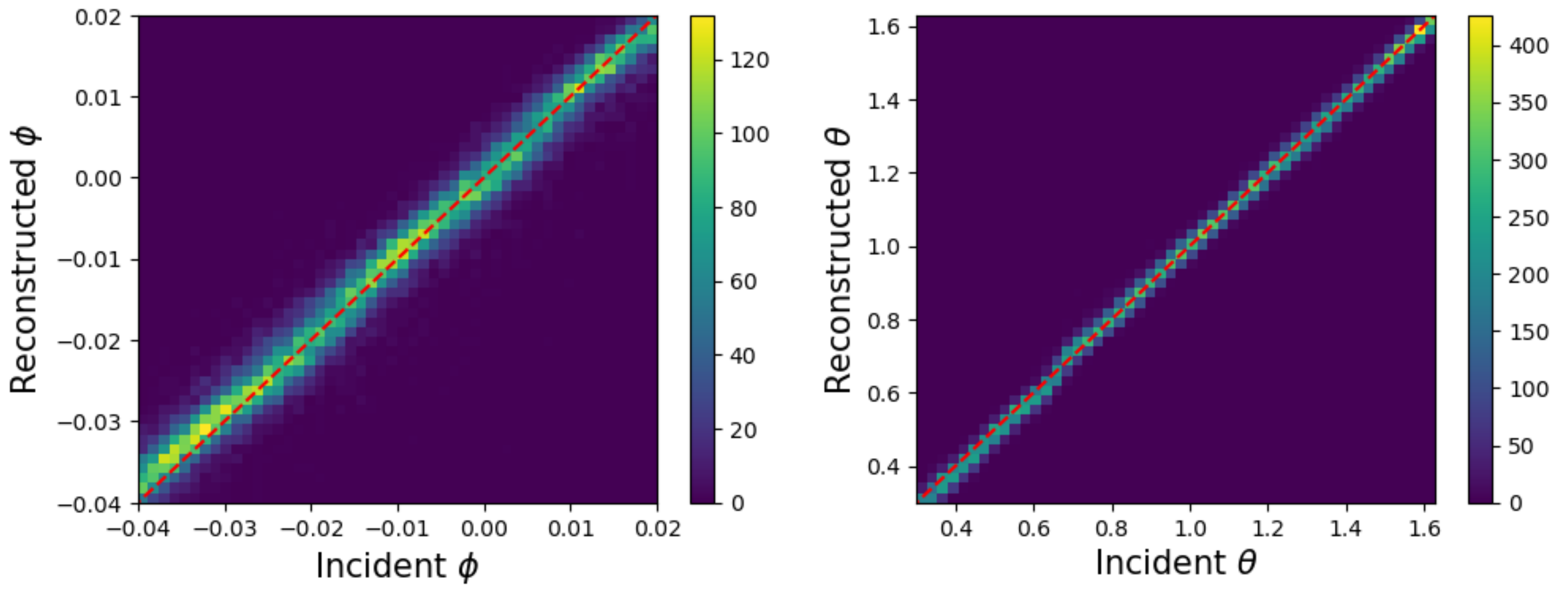


## Energy reconstruction

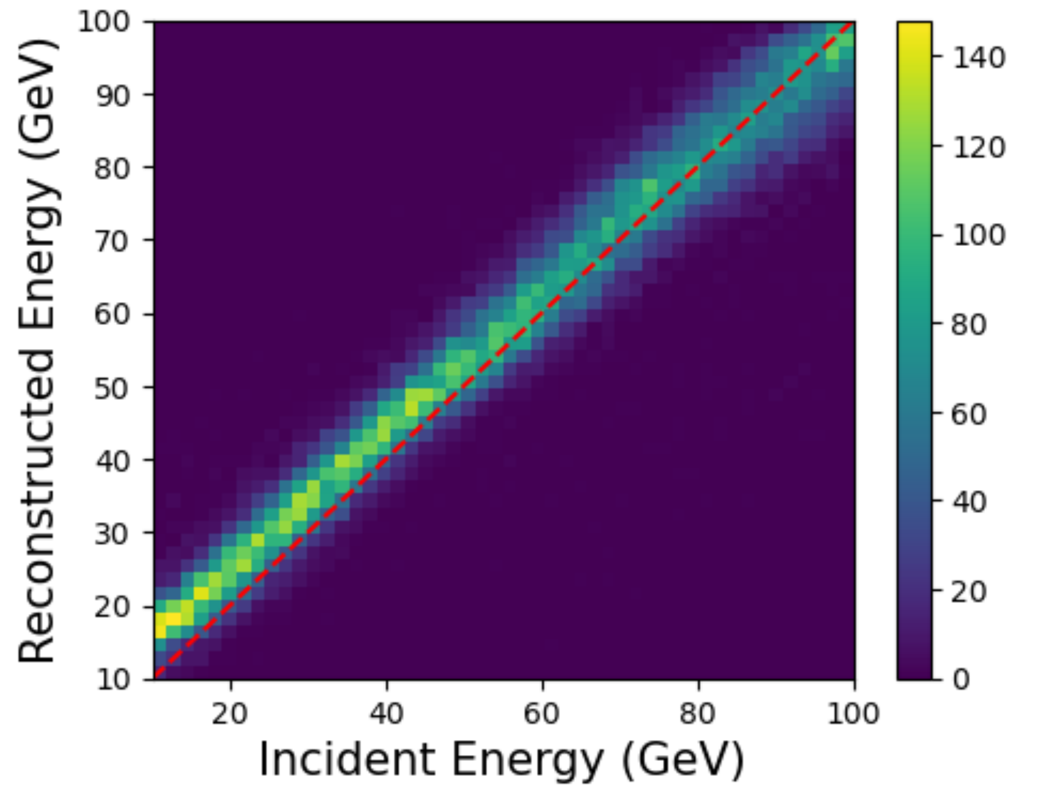

# Comparison of Dual-Readout Calorimeter of different absorbers

## Based on GEANT4 simulation, compared performance of Dual-Readout Calorimeter of various absorbers.

- Copper, Brass, Iron, Lead, Tungsten absorbers are compared

  -> For **EM particles**, results **show high relation to absorber's Z value**, relatively better energy resolution on low Z absorbers – Cu, Brass, Fe.

  -> For **single charge pion**, stochastic term of DR corrected energy is **under 30%**, regardless of absorber except Pb.

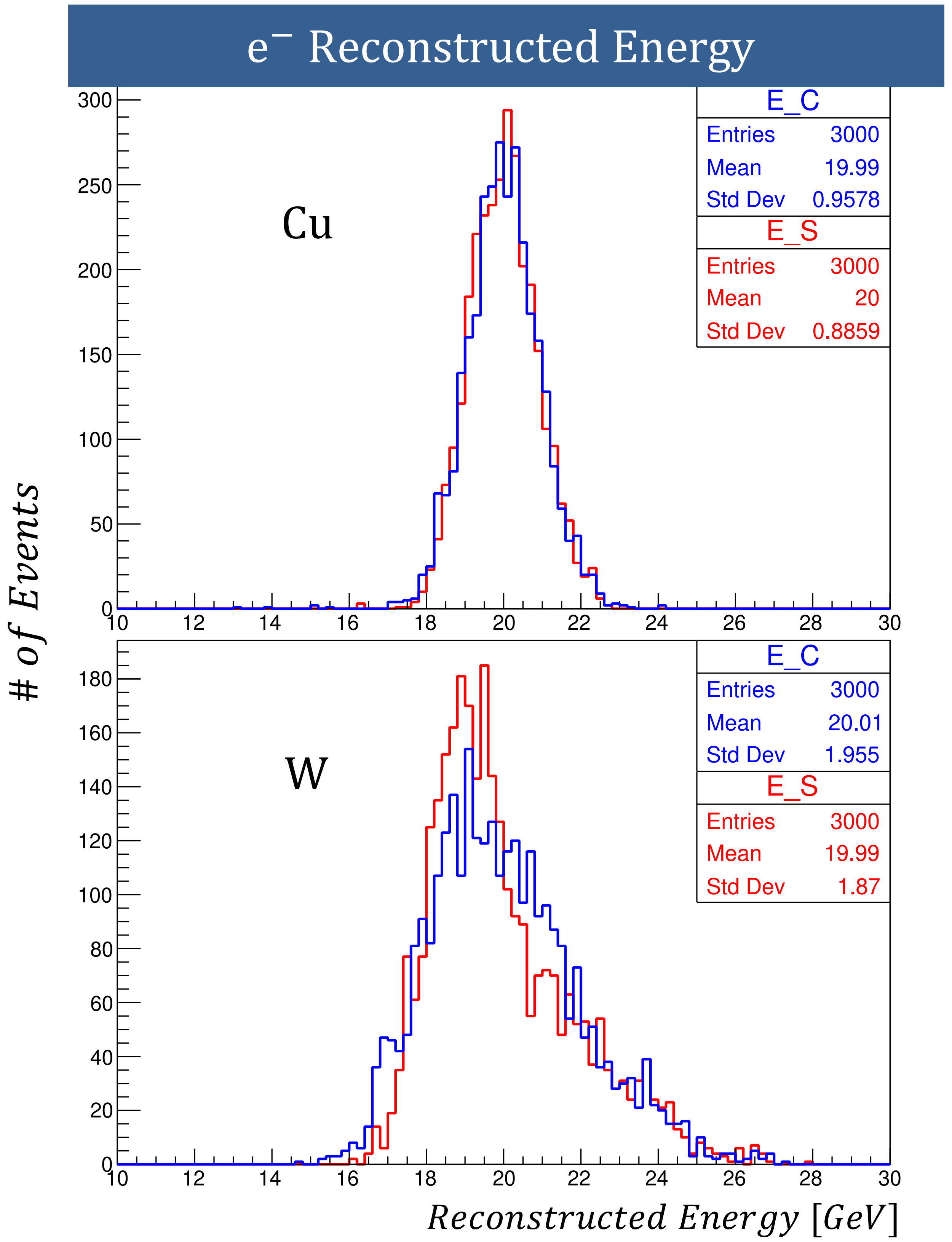


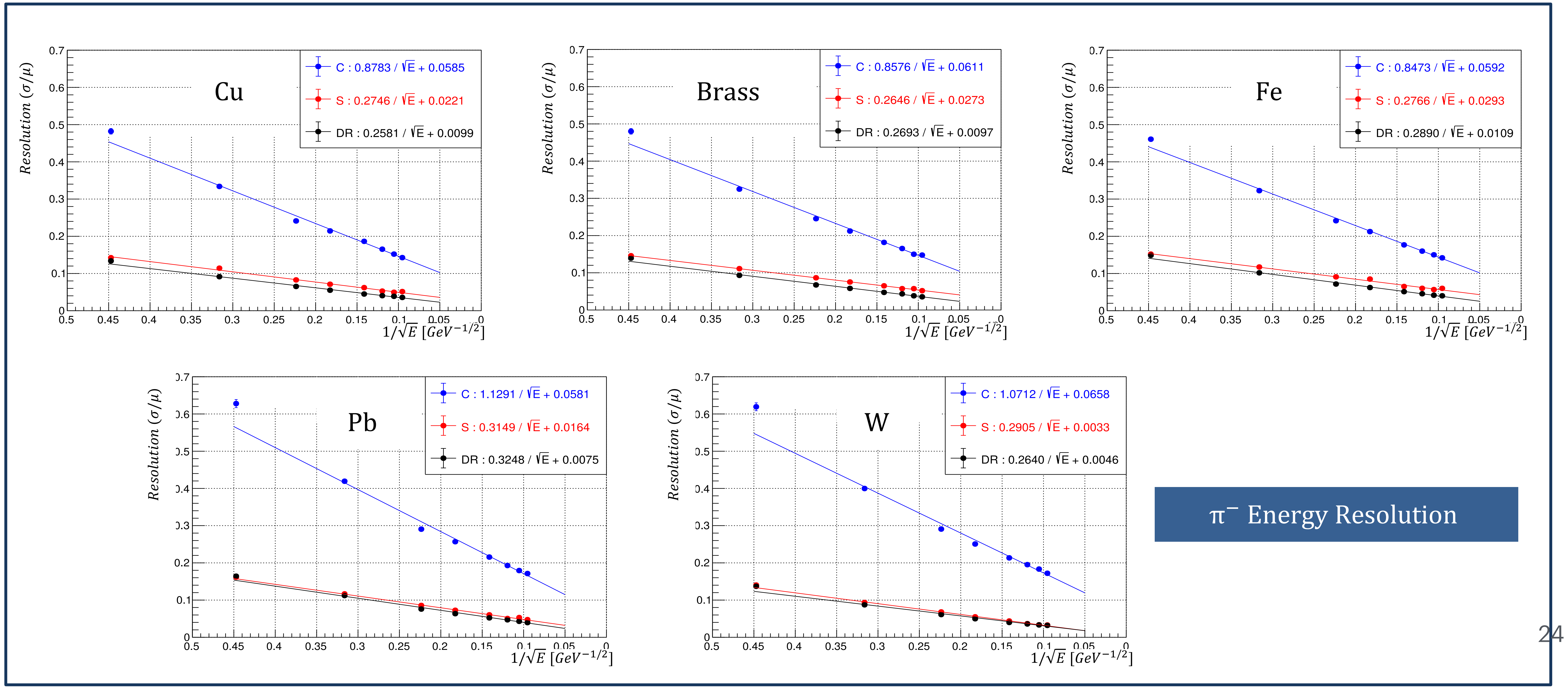

# 2023 Test beam with DRC at CERN

- Korean DRC collaboration had **test beam (TB)** with **50cm DRC module** at **CERN** east area T9
- Analyzed the data taken with **low energy (1~5 GeV) positron** beam
- The **DRC combined channel** showed energy resolution of $\frac{14.7\%}{\sqrt{E}} \oplus 2\%$
- The 3D and SFHS(top) tower showed **uniform energy response** to various beam spots

Sungwon Kim, May 23

50 cm DRC module

EM energy resolution

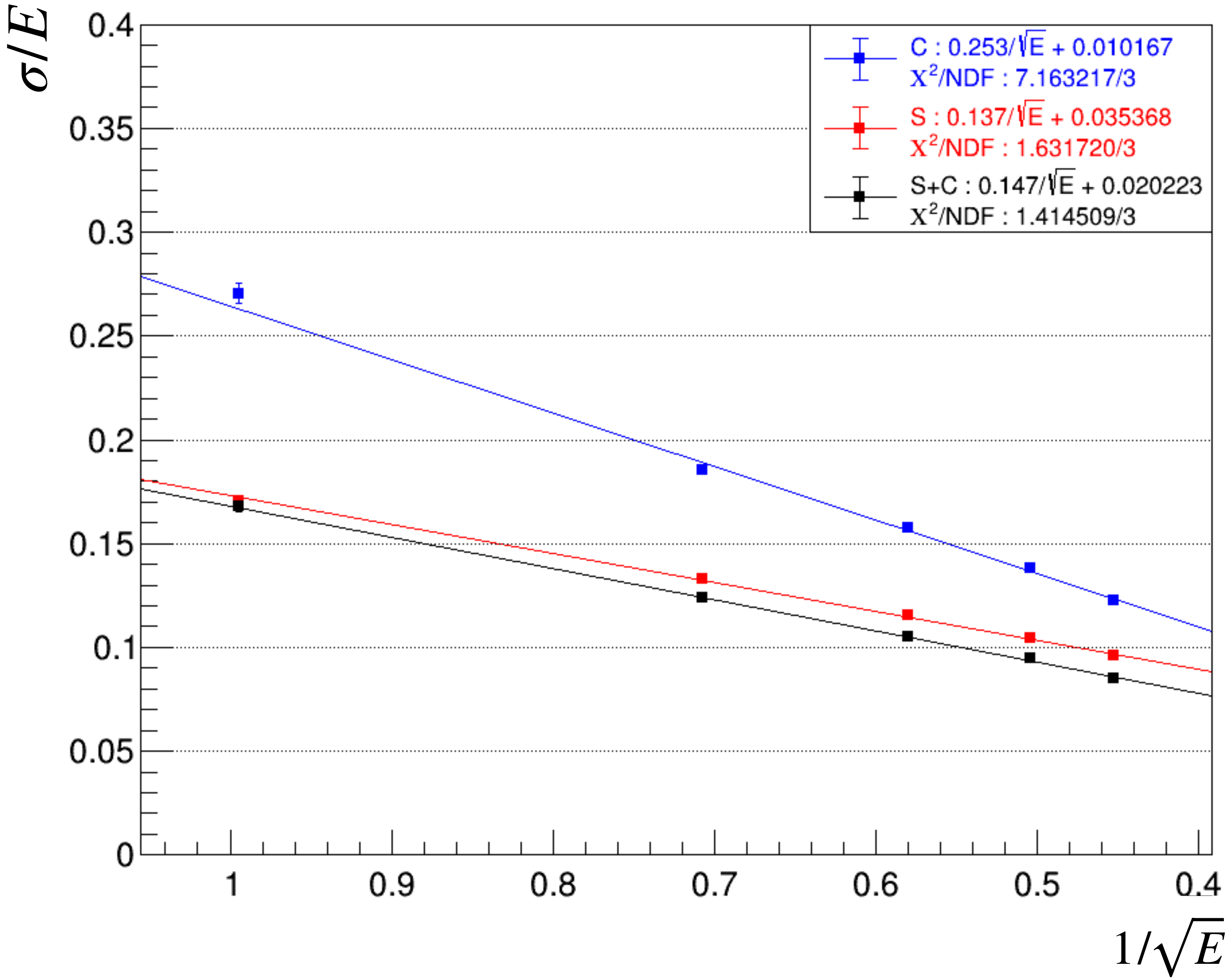


3D tower uniformity

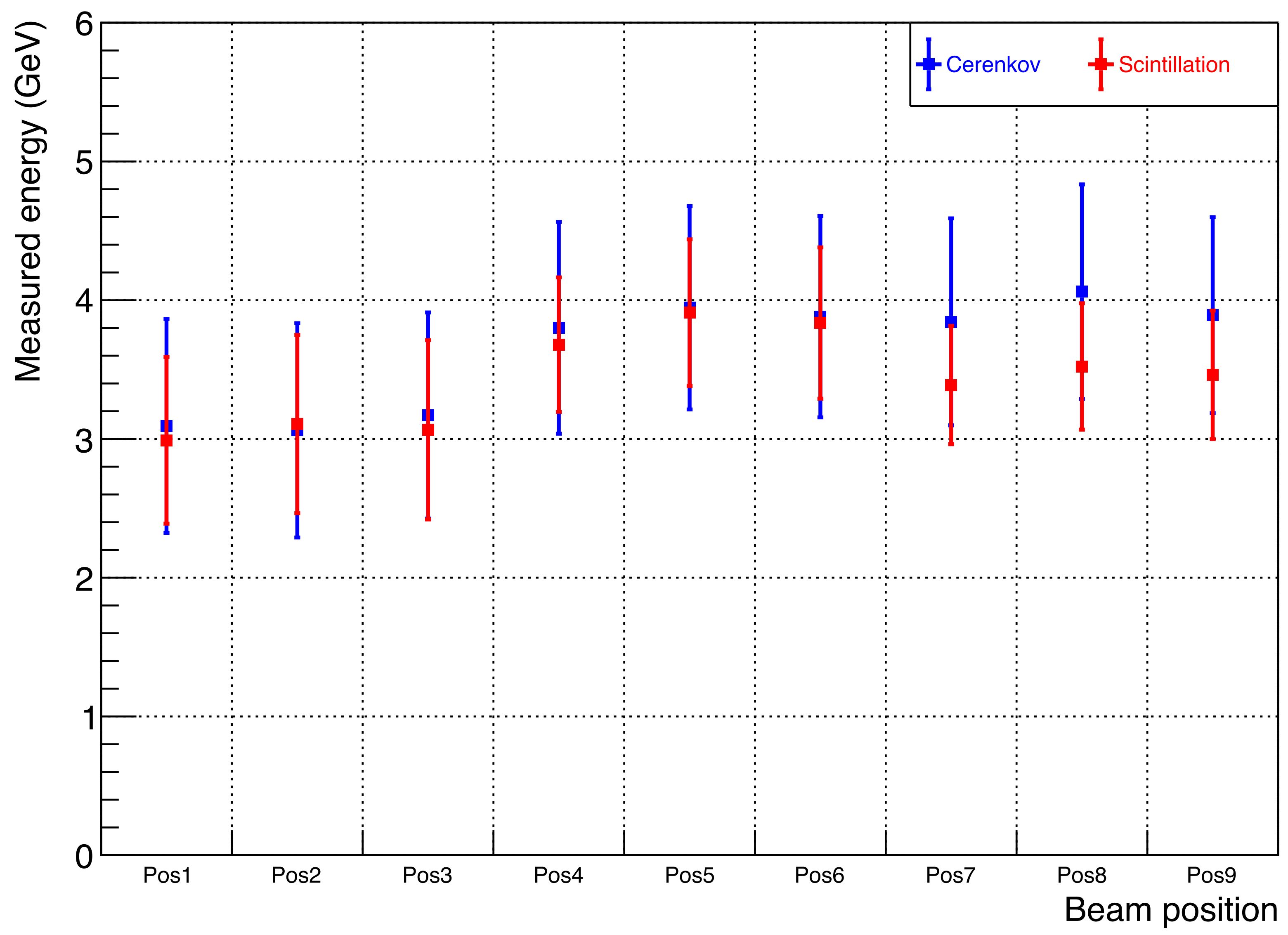


SFHS tower uniformity

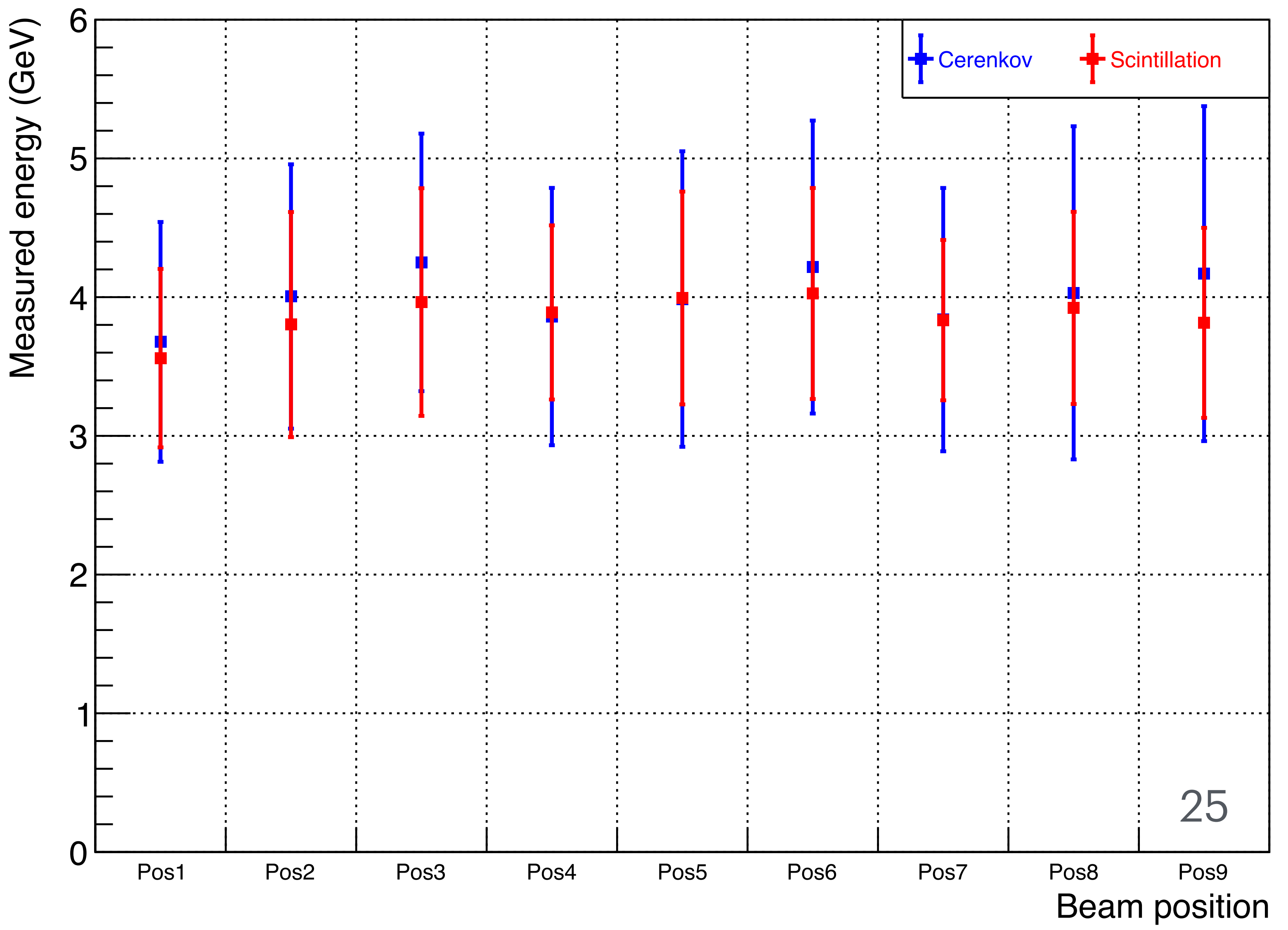

# Summary

- The dual-readout principle was proved with test beam data and provides high-quality energy measurement, especially for single hadrons and jets.

- Various studies on dual-readout calorimetry have been done over the last 25 years.

    - All results are at: http://www.phys.ttu.edu/~dream/results/publications/publications.html

- Our studies on the dual-readout calorimeter are ongoing for future experiments.

# Backup

# Neutron Signals for Dual-Readout Calorimetry

## NIM A 598 (2009) 710

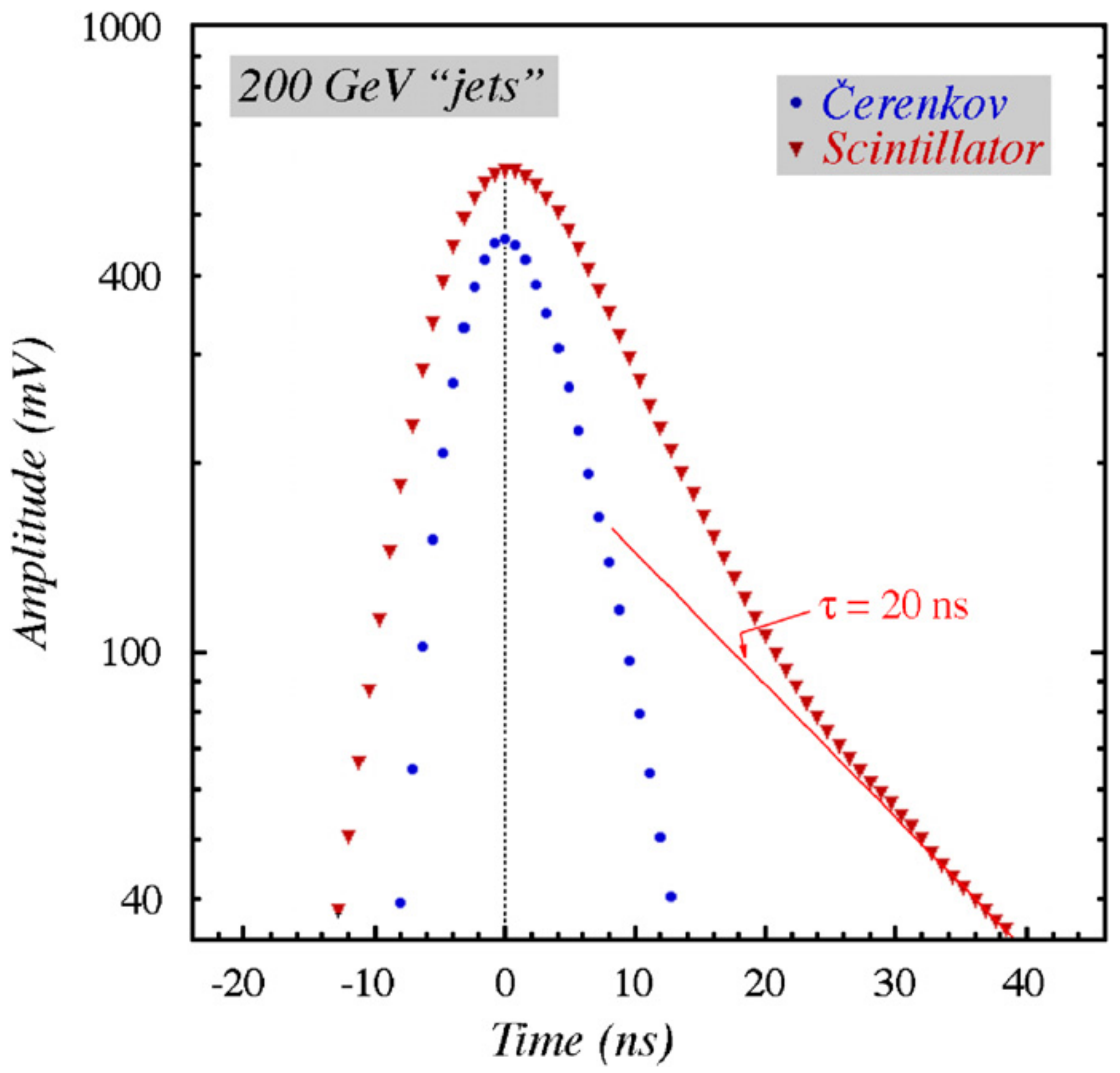


**Fig. 4.** Average time structure of the Cherenkov and scintillation signals recorded for 200 GeV "jets" developing in the DREAM calorimeter. The scintillation signals exhibit a tail with a time constant of about 20 ns, which is absent in the Cherenkov signals.

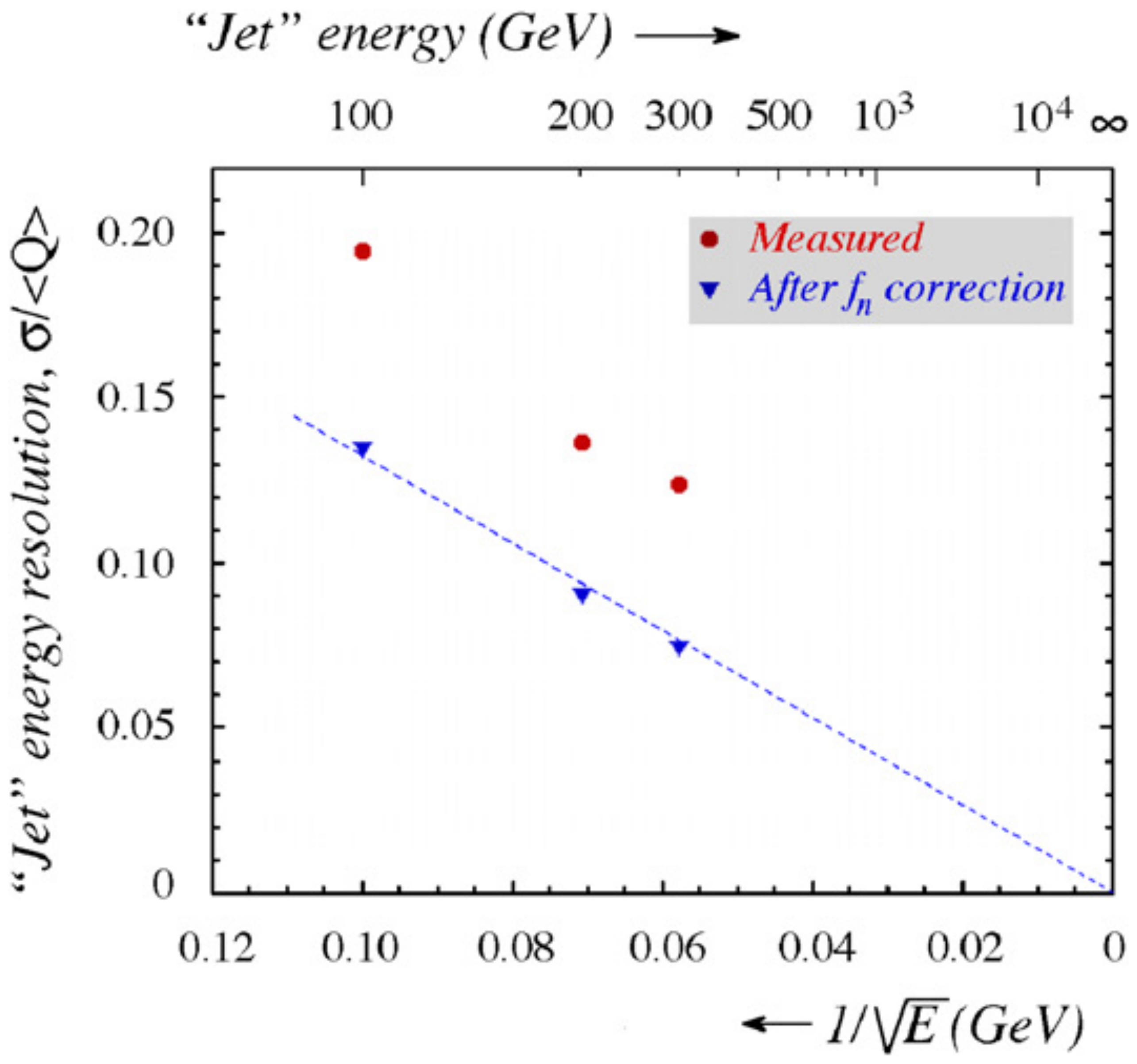


**Fig. 11.** Relative width of the Cherenkov signal distribution for "jets" as a function of energy, before and after a correction that was applied on the basis of the relative contribution of neutrons to the scintillator signals.

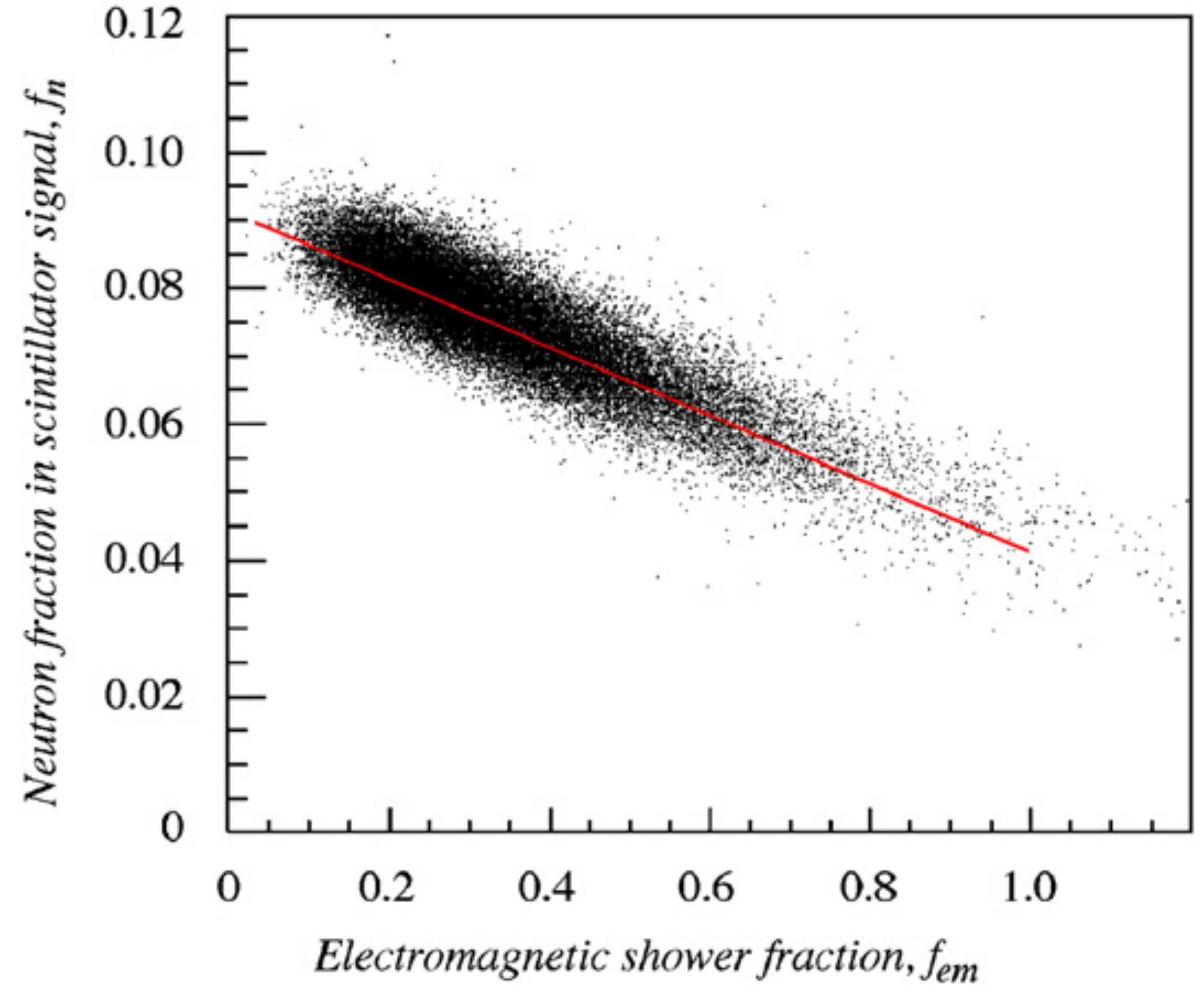


**Fig. 12.** Relationship between the average fractional contribution of neutrons to the scintillator signals and the em fraction of the showers induced by 200 GeV "jets".

# Dual-readout calorimetry with a full-size BGO electromagnetic section

# NIM A 610 (2009) 488

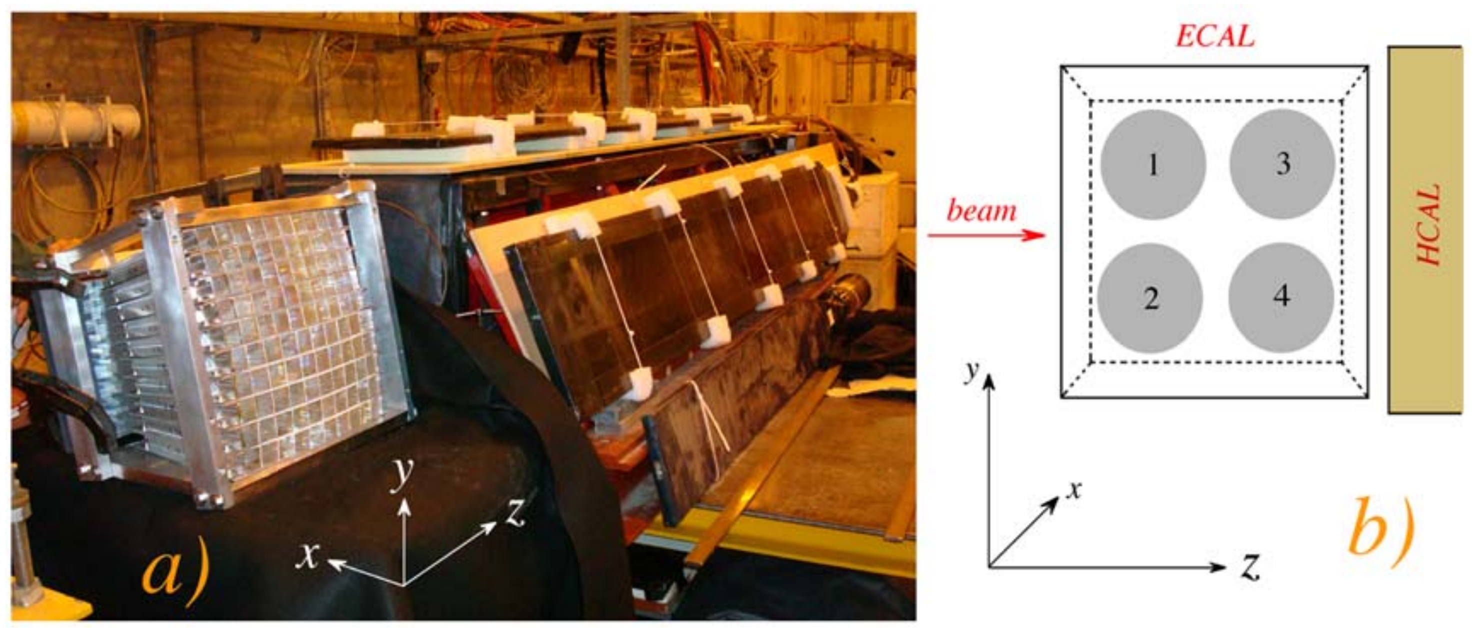


**Fig. 1.** The calorimeter during installation in the H4 test beam, which runs from the bottom left corner to the top right corner in this picture. The 100-crystal BGO matrix is located upstream of the fiber calorimeter, and is read out by four PMTs on the left (small end face) side. Some of the leakage counters are visible as well (a). The location and numbering of the PMTs reading out the BGO crystal matrix (b).

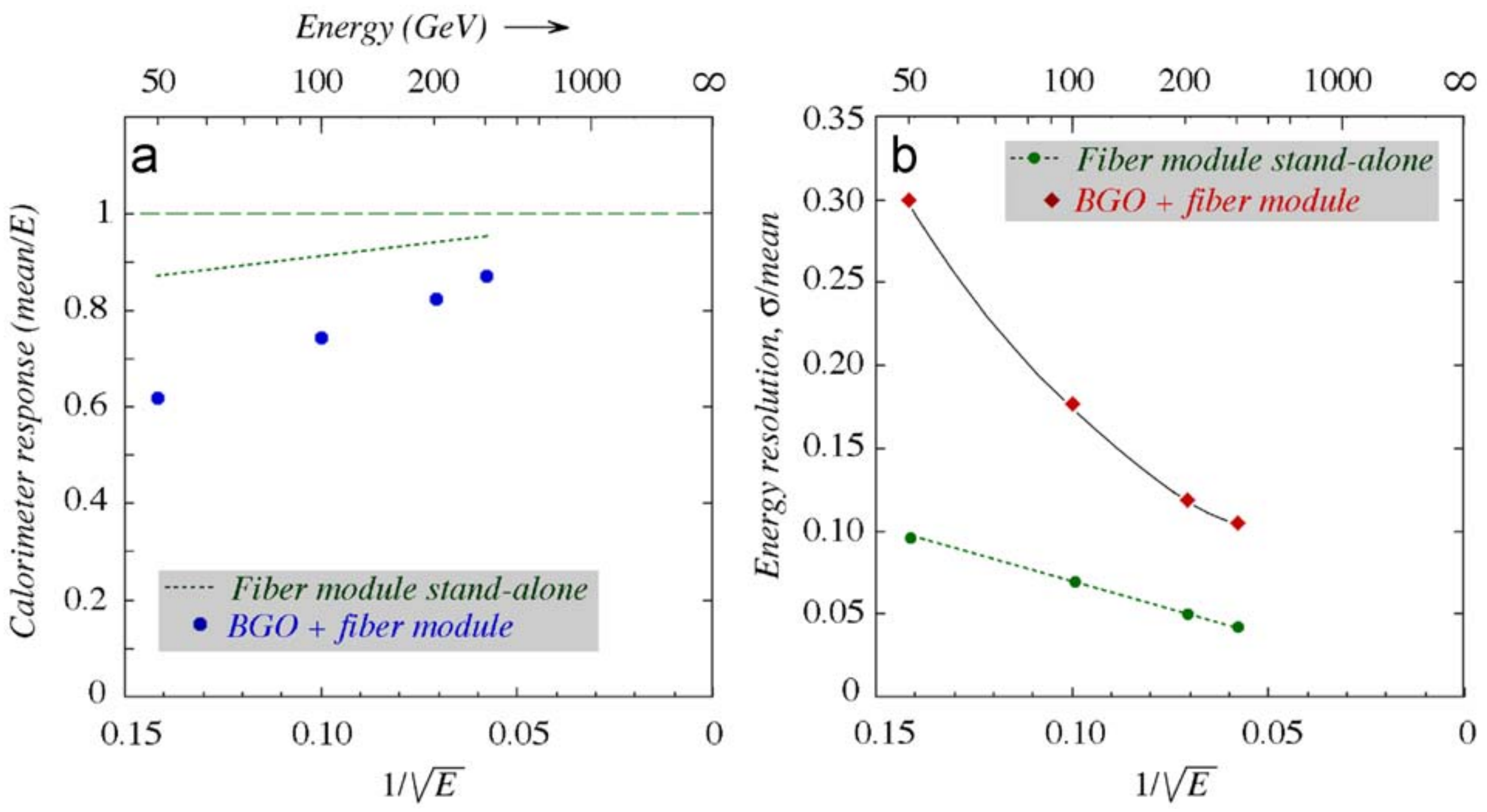


**Fig. 18.** The calorimeter response (a) and the energy resolution (b) for "jet" events detected in the BGO + fiber calorimeter system, corrected for the effects of fluctuations in $f_{em}$ by means of Eq. (4) (using $\xi_{eff} = 0.4$), as function of the "jet" energy. The results obtained previously for the fiber calorimeter module in stand-alone mode [4] are indicated by dotted lines.

# Particle identification in the longitudinally unsegmented RD52 calorimeter

## NIM A 735 (2014) 120

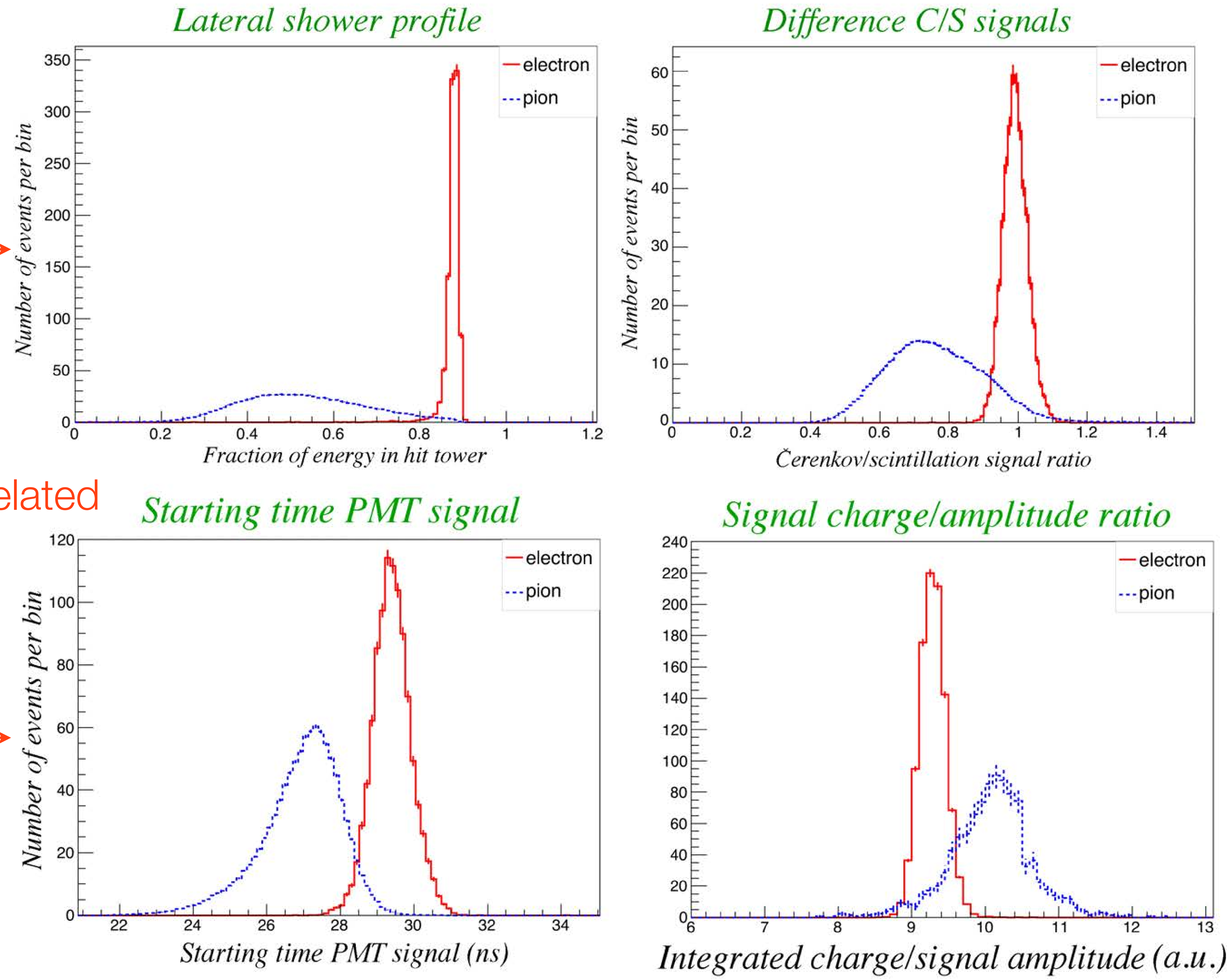


Uncorrelated

Input variables for 60 GeV $e^-$ and $\pi^-$

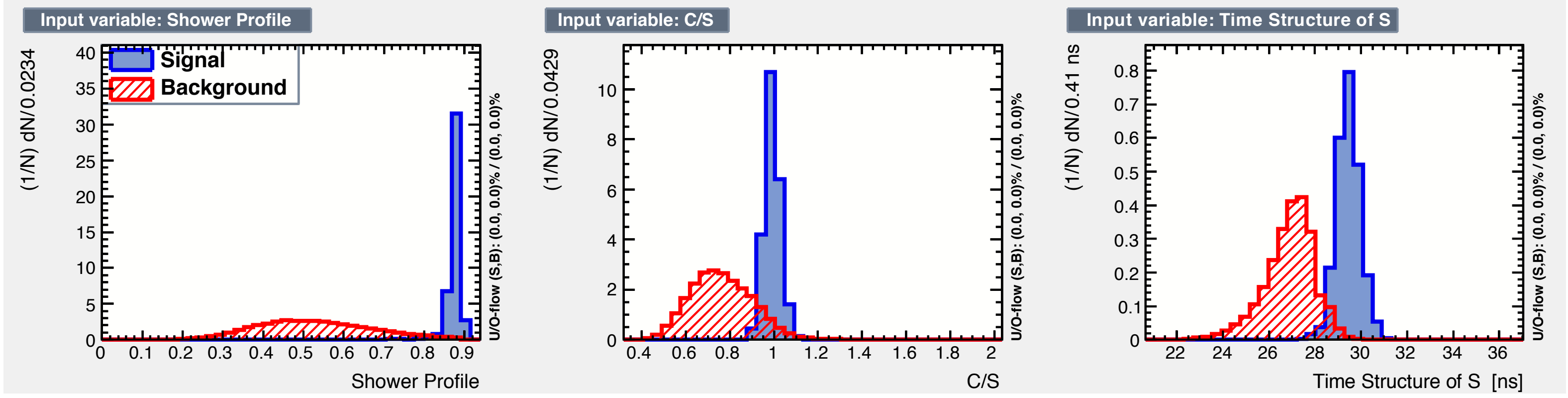


Optimal

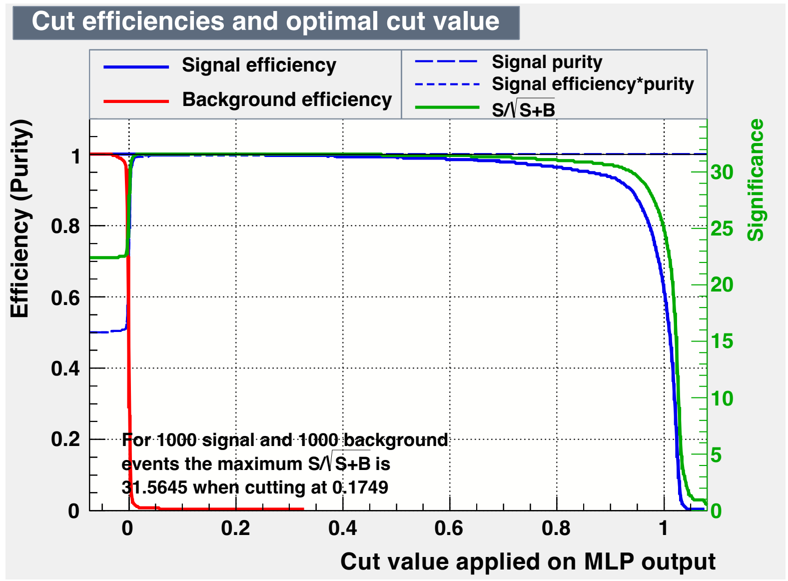


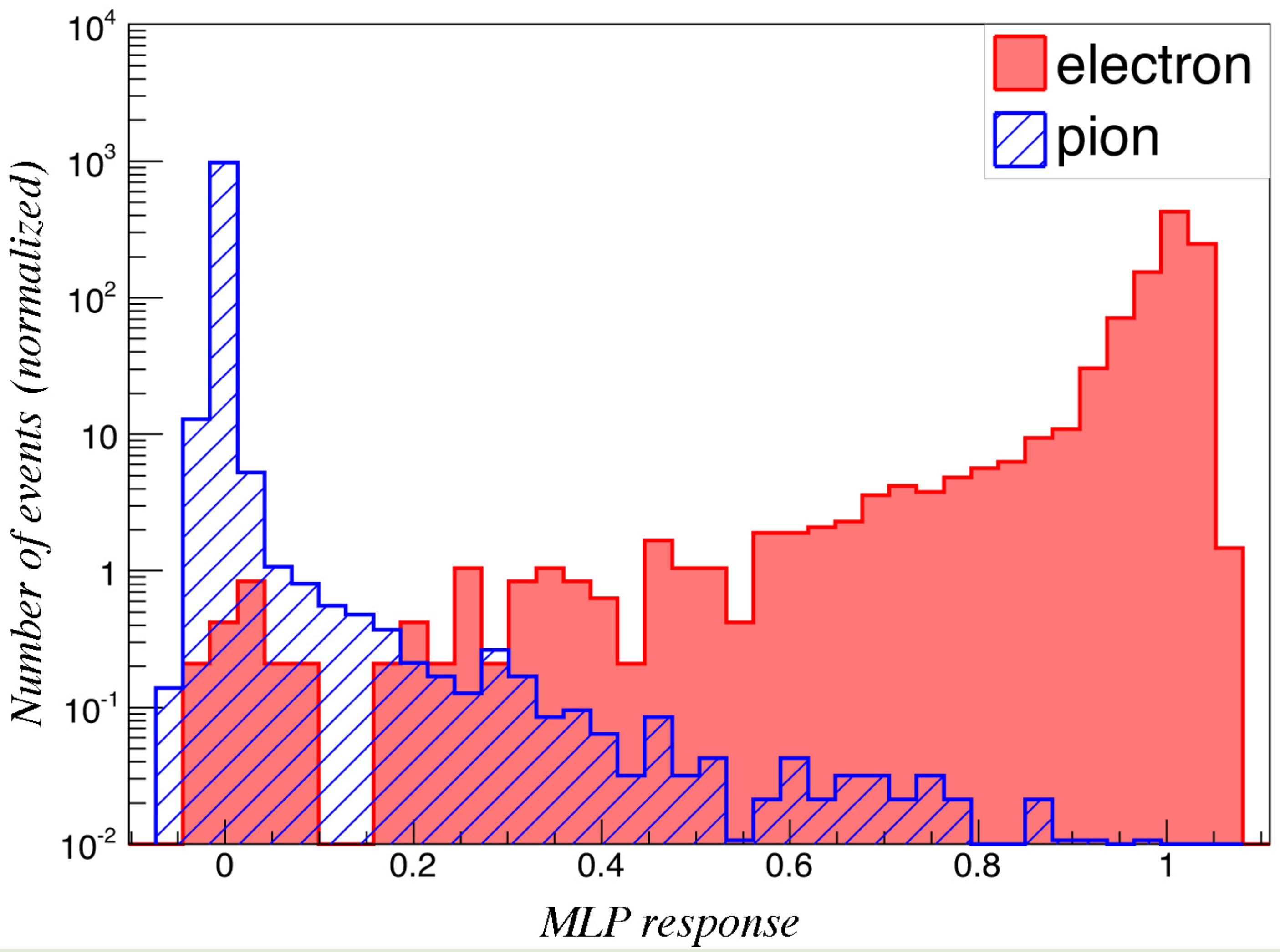


(Lateral shower profile > 0.7, $t_s$ > 28.0 ns): 99.1 % electron ID, 0.5 % pion mis-ID

**99.8 % electron ID**, **0.2 % pion mis-ID** for MLP > 0.17